

STOCHASTIC OPTIMIZATION BASED
APPROACH TOWARDS OPTIMAL CONTROL
IN DISSOCIATIVE DYNAMICS OF SMALL
MOLECULES

(Research project funded by UGC, New Delhi, India.)

Sanction No. : F.42-301/2013(SR) dt. 12.03.2013

FINAL COMPLETION REPORT



P. I. : Dr. Pinaki Chaudhury ,
Professor , Department of Chemistry ,
University of Calcutta

Final Report Assessment / Evaluation Certificate
(Two Members Expert Committee Not Belonging to the Institute of Principal Investigator)
 (to be submitted with the final report)

It is certified that the final report of Major Research Project entitled” **_Stochastic Optimization Based Approach Towards Optimal Control in Dissociative Dynamics of Small Molecules_**” by Dr./Prof. **Pinaki Chaudhury** of **Dept. of Chemistry, University of Calcutta** has been assessed by the committee consisting the following members for final submission of the report to the UGC, New Delhi under the scheme of Major Research Project.

Comments/Suggestions of the Expert Committee:-

The work carried out is satisfactory and the objective of the project has been achieved to a large extent with publications in reputed journals.

Name & Signatures of Experts with Date:-

Name of Expert	University/College name	Signature with Date
1. Prof. Suman Kumar Banik	Bose Institute, Kolkata	 15/2/21
2. Prof. Sudip Kumar Chattopadhyay	IEST, Shibpur, West Bengal	 15/2/21

It is certified that final report, Executive summary of the report, Research documents, monograph academic papers provided under Major Research Project have been posted on the website of the University/College.


 (Registrar/Principal)
 Seal
 REGISTRAR
 UNIVERSITY OF CALCUTTA



Development & Planning Officer
CALCUTTA UNIVERSITY

No. UGC/156/Aud. Utili. Cert./2016.

When replying please quote
Number, Date and Subject

Dated: 25/02/2016.

To
The Under Secretary,
[MRP(SR)],
University Grants Commission,
Bahadur Shah Zafar Marg,
New Delhi- 110002.

Subject: Submission of Statement of Expenditure & Utilisation Certificate in respect of Project of
Dr. (Prof.) Pinaki Chaudhury,
Department of Chemistry,
University of Calcutta, Ref. No. F. 42-301/2013(SR) dt. 12.03.2013
Attention:- Mrs. G. S. Arulak, Room No. - 319.

Dear Sir / Madam,

I am forwarding herewith the Utilisation Certificate and Statement of Expenditure in respect of Project of
Dr. (Prof.) Pinaki Chaudhury Principal Investigator, Department of Chemistry,
University of Calcutta, duly audited by the M/S. Mitra Deb Mallik & Co., Chartered Accountants,
West Bengal and endorsed by the Audit & Finance Officer and the Registrar, University of
Calcutta. Accounts

As per the Audit Report, the excess amount of Rs. _____ (Rupees _____)
only incurred for the purpose of above project may kindly be released as early as possible from the total
approved allocation as committed by the Commission to the University.

An early action in this regard is requested from your end.

Thanking you,
Yours faithfully,

Sd/-
Development & Planning Officer,
University Of Calcutta.

Memo No. UGC/156A/Aud. Utili. Cert./2016,

Dated-25/02/2016.

Copy forwarded to :-

1. Dr. (Prof.) Pinaki Chaudhury, Deptt. of Chemistry, University of Calcutta.
2. The Accounts Officer, University of Calcutta.

A.O.-II
Development & Planning Officer,
University of Calcutta.

Kanika Pal 25.02.16

A.O.
22.02.16

**STOCHASTIC OPTIMIZATION BASED APPROACH
TOWARDS OPTIMAL CONTROL IN DISSOCIATIVE
DYNAMICS OF SMALL MOLECULES**

(Research Project funded by U.G.C., New Delhi)

P.I. : Dr. Pinaki Chaudhury, Dept. of Chemistry,
University of Calcutta

Sanction No. : F.42-301/2013(SR) dt. 12.03.2013

AUDIT REPORT

MITRA DEBMALLIK & Co.

Chartered Accountants

9, Kiran Sankar Roy Road,

Kolkata - 700 001



MITRA DEBMALLIK & CO.

Chartered Accountants

S. Mitra M. Com., F.C.A.

M. Debmallik, B.Sc., F.C.A.

Date.....

UTILIZATION CERTIFICATE

Certified that UNIVERSITY GRANTS COMMISSION, NEW DELHI released a sum of Rs.12,00,000/- to Calcutta University towards the Research Project entitled "STOCHASTIC OPTIMIZATION BASED APPROACH TOWARDS OPTIMAL CONTROL IN DISSOCIATIVE DYNAMICS OF SMALL MOLECULES" under Dr. Pinaki Chaudhury, of the Department of Chemistry vide Sanction No. F.42-301/2013(SR) dt. 12.03.2013. There was a further credit of Rs.57,729/- by the Bank as interest, thereby making the total amount available under the Project Rs.12,57,729/-. Out of the said amount an amount of Rs.11,94,050/- was actually spent towards the purpose of Research Project thereby leaving a balance of Rs.63,679/- in the Bank. The Project is now completed and so after clearing the Auditors Remuneration of Rs.1,000/-, the balance amount of Rs.62,679/- is to be refunded to the funding Agency.

For MITRA DEBMALLIK & CO.

Chartered Accountants

(S. MITRA)
Partner

Date : 22nd September, 2015



Pinaki Chaudhury

20/1/2016

DR. PINAKI CHAUDHURY
Associate Professor
Dept. of Chemistry
UNIVERSITY OF CALCUTTA
92, A.P.C. Road, Kolkata-700009

A3 22/1/16
ACCOUNTS OFFICER
UNIVERSITY OF CALCUTTA

COUNTER-SIGNATURE

[Signature]
REGISTRAR
UNIVERSITY OF CALCUTTA

28/01/16

STOCHASTIC OPTIMIZATION BASED APPROACH TOWARDS OPTIMAL CONTROL IN DISSOCIATIVE DYNAMICS OF SMALL MOLECULES

Name of the Funding Agency : UNIVERSITY GRANTS COMMISSION, NEW DELHI
 Sanction No. : F.42-301/2013(SR) dt. 12.03.2013
 Name of the P.I. : Dr. PINAKI CHAUDHURY
 Dept. of Chemistry, University of Calcutta

RECEIPTS & PAYMENTS ACCOUNT For the year ended 31st March 2013

<u>RECEIPTS</u>	<u>AMOUNT</u>	<u>PAYMENTS</u>	<u>AMOUNT</u>
To Grant Received	1,200,000	By Closing Balance	1,200,000
	1,200,000		1,200,000

RECEIPTS & PAYMENTS ACCOUNT For the year ended 31st March 2014

<u>RECEIPTS</u>	<u>AMOUNT</u>	<u>PAYMENTS</u>	<u>AMOUNT</u>
To Opening Balance	1,200,000	By Equipment & Accessories	1,194,050
To Bank Interest	35,332	By Closing Balance	41,282
	1,235,332		1,235,332

RECEIPTS & PAYMENTS ACCOUNT For the year ended 31st March 2015

<u>RECEIPTS</u>	<u>AMOUNT</u>	<u>PAYMENTS</u>	<u>AMOUNT</u>
To Opening Balance	41,282	By Closing Balance	62,440
To Bank Interest	21,158		
	62,440		62,440

RECEIPTS & PAYMENTS ACCOUNT For the Period from 1st April 2015 to 31st July 2015

<u>RECEIPTS</u>	<u>AMOUNT</u>	<u>PAYMENTS</u>	<u>AMOUNT</u>
To Opening Balance	62,440	By Closing Balance	63,679
To Bank Interest	1,239		
	63,679		63,679

AUDITORS' REPORT

We have audited the above Receipts & Payments Account of the Research undertaken by Dr. PINAKI CHAUDHURY, of the Development of Chemistry, Calcutta University with the books of accounts, vouchers and all other records as maintained and produced before us and found them correct.

9, Kiran Sankar Roy Road

Kolkata - 700 001.

Pinaki Chaudhury
20/11/2016

Dated : 22nd September 2015

DR. PINAKI CHAUDHURY
Associate Professor
Dept. of Chemistry
UNIVERSITY OF CALCUTTA
92, A.P.C. Road, Kolkata-700009

A3
22/11/16
ACCOUNTS OFFICER
UNIVERSITY OF CALCUTTA



For MITRA DEBMALLIK & CO.

Chartered Accountants

(Signature)

(S. MITRA)
Partner

**STOCHASTIC OPTIMIZATION BASED APPROACH TOWARDS OPTIMAL
CONTROL IN DISSOCIATIVE DYNAMICS OF SMALL MOLECULES**

Name of the Funding Agency : UNIVERSITY GRANTS COMMISSION, NEW DELHI
Sanction No. : F.42-301/2013(SR) dt. 12.03.2013
Name of the P.I. : Dr. PINAKI CHAUDHURY
 Dept. of Chemistry, University of Calcutta

CONSOLIDATED STATEMENT OF EXPENDITURE

	<u>Grant Released</u>	<u>Expenditure Incurred</u>	<u>Expenditure to be incurred</u>	<u>Total Expenditure</u>	<u>Balance</u>
	1,200,000	1,194,050	--	1,194,050	5,950
Additional Grant :					
Bank Interest	57,729	--	1,000 *	1,000	56,729
	<u>1,257,729</u>	<u>1,194,050</u>	<u>1,000</u>	<u>1,195,050</u>	<u>62,679</u>

* Audit Fee Payable



Pinaki Chaudhury
20/11/2016

DR. PINAKI CHAUDHURY
Associate Professor
Dept. of Chemistry
UNIVERSITY OF CALCUTTA
92, A.P.C. Road, Kolkata-700009

A3
22/1/16
ACCOUNTS OFFICER
UNIVERSITY OF CALCUTTA

COUNTER-SIGNATURE

Ejn
REGISTRAR
UNIVERSITY OF CALCUTTA
28/01/16

Stochastic Optimization Based Approach Towards Optimal Control in Dissociative Dynamics of Small Molecules

Pinaki Chaudhury¹

¹*Department of Chemistry, University of Calcutta,
92, A.P.C. Road, Kolkata 700 009, INDIA.*

(Dated: March 10, 2020)

I. DETAILS OF WORK DONE

As was laid down in the objective of the work, we have done substantial work on selective bond dissociation by designing optimum pulses both in *HOD* and *O₃* systems. In *HOD* we have been able to design pulses, which gives substantially high dissociation fluxes in the target dissociation channels separately i.e. O – H and O – D bonds in *HOD*. We stress upon the point that the individual fluxes obtained are much higher than those obtained in earlier reports using single standard pulses, which are more common. We have published our work in the Journal of Chemical Physics (139 (2013) 034310). A copy of the published paper is given in the list of reprints supplied.

The second important system that we have studied in the project is on selective bond dissociation dynamics in *O₃*. However in this systems one of the terminal oxygen atoms is ¹⁸O. This creates two separate channels of dissociation ¹⁸O + ¹⁶O – ¹⁶O and ¹⁸O – ¹⁶O + ¹⁶O. Dissociating these bonds in itself is difficult because this system suffers from very strong Intra Molecular vibrational Relaxation (IVR). This makes excitation of the molecule with a target laser pulse difficult as the population enhancement in the excited state does not stay for a reasonable amount of time for the following dynamics to take place. However, we with our optimized pulse have been able to get reasonably good dissociating fluxes in the two channels. The manuscript has been published Journal of Chemical Physics (139, (2013) 164312).

The problem of dissociating bonds selectively in *HOD* has also been investigated differently. Since Stochastic Algorithms can differ in their mode of operation as well as in complexity. To examine this aspect we have used Genetic Algorithms to see if there is an enhancement in branching ratios of the two channels of dissociation. The results have been published in Molecular Physics (15 (2017) 1786) A copy of the reprint is supplied.

Since Optimal control theory can extend to controlling other chemical events, we have also made a few publications in analogous areas like controlling tunnelling in relevant potentials, and other applications of stochastic optimization techniques to study complex structural patterns . We acknowledge with humility, the assistance from UGC, which has helped us achieve these goals since the commencement of the project. The complete list of publications is provided in a separate section along with the reprints.

We now present the titles and abstracts of some of our publications in the field of optimal control.

1) Enhancing the branching ratios in the dissociation channels for ¹⁶O¹⁶O¹⁸O molecule by designing optimum laser pulses: A study using stochastic optimization

The Journal of Chemical Physics 143 (2015) 144109

We propose a strategy of using stochastic optimization technique, namely, Simulated Annealing to design optimum laser pulses (both IR and UV) to achieve greater fluxes along the two dissociating channels ($O^{18} + O^{16}O^{16}$ and $O^{16} + O^{16}O^{18}$) in $^{16}O^{16}O^{18}O$ molecule. We clearly show that the integrated fluxes obtained along the targeted dissociating channel is much larger with the optimized pulse than with the unoptimized one. The flux ratios are also more impressive with the optimized pulse than with the unoptimized one. To explain clearly, why we are achieving better results we look at the evolution contours of the wavefunctions along the two channels with time after the actions of both the IR and UV pulses. We also report the pulse parameters obtained as well as the final shapes they take.

2) Selective bond breaking mediated by state specific vibrational excitation in model *HOD* molecule through optimized femtosecond IR pulse: A simulated annealing based approach

The Journal of Chemical Physics 139 (2013) 034310

The selective control of *OH/OD* bond dissociation in reduced dimensionality model of *HOD* molecule has been explored through IR + UV femtosecond pulses. The IR pulse has been optimized using simulated annealing stochastic approach to maximize population of a desired low quantum vibrational state. Since those vibrational wavefunctions of the ground electronic states are preferentially localized either along the *OH* or *OD* mode, the femtosecond UV pulse is used only to transfer vibrationally excited molecule to the repulsive upper surface to cleave specific bond, *OH* or *OD*. While transferring from the ground electronic state to the repulsive one, the optimization of the UV pulse is not necessarily required except specific case. The results so obtained are analyzed with respect to time integrated flux along with contours of time evolution of probability density on excited potential energy surface.

3) Coherent destruction of tunneling with optimally designed polychromatic external field

Chemical Physics 425 (2013) 73

A suitably designed polychromatic field with a very low field strength and low frequency (10^{-5} atomic unit) can bring about coherent destruction of tunneling (CDT) in a symmetric double well system. It is analyzed that in the presence of an external perturbation the difference of energy between the two lowest quasi-energy states may increase or decrease depending on the spatial and temporal nature of the perturbation. We have designed sets of polychromatic fields both spatially symmetric and antisymmetric, which cause CDT in symmetric double well system. A stochastic optimizer (Simulated Annealing) has been used to design such a polychromatic field periodic in time. Both spatial symmetry preserving or symmetry breaking perturbations may cause CDT for a symmetric double well potential.

4) Optimal designing of polychromatic field for maximum dissociation of *LiH* molecule

Indian Journal of Physics 87 (2013) 865

We present a strategy for enhancing the dissociation probability of a diatomic molecule, namely *LiH*, by designing optimal laser pulse. Dissociation dynamics is followed by solving time-dependent

Schrodinger equation using time-dependent Fourier Grid Hamiltonian technique with optimal laser pulse function, generated by using the stochastic optimization technique of simulated annealing. We show that as we increase number of variable parameters while designing the optimal time dependent perturbation, higher dissociation is obtained. The step-wise increase in dissociation probability with the increase in complexity of designed pulse is clearly shown

5) Selective bond dissociation of HOD molecule by optimally designed polychromatic IR+UV pulse: a genetic-algorithm-based study

Molecular Physics 115 (2017) 1786

A theoretical investigation of selective bond dissociation of OH or OD bond of HOD molecule is carried out by optimally designed electromagnetic field where optimisation is performed by Genetic Algorithm (GA). Two strategies depending upon the objective function and variable space for optimisation have been followed to achieve selective photodissociation. In Strategy I flux along a particular channel ($JH + OD / JD + OH$) in the repulsive excited state of HOD is considered in defining the objective function with a polychromatic IR pulse of eight components and a UV radiation of two components being optimally found out by GA. The polychromatic IR pulse distributes the population among the low quanta vibrational states of OH or OD stretching mode in ground electronic state and the subsequent UV pulse transfers the population to the excited state where photodissociation occurs. According to the direction of population along OH or OD stretch in ground electronic state, fluxes in the channels may be expected. We have obtained a maximum value of 92.38% and 74.12% along $JH + OD$ and $JD + OH$ channels, respectively. The Strategy II is the conventional strategy of selective vibrational excitation followed by population transfer to excited state by single UV pulse. In this case, the polychromatic IR fields are optimised by GA to achieve selective vibrational excitation on $-1, 0, -2, 0, -0, 1$ and $-0, 2$ states and the matching single UV pulse is fired for electronic excitation. The first two states correspond to the OH stretch and population transfer from these states to excited state result in predominant flux along H+OD channel and similar scheme from the last two states result in D+OH dissociation as they are effectively of OD character. The best values of $JH + OD$ and $JD + OH$ are 86.91% and 65.94% obtained by using Strategy II.

Papers Published

(1) Enhancing the branching ratios in the dissociation channels for $^{16}O^{16}O^{18}O$ molecule by designing optimum laser pulses: A study using stochastic optimization

S Talukder, S Sen, BK Shandilya, R Sharma, **P Chaudhury**, S Adhikari
The Journal of Chemical Physics 143 (2015) 144109

(2) Selective bond breaking mediated by state specific vibrational excitation in model HOD molecule through optimized femtosecond IR pulse: A simulated annealing based approach

BK Shandilya, S Sen, T Sahoo, S Talukder, **P Chaudhury**, S Adhikari
The Journal of Chemical Physics 139 (2013) 034310

(3) Coherent destruction of tunneling with optimally designed polychromatic external field

S Ghosh, S Talukder, S Sen, **P Chaudhury**
Chemical Physics 425 (2013) 73

(4) Optimal designing of polychromatic field for maximum dissociation of LiH molecule

S Sen, S Talukder, **P Chaudhury**

Indian Journal of Physics 87 (2013) 865

(5) Selective bond dissociation of HOD molecule by optimally designed polychromatic IR+ UV pulse: a genetic-algorithm-based study

S Talukder, **P Chaudhury**, S Adhikari

Molecular Physics 115 (2017) 1786

Enhancing the branching ratios in the dissociation channels for $O^{16}O^{16}O^{18}$ molecule by designing optimum laser pulses: A study using stochastic optimization

Cite as: J. Chem. Phys. **143**, 144109 (2015); <https://doi.org/10.1063/1.4932333>

Submitted: 02 July 2015 . Accepted: 21 September 2015 . Published Online: 12 October 2015

Srijeeta Talukder, Shrabani Sen, Bhavesh K. Shandilya, Rahul Sharma , Pinaki Chaudhury, and Satrajit Adhikari



View Online



Export Citation



CrossMark

ARTICLES YOU MAY BE INTERESTED IN

Selective bond breaking mediated by state specific vibrational excitation in model HOD molecule through optimized femtosecond IR pulse: A simulated annealing based approach
The Journal of Chemical Physics **139**, 034310 (2013); <https://doi.org/10.1063/1.4813127>

Beyond Born-Oppenheimer theory for ab initio constructed diabatic potential energy surfaces of singlet H_3^+ to study reaction dynamics using coupled 3D time-dependent wave-packet approach
The Journal of Chemical Physics **147**, 074105 (2017); <https://doi.org/10.1063/1.4998406>

Conical intersections and diabatic potential energy surfaces for the three lowest electronic singlet states of H_3^+

The Journal of Chemical Physics **141**, 204306 (2014); <https://doi.org/10.1063/1.4901986>

Lock-in Amplifiers

Find out more today



Zurich
Instruments



Enhancing the branching ratios in the dissociation channels for $O^{16}O^{16}O^{18}$ molecule by designing optimum laser pulses: A study using stochastic optimization

Srijeeta Talukder,¹ Shrabani Sen,² Bhavesh K. Shandilya,³ Rahul Sharma,⁴ Pinaki Chaudhury,^{1,a)} and Satrajit Adhikari^{5,b)}

¹Department of Chemistry, University of Calcutta, 92 A P C Road, Kolkata 700 009, India

²Department of Chemistry, Rammohan College, 102/1, Raja Rammohan Sarani, Kolkata 700 009, India

³Department of Chemistry, Indian Institute of Technology Bombay, Powai, Mumbai 400 076, India

⁴Department of Chemistry, St. Xavier's College, 30 Mother Teresa Sarani, Kolkata 700 016, India

⁵Department of Physical Chemistry, Indian Association for the Cultivation of Science, Jadavpur, Kolkata 700 032, India

(Received 2 July 2015; accepted 21 September 2015; published online 12 October 2015)

We propose a strategy of using a stochastic optimization technique, namely, simulated annealing to design optimum laser pulses (both IR and UV) to achieve greater fluxes along the two dissociating channels ($O^{18} + O^{16}O^{16}$ and $O^{16} + O^{16}O^{18}$) in $O^{16}O^{16}O^{18}$ molecule. We show that the integrated fluxes obtained along the targeted dissociating channel is larger with the optimized pulse than with the unoptimized one. The flux ratios are also more impressive with the optimized pulse than with the unoptimized one. We also look at the evolution contours of the wavefunctions along the two channels with time after the actions of both the IR and UV pulses and compare the profiles for unoptimized (initial) and optimized fields for better understanding the results that we achieve. We also report the pulse parameters obtained as well as the final shapes they take. © 2015 AIP Publishing LLC. [<http://dx.doi.org/10.1063/1.4932333>]

I. INTRODUCTION

The quest for doing selective chemistry at a particular site in a molecule by leaving the rest of the molecular backbone intact, or as it is, has been a much sought after goal for chemists over the years. With the use of light as a source of perturbation and in particular the invention and extensive use of lasers as a tool, the goal has been realized to a large extent. The traditional view of using thermal energy to control and direct a chemical process obviously is the more popular one but if the quest is for doing site selective chemistry or optimally controlling a chemical event, such a route is not the favoured one.

The use of laser pulses in doing selective chemistry is popular and both experimental and theoretical applications are impressive in number. Many theoretical studies have been performed through the years showing that how optimal control theory (OCT) is used to design the radiative field by which a chemical phenomena may be controlled.^{1–15} OCT provides the framework to optimize the laser pulse shape or the field parameters to achieve the desired goal. Different methods are demonstrated by several authors for the optimization of the external electromagnetic perturbation.^{16–22} Stochastic optimizers are also being reported to be used in some recent papers.^{23–27} There are also plenty of books and reviews, demonstrating the use of coherent control of quantum dynamics.^{28–35} Experimental studies on designing laser field are also reported.^{35–40}

Applications ranging from selective vibrational mode excitation in Morse potential systems and controlling the dissociation probability of a bond²⁶ or tuning the efficiency of tunnelling events²⁷ are reports worth looking into. A rather more appealing question to a practising chemist is whether a molecular system, which is multi-bonded, can be subjected to an appropriate time-dependent perturbation incorporating a laser pulse and suffer selective breaking of a particular bond leaving the others intact. This objective is immensely important, since a bond cleavage, which has been done selectively, opens up a reactive site in the molecular system, which can undergo further chemical transformation with the rest of the molecular framework remaining as it is.

There are impressive experimental works which focus on using shaped laser pulses to control a chemical event like opening a particular reacting channel *in lieu* of the other available ones. The work on photodissociation of dicarbonylchloro(η^5 -cyclopentadienyl)iron by using femtosecond laser control to produce different product ratios was carried out by the group of Gerber.⁴¹ There are other reports on experimental investigations carried out on chemical systems of diverse nature on laser pulse controlled chemical events.^{42–64} These references use the principle of coherent control. One must emphasize that photochemistry can be tuned or controlled by using techniques which are not dependent on coherence also. One possibility can be the use of excitations which are bond selective.^{65–78} However, one must recognise that this approach is practically feasible when the molecule under investigation has very low intra-molecular-vibrational redistribution (IVR). Another method is to excite the system to different excited states with

^{a)}Electronic mail: pinake@rediffmail.com

^{b)}Electronic mail: pcsa@iacs.res.in

the use of different wavelength as is the case with photodissociation of CH_2IBr .^{79–81}

Two triatomic systems which have found appreciable attention are the HOD^{25,82–86} and the $\text{O}^{16}\text{O}^{16}\text{O}^{18}$ ^{87–90} systems. Both have two dissociating channels ($\text{HOD} \rightarrow \text{H} + \text{OD}$ and $\text{D} + \text{OH}$; $\text{O}^{16}\text{O}^{16}\text{O}^{18} \rightarrow \text{O}^{18} + \text{O}^{16}\text{O}^{16}$ and $\text{O}^{16} + \text{O}^{16}\text{O}^{18}$). However, the two systems are inherently different in levels of complexity. For HOD system, the normal route followed is to initially excite the system in an excited vibrational eigenstate of the ground electronic state. In HOD, fortunately, the excited vibrational eigenstates are principally of a local mode type and the vibrational levels are predominantly of OH or OD type. Once the initial excitation using an IR pulse is done to a particular excited eigenstate, a follow up UV pulse is applied which takes the system to a totally repulsive excited electronic state and the system suffers dissociation mainly in the OH or OD channel dependent upon the initial vibrational excitation. Thus, an adequately designed hybrid IR and UV pulse can enhance the fluxes in the two channels appreciably.^{82,90} In our previous paper, we have been able to design proper polychromatic electric field which has been shown to perform better than a single standard analytical pulse.²⁵

The subject of the present study is the $\text{O}^{16}\text{O}^{16}\text{O}^{18}$ system. Authors in previous works⁹⁰ have explained the inherent complexity of the system with regards to selective bond breaking. As in HOD, the isotope substituted ozone molecule also has an excited electronic state from which it can dissociate. So, a similar strategy of initial vibrational excitation in the ground electronic state followed by a transition to the dissociative excited electronic state should work, if selective bond breaking is the sought after objective. However, in this system, IVR is dominant and this affects the initial excitation. Moreover the vibrational eigenstates are more of a normal mode rather than a local mode type. This makes it extremely difficult to prepare the system predominantly in the $\text{O}^{18} + \text{O}^{16}\text{O}^{16}$ or $\text{O}^{16} + \text{O}^{16}\text{O}^{18}$ channel⁹⁰ before the UV pulse is applied which breaks a particular bond. Authors in earlier reports have tried using a gaussian IR pulse for initial excitation followed by an UV pulse. It has been reported⁹⁰ that shorter is the UV pulse, greater is the branching ratio in the two channels. Since IVR is prominent, the other factor that must be kept in mind is that the UV pulse should act before the IR pulse has completely died away.

We in this report, would like to present a strategy, which is an extension of those already reported. Instead of using a single gaussian IR pulse, a hybrid pulse generated by combining gaussians with different half widths along with other pulse parameters will be the one that will be used. This pulse, in our opinion, directs the system with greater wavefunction amplitude along the $\text{O}^{18} + \text{O}^{16}\text{O}^{16}$ or $\text{O}^{16} + \text{O}^{16}\text{O}^{18}$ channel, as the case might be and the subsequent action of an UV would then generate fluxes which are greater in the two dissociating channels and hence a greater branching ratio. It is true that the coupling between the local modes is an inherent feature of the system and cannot be done away with, but the hybrid IR pulse should, even in this scenario, be able to direct the system to a greater extent along one of the modes.

Since our proposed and used strategy completely depends on the generation of the hybrid pulse, the question is how do we

go about it. We use a potent optimization technique, namely, Simulated Annealing (SA)⁹¹ to find the optimum pulse parameters in generating hybrid pulses. SA is a technique which uses stochastic principles in finding an optimum solution in a complicated search space. SA has been used very effectively in problems relating to both structural^{92–102} and dynamical aspect of chemistry.^{25–27} It has been shown in numerous applications that a stochastic optimization scheme is better suited to handle tough problems as opposed to deterministic methods. Deterministic methods more often than not suffer from premature convergence and fails to find out the best solution in a space comprising of multiple solutions differing in quality. SA has been used to generate optimum pulse parameters in some reports already existing.^{25–27} We in this present work would like to see how the optimized pulse parameters are better in generating fluxes of greater magnitude in the two channels as opposed to the unoptimized pulse.

Our strategy will be to generate a given pulse and then do the dynamics using the *ab initio*-fitted potential energy surface available for $\text{O}^{16}\text{O}^{16}\text{O}^{18}$.⁸⁹ The Lanczos scheme¹⁰³ will be used for the time propagation. The system will be described on a two dimensional grid. Once the fluxes in the channels are found out, we use SA to design a new pulse and calculate the next fluxes and hence the branching ratio. This process is carried out until a steady high branching ratio is achieved.

We discuss the theoretical framework in Sec. II, followed by a discussion on the results obtained.

II. METHODOLOGY

A. The Hamiltonian for the system

In O_3^{16} , the three lowest energy transitions corresponding to symmetric stretch, asymmetric stretch, and bending transitions are observed at around 1101 cm^{-1} , 1043 cm^{-1} , and 698 cm^{-1} , respectively. For isotopomer of O_3^{16} , the values are near to these quantities. As mentioned in a detailed study on vibrational energies of O_3 , upto dissociation threshold by Schinke *et al.*,¹⁰⁴ the lower energy states are of normal mode type and near the dissociation threshold, the states assume local mode character. Mixing between states are seen to occur for higher energy situations which can be probed by high quanta excitations. If a given state is labelled by three quantum numbers ν_1 , ν_2 , and ν_3 , where these represent excitation along symmetric stretch, bending, and asymmetric stretch, respectively, a given state can be represented as (ν_1, ν_2, ν_3) . For example, for a state with $\nu_1 + \nu_2 + \nu_3 = 5$, the (3,1,1) state is seen to be coupled with (0,0,5) or where $\nu_1 + \nu_2 + \nu_3 = 7$, the state (2,2,3) is coupled to (1,1,5). So, only when high quanta excitations are probed, does one need to consider mixing. In our study, we excite the system from (0,0,0) to (1,0,0) or (0,0,1) and since the fundamental bending frequency (700 cm^{-1}) is much less than the fundamental stretching frequencies (1050 cm^{-1} or 1100 cm^{-1}), we need not consider the mixing while studying the dynamics. However, it must again be reiterated that if high quanta excitations were needed, one must consider mixing of states.

The rotational motion of the system is also not considered since the frequency of rotational motion is even less than

the bending vibrational motion. So, the time scale in which the dynamics is studied guarantees the absence of rotational contribution. It needs to be further stressed that the molecule is assumed to be pre-oriented^{105–108} before action of the laser pulses in the subsequent dynamics. In the potential that is used for describing the O¹⁶O¹⁶O¹⁸ system, the rotational and bending motions are neglected, in the two degree of freedom potential being used. Moreover, for the excited state (ES) O¹⁶O¹⁶O¹⁸, the bending angle gets reduced by about 10°, but this reduction takes place only after 10 fs. So for the electronic excitation if a short UV pulse with width around 10 fs is used, we can still neglect the bending motion. If r_1 and r_2 represent the coordinates for the O¹⁶–O¹⁸ and O¹⁶–O¹⁶ and the corresponding conjugate momenta are P_1 and P_2 , the internal kinetic energy operator^{25,90} assumes the form

$$\hat{T} = \frac{\hat{P}_1^2}{2\mu_1} + \frac{\hat{P}_2^2}{2\mu_2} + \frac{\hat{P}_1\hat{P}_2}{m(^{16}\text{O})} \cos \theta, \quad (2.1)$$

with

$$\hat{P}_j = \frac{\hbar}{i} \frac{\partial}{\partial r_j}, \quad j = 1, 2,$$

and

$$\mu_1 = \frac{m(^{18}\text{O})m(^{16}\text{O})}{[m(^{18}\text{O}) + m(^{16}\text{O})]}, \quad \mu_2 = \frac{m(^{16}\text{O})m(^{16}\text{O})}{[m(^{16}\text{O}) + m(^{16}\text{O})]}.$$

In expression (2.1), the subscript “1” refers to O¹⁶–O¹⁸ and “2” refers to O¹⁶–O¹⁶. The angle θ is kept frozen at 116.8°, since we are not considering bending contributions as has already been described. However, we must admit that after the UV pulse has been applied, i.e., after 10 fs, there will be a switching of the bending by about 10°, and this might cause small changes in the results (which will be discussed in Sec. III) during the next 150 fs.

For interaction with the external radiation, the dipole moment surface is essential. For the electronic ground state (GS), the dipole moment vector has two components μ_x along the bisector of the two bonds and μ_y is along the perpendicular to the bisector.⁸⁸ We in Sec. II B will discuss in some detail, both the potential energy surface as well as the dipole moment function.

For evolving the system in time in the ground and excited states, the time-dependent Schrödinger equation is employed with the evolution of the ground and excited states being

$$i\hbar \frac{\partial}{\partial t} \begin{pmatrix} \Psi_g \\ \Psi_e \end{pmatrix} = \begin{pmatrix} \hat{H}_g + \hat{H}_{IR}(t) & \hat{H}_{uv}(t) \\ \hat{H}_{uv}(t) & \hat{H}_e \end{pmatrix} \begin{pmatrix} \Psi_g \\ \Psi_e \end{pmatrix}. \quad (2.2)$$

Now, Ψ_g and Ψ_e are the wavefunctions for the nuclear motion in the ground and the excited electronic states. \hat{H}_g and \hat{H}_e are the nuclear Hamiltonian for the two states. $\hat{H}_{IR}(t)$ captures the interaction of the molecule with the external IR radiation in ground electronic state and $\hat{H}_{UV}(t)$ is the term which couples the two states when the external UV field is switched on.

To start the time propagation, the starting eigenstates needs to be found out. So a field free calculation is done at $t = 0$, to get the Ψ_g wavefunction as well as the vibrational eigenvalues of the ground electronic state, using the two dimensional Fourier Grid Hamiltonian (FGH) method. Once the stationary states are obtained, the Schrödinger equation is solved to get $\Psi_g(t)$ and $\Psi_e(t)$ at various times. To get the effect of the kinetic energy operators on the wavefunction, the Fast Fourier Transformation (FFT) algorithm¹⁰⁹ is used and the time progression is done with the Lanczos scheme.¹⁰³ Since we work on a grid to represent the wavefunctions, it is done on both the directions r_1 and r_2 with bond lengths between $2a_0$ and $11a_0$. The total points on the grid used is 256 and the interpoint spacings are $\Delta r_1 = \Delta r_2 = 0.035a_0 \approx 0.0189 \text{ \AA}$. The external radiation (both IR and UV) couples with $\hat{\mu}_{IR}$ and $\hat{\mu}_{UV}$ (the dipole moment operators) to generate $\hat{H}_{IR}(t)$ and $\hat{H}_{UV}(t)$. $\hat{\mu}_{IR}$ couples with the external IR field $E_{IR}(t)$ (for vibrational excitation). $E_{IR}(t) = \sum_i S_{IR}^i(t)$, where $E_{IR}(t)$ is made up of a combination of gaussian IR pulse with associated frequencies and intensities ($S_{IR}^i(t)$). The $\hat{\mu}_{UV}(t)$ couples with the $E_{UV}(t)$, which comprises of a single Gaussian UV pulse. The pulse parameters are optimizable and effectively done using SA to maximize the dissociation along particular channels. Once the dynamics with a particular perturbation is complete, total fluxes along the two dissociation channels O¹⁸ + O¹⁶O¹⁶ ($J_{\text{O}^{18}+\text{O}^{16}\text{O}^{16}}$) and O¹⁶ + O¹⁶O¹⁸ ($J_{\text{O}^{16}+\text{O}^{16}\text{O}^{18}}$) are evaluated using the following expressions:²⁵

$$J_{\text{O}^{18}+\text{O}^{16}\text{O}^{16}} = \int_0^{r_2^d} \int_0^T [j_1(r_1 = r_1^d) + j_2(r_1 = r_1^d)] dr_2 dt, \quad (2.3)$$

with

$$j_1 = \frac{\hbar}{2i} \frac{1}{\mu_1} \left(\Psi^* \frac{\partial \Psi}{\partial r_1} - \Psi \frac{\partial \Psi^*}{\partial r_1} \right), \quad j_2 = \frac{\hbar}{2i} \frac{\cos \theta}{m(^{16}\text{O})} \left(\Psi^* \frac{\partial \Psi}{\partial r_2} - \Psi \frac{\partial \Psi^*}{\partial r_2} \right),$$

and

$$J_{\text{O}^{16}+\text{O}^{16}\text{O}^{18}} = \int_0^{r_1^d} \int_0^T [j_2(r_2 = r_2^d) + j_1(r_2 = r_2^d)] dr_1 dt, \quad (2.4)$$

with

$$j_1 = \frac{\hbar}{2i} \frac{\cos \theta}{m(^{16}\text{O})} \left(\Psi^* \frac{\partial \Psi}{\partial r_1} - \Psi \frac{\partial \Psi^*}{\partial r_1} \right), \quad j_2 = \frac{\hbar}{2i} \frac{1}{\mu_2} \left(\Psi^* \frac{\partial \Psi}{\partial r_2} - \Psi \frac{\partial \Psi^*}{\partial r_2} \right),$$

where μ_i is the corresponding reduced mass and r_i^d represents a grid point for the asymptotic region of the particular i th channel. r_1^d and r_2^d are both kept at $8.5a_0$. The integrands consists of a summation of two operators, the second representing the kinetic coupling between the two $O^{16}-O^{18}$ and $O^{16}-O^{16}$ modes. We take the upper limit of integration (T) to be 320 fs.

B. Potential energy surface and dipole moment function

The potential energy surface constructed for O_3 , as used by other workers, considers four surfaces labelled X , A , B , and R .⁸⁷ For studying the dissociating dynamics of ozone, the ground state considered is X and the excited state as B . We use the analytically fitted potential energy surfaces for X and B states as used in the paper by Morokuma.⁸⁹ The parameters of the fitted surface can be found in this paper. The B state shows the existence of a potential well, which earlier works had failed to predict. The success of this potential is that it is able to show the relative positions as well as intensities of the Huggins band with good accuracy when compared with experiment (within 100 cm^{-1}).

We have also used the analytic dipole moment function from the same paper by Morokuma.⁸⁹ In this form, the components μ_x are the molecular plane for the $X-B$ transition and also the one located perpendicular to the angle bisector (μ_y) is represented as linear combinations of terms upto fourth order in magnitude. The magnitude of terms appearing in the expressions for dipole moments can again be found in this paper.

To eliminate the effect of unphysical reflection from the edges, an absorbing potential placed at the asymptotic cut is used. The absorbing potential is linearly dependent on coordinate and this term is present as an exponent in the overall decaying exponential function.

C. Representation of the pulses

As discussed in Sec. II A, we use a combination of Gaussian IR pulse with associated parameters to model the IR radiation field ($E_{IR}(t)$). The UV radiation field ($E_{UV}(t)$) is a single Gaussian UV pulse,

$$E_{IR}(t) = \sum_i S_{IR}^i(t), \quad (2.5)$$

where

$$S_{IR}^i = \epsilon_0^i \cos(\omega_i t) \exp[-\gamma_i(t - t_0)^2], \quad (2.6)$$

and the full width at half maxima,

$$\text{FWHM} = \sqrt{\frac{4\ln 2}{\gamma}}, \quad (2.7)$$

where ϵ_0^i is the intensity, ω_i the frequency, and γ_i and t_0^i are the parameters for the i th Gaussian IR pulse. A total of eight such individual pulses were combined to generate the optimum pulse shape. ω_i , ϵ_0^i , and γ_i were optimized using SA and fed into the time propagation to check whether greater value of flux along a given channel is obtained or not. A check on the

individual values of ϵ_0^i 's was kept so that the value of field strength did not exceed the value which causes ionization of electron in hydrogen atom.

The UV pulse perturbation $E_{UV}(t)$ is used as

$$E_{UV}(t) = \epsilon_0^{UV} \cos(\omega_{UV} t) \exp - [\gamma_{UV}(t - t_0^{UV})^2]. \quad (2.8)$$

The parameters ϵ_0^{UV} (intensity), ω_{UV} (frequency), and the gaussian parameters γ_{UV} and t_0^{UV} were also optimized using SA and fed into time propagation scheme.

D. Optimizing the pulse parameters using SA

The parameters described in Sec. II C were changed randomly using stipulated random maximum allowable variation by using SA. SA is a stochastic optimizer which draws its working principle mimicking the metallurgical process of annealing⁹¹ and uses Metropolis sampling scheme to set criteria for selecting a given set of parameters. The working principles of SA is described in detail in earlier publications by our group.⁹⁹⁻¹⁰² Since SA is an optimizer, it will work only if a functional (popularly called cost functional) is written down and the goal of the search would be to minimize the cost functional. Since our objective is to maximize the integrated flux along a given direction, we choose two functionals $\text{cost}^{O^{18}+O^{16}O^{16}}$ and $\text{cost}^{O^{16}+O^{16}O^{18}}$ for $O^{18} + O^{16}O^{16}$ and $O^{16} + O^{16}O^{18}$ channels, respectively. $\text{cost}^{O^{18}+O^{16}O^{16}}$ and $\text{cost}^{O^{16}+O^{16}O^{18}}$ are defined as

$$\text{cost}^{O^{18}+O^{16}O^{16}} = [1 - (J_{O^{18}+O^{16}O^{16}} - J_{O^{16}+O^{16}O^{18}})]^2 \quad (2.9)$$

and

$$\text{cost}^{O^{16}+O^{16}O^{18}} = [1 - (J_{O^{16}+O^{16}O^{18}} - J_{O^{18}+O^{16}O^{16}})]^2 \quad (2.10)$$

where $J_{O^{18}+O^{16}O^{16}}$ and $J_{O^{16}+O^{16}O^{18}}$ are given in Equations (2.3) and (2.4). We use the flux values after total time propagation to get the magnitudes of the cost functions.

Having defined the cost functions along the two channels in Equations (2.9) and (2.9), it must be stated that this particular choice is by no means the only one available. One could just write a cost function containing the appropriate flux and set the goal of optimization as the maximization of that flux. However, the cost functions we are using does two jobs. First, it tries to maximize the flux along the observed channel and also tries to reduce the flux in the counter channel. It is clear that as the difference between say $J_{O^{18}+O^{16}O^{16}}$ and $J_{O^{16}+O^{16}O^{18}}$ increases with $J_{O^{18}+O^{16}O^{16}} > J_{O^{16}+O^{16}O^{18}}$, $\text{cost}^{O^{18}+O^{16}O^{16}}$ decreases. So minimizing $\text{cost}^{O^{18}+O^{16}O^{16}}$ will direct the system to dissociate more along $O^{18} + O^{16}O^{16}$ channel and vice-versa. So our cost function guarantees the obtainment of a good flux ratio in the end. One thing that must be mentioned here is that the integrated flux calculated with Equations (2.3) and (2.4) is unitless quantity.

Now, we have to optimize the pulse parameters ω_i , ϵ_0^i , γ_i , ϵ_0^{UV} , ω_{UV} , γ_{UV} , and t_0^{UV} in order to minimize the cost function and we will be able to direct the dissociation along a particular mode. To conclude this section, one must also add an important criterion that must be kept in mind for firing the UV pulse. As the system oscillates along the r_1 and r_2 directions in the excited vibrational state of the ground electronic state, the UV

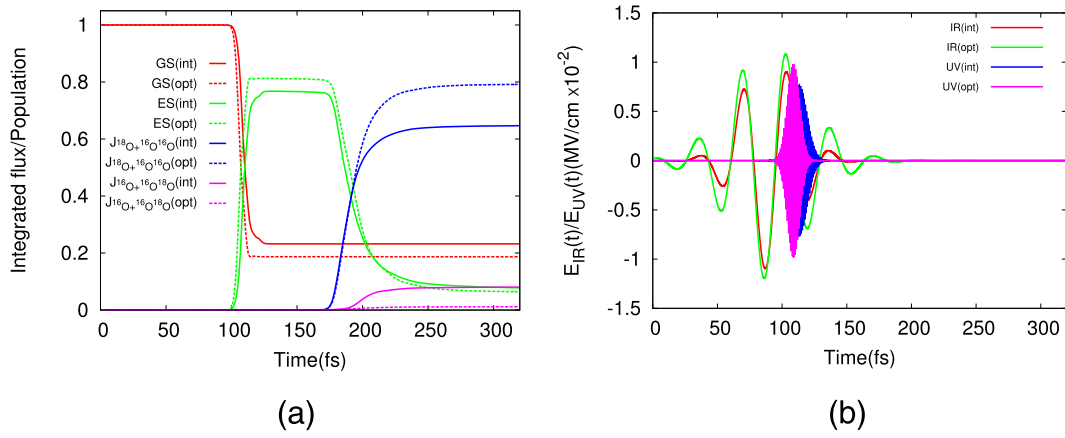


FIG. 1. The plots are obtained while optimizing the flux along $J_{O^{18}+O^{16}O^{16}}$ mode. (a) The initial and optimized profile for the population of both ground (GS) and excited (ES) electronic states and also the fluxes along $J_{O^{18}+O^{16}O^{16}}$ and $J_{O^{16}+O^{16}O^{18}}$ modes with time. (b) The initial and optimized pulse with time.

must be fired at a time the system is more localized along r_1 or r_2 if we are aiming to cleave a $O^{16}-O^{18}$ or $O^{16}-O^{16}$ bond.

Having defined our cost functions, which will drive the optimization towards its goal, it must be mentioned that one can use different forms of cost functions to study the problem. Since it is important to keep the used field strength below a permissible low value, one can add a term which penalizes the field strength.

III. RESULTS AND DISCUSSION

Having underlined the concept and working principles of optimal control in the selective bond breaking of $O^{16}O^{16}O^{18}$, we present the objectives achieved by the use of the optimized IR and UV pulses using SA. In all our analysis, we will stress on the point as to how the optimized pulse gives us better fluxes and branching ratios along a particular mode vis-a-vis the unoptimized one.

We first concentrate on the $O^{18} + O^{16}O^{16}$ channel (which is for dissociation of the $O^{16}-O^{18}$ bond). Fig. 1(a) shows both the integrated flux and the population of the GS as well as ES. GS(int)/ES(int) and GS(opt)/ES(opt) depict the variations in population with the initial pulse (int) and the optimized pulse (opt) with time. What is noticeable is the relatively rapid fall of the ground state population and the rapid rise of the excited state populations with the optimized pulse. The population in all the situations shows a saturation behaviour in the large time limit. However, to see whether we are getting better optimal control or not, the variation of integrated fluxes for both the channels $J_{O^{18}+O^{16}O^{16}}$ and $J_{O^{16}+O^{16}O^{18}}$ with optimized (opt) and unoptimized initial (int) should be better parameters to study. Since, we are concentrating on the $O^{18} + O^{16}O^{16}$ channel, $J_{O^{18}+O^{16}O^{16}}(\text{opt})$ shows a final value of over 79% (79.3%) while $J_{O^{18}+O^{16}O^{16}}(\text{int})$ is 64.67%. $J_{O^{16}+O^{16}O^{18}}(\text{int})$ and $J_{O^{16}+O^{16}O^{18}}(\text{opt})$ on the other hand should be as low as possible to get better branching ratios. $J_{O^{16}+O^{16}O^{18}}(\text{opt})$ is seen to be less than $J_{O^{16}+O^{16}O^{18}}(\text{int})$. So we get a better difference

TABLE I. IR and UV hybrid pulse parameters for both initial and optimized states for $O^{18} + O^{16}O^{16}$ channel.

Pulse number	IR pulse parameter						UV pulse parameter							
	ϵ_{IR}^0 (a.u.)		ω_{IR} (cm^{-1})		FWHM _{IR} (fs)		ϵ_{UV}^0 (a.u.)		ω_{UV} (cm^{-1})		FWHM _{UV} (fs)		t_{UV}^0 (fs)	
	in	opt	int	opt	int	opt	int	opt	int	opt	int	opt	int	opt
1	0.0060	0.005 84	942.0	969.82	47.0	44.74								
2	0.0065	0.006 11	947.0	959.96	48.0	104.70								
3	0.0070	0.008 71	952.0	976.24	49.0	60.51								
4	0.0075	0.007 93	957.0	963.50	50.0	78.45								
5	0.0080	0.008 33	962.0	977.15	51.0	55.07								
6	0.0085	0.011 46	967.0	969.13	52.0	63.53								
7	0.0090	0.008 52	972.0	968.48	53.0	83.35								
8	0.0095	0.009 82	977.0	965.96	54.0	75.56								
Single pulse	0.015	0.0192	35 619.0	34 131.32	15.0	11.26	113.0	108.81						

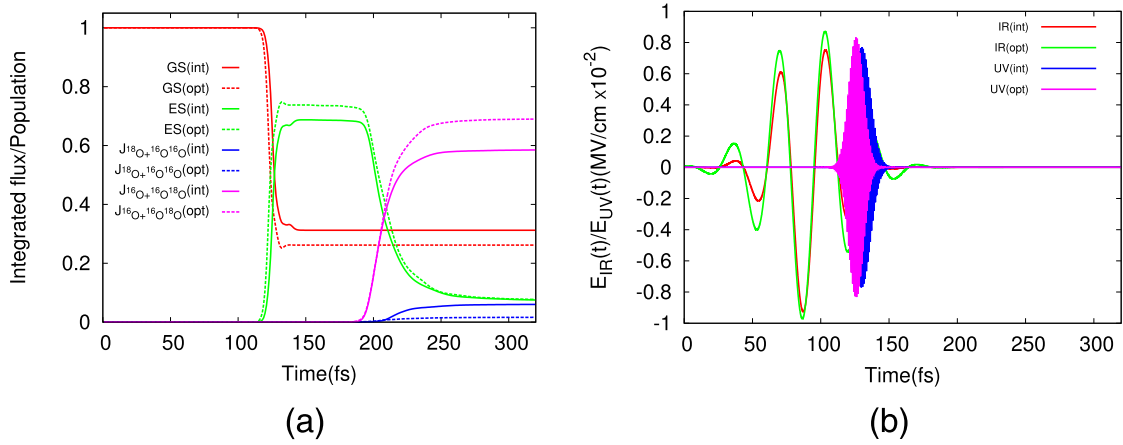


FIG. 2. The plots are obtained while optimizing the **flux along $J_{O^{16}_+O^{16}O^{18}}$ mode**. (a) The initial and optimized profiles for the population of both ground (GS) and excited (ES) electronic state and also the fluxes along $J_{O^{18}_+O^{16}O^{16}}$ and $J_{O^{16}_+O^{16}O^{18}}$ modes with time. (b) The initial and optimized pulses with time.

in integrated fluxes for the two channels with the optimized pulse ($J_{O^{18}_+O^{16}O^{16}}(\text{opt}) - J_{O^{16}_+O^{16}O^{18}}(\text{opt})$), which is greater than ($J_{O^{18}_+O^{16}O^{16}}(\text{int}) - J_{O^{16}_+O^{16}O^{18}}(\text{int})$). Fig. 1(b) depicts both the initial IR (IR(int)) and optimized IR (IR(opt)) and initial UV (UV(int)) and optimized UV (UV(opt)) pulse shapes. In both cases, it is observed that the final optimal IR and UV pulses have changed from the initial starting pulses. It is worth noting the increase in the maximum pulse amplitude for both the IR and UV optimized pulses. The UV(opt) pulse is also seen to be shorter in width as compared to the UV(int). However, it needs to be mentioned that the initial pulses in all the situations have been chosen as combination of gaussians and hence they are learned guesses which on optimization have been refined further. This is expected as a shorter UV pulse is expected to give better branching ratio for the system being studied.⁹⁰ However, we must stress on the point that our high branching ratio has not been obtained by merely shortening the UV pulse which is a possibility.⁹⁰ Our results stems from the optimi-

zation of both the IR and UV radiations. Table I shows the associated pulse parameters for both IR and UV (initial and final) while following the dissociation of the $O^{18} + O^{16}O^{16}$ channel.

We now turn our attention to a similar plot for dissociating the $O^{16} + O^{16}O^{18}$ channel ($O^{16} + O^{16}O^{18}$). Fig. 2(a) shows the variations of populations for ground and excited states as well as the variation of the integrated fluxes $J_{O^{16}_+O^{16}O^{18}}$ and $J_{O^{18}_+O^{16}O^{16}}$ with both initial (int) and optimized (opt) pulses. The variations are in a similar line with the earlier situation with the optimum pulses being better in starting the fall of the ground state and rise of the excited state populations at relative faster rates. As we are following the $O^{16} + O^{16}O^{18}$ channel, we notice a larger final integrated flux value $J_{O^{16}_+O^{16}O^{18}}$. With $J_{O^{16}_+O^{16}O^{18}}(\text{opt})$, it is about 69.15% and for the initial pulse, $J_{O^{16}_+O^{16}O^{18}}(\text{int})$ is 58.94%. The other mode ($^{16}O - ^{18}O$) as expected shows lower values of $J_{O^{18}_+O^{16}O^{16}}(\text{opt})$ and $J_{O^{18}_+O^{16}O^{16}}(\text{int})$. $J_{O^{18}_+O^{16}O^{16}}(\text{opt})$ (1.71%) is also lower than

TABLE II. IR and UV hybrid pulse parameters for both initial and optimized state for $O^{16} + O^{16}O^{18}$ channel.

IR pulse parameter								
Pulse number	ϵ_{IR}^0 (a.u.)		ω_{IR} (cm ⁻¹)		FWHM _{IR} (fs)			
	int	opt	int	opt	int	opt		
1	0.0040	0.003 41	942.0	974.98	47.0	73.26		
2	0.0060	0.007 08	947.0	973.76	48.0	63.14		
3	0.0080	0.009 12	952.0	984.521	49.0	65.30		
4	0.0100	0.008 96	957.0	971.10	50.0	64.12		
5	0.0090	0.008 80	962.0	962.57	51.0	72.58		
6	0.0070	0.005 85	967.0	965.41	52.0	79.30		
7	0.0050	0.005 84	972.0	961.50	53.0	61.13		
8	0.0030	0.002 79	977.0	973.63	54.0	56.32		
UV pulse parameter								
Pulse number	ϵ_{UV}^0 (a.u.)		ω_{UV} (cm ⁻¹)		FWHM _{UV} (fs)		t_{UV}^0 (fs)	
	int	opt	int	opt	int	opt	int	opt
Single pulse	0.015	0.0161	35 619.0	34 744.16	15.0	12.75	130.0	125.32

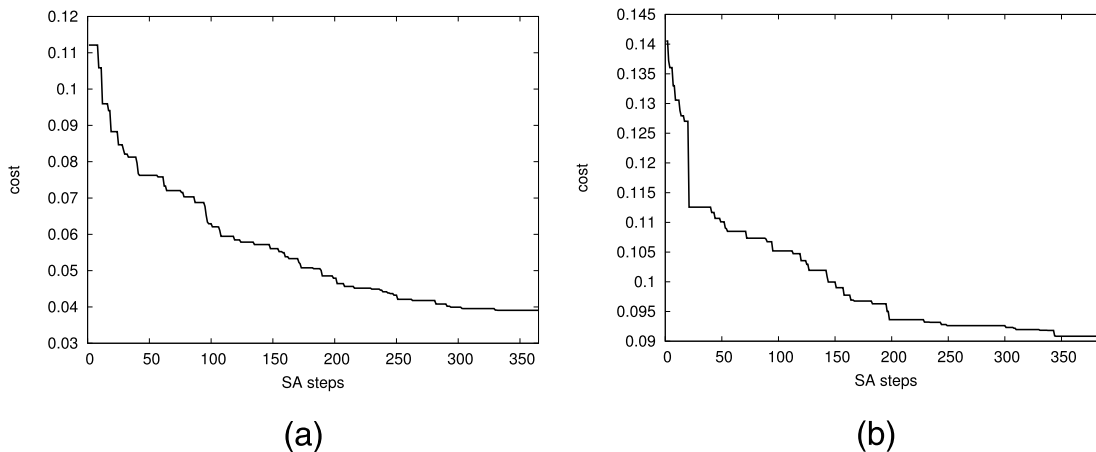


FIG. 3. (a) Cost profile with SA steps while optimizing the flux along $J_{O^{18}+O^{16}O^{16}}$ mode. (b) Cost profile with SA steps while optimizing the flux along $J_{O^{16}+O^{16}O^{18}}$ mode.

$J_{O^{18}+O^{16}O^{16}}(\text{int})$ (6.02%). This gives a relatively large value for the differences in the fluxes in the two modes with the optimized one [$(J_{O^{18}+O^{16}O^{16}}(\text{opt}) - J_{O^{16}+O^{16}O^{18}}(\text{opt})) > (J_{O^{18}+O^{16}O^{16}}(\text{int}) - J_{O^{16}+O^{16}O^{18}}(\text{int}))$]. To follow the nature of the pulse which has been able to achieve this better flux difference, we depict the optimized and the initial pulses for both IR and UV in Fig. 2(b). The IR(opt) has changed from the IR(int) with greater maximum peak amplitude. The UV(opt) shows as similar behaviour (as seen in the $O^{18} + O^{16}O^{16}$ channel) as compared to UV(int) and has a shorter width as expected. Table II lists all the associated pulse parameters for both the IR and UV while trying to selectively dissociate this mode. It must be mentioned here that the peak intensity values of the combined IR + UV laser pulses are 26.94 TW/cm² along $O^{18} + O^{16}O^{16}$ mode and 6.29 TW/cm² along $O^{16} + O^{16}O^{18}$ mode.

Since our idea has centred around optimizing the pulse with SA, we show in Figs. 3(a) and 3(b) a representation of how this has been achieved. In both the cases, we plot the variation in the cost functions (defined earlier, Eqs. (2.9) and (2.9)) with the number of SA steps. For both the cases, a steady low cost function value is achieved at around 350 steps.

Now, we turn our attention to the contour plots for the wavefunctions during the entire dynamics process. Fig. 4 show snapshots of contours of population with time in the ground state along the $r_{O^{16}-O^{18}}$ and $r_{O^{16}-O^{16}}$, where UV pulse has not been fired. This was when the stress was on dissociating the $O^{16}-O^{18}$ bond (i.e., $J_{O^{18}+O^{16}O^{16}}$ channel). Column (a) of Fig. 4 is with unoptimized IR pulse and column (b) of the same figure depict the scenario with optimized IR pulse. The contours for 107 fs, 115 fs give successively higher disposition or concentration of the system along the $O^{18} + O^{16}O^{16}$ channel, whereas at 130 fs, concentration increases along $O^{16} + O^{16}O^{18}$ channel. It is clear from these snapshots that the ground state population oscillates between the two modes. Thus, UV pulse should be fired at that particular point of time when the ground state population is relatively more on the targeted channel than the other channel. For aiming to optimize flux at $O^{18} + O^{16}O^{16}$ mode, we thus set the UV pulse maximum at 113 fs as the initial value and for $O^{16} + O^{16}O^{18}$ channel, it is set at 130 fs initially (see Tables I and II). Now, what is more noticeable is the relatively higher

disposition on $O^{18} + O^{16}O^{16}$ channel with optimized pulses (Fig. 4(b)) as compared to the unoptimized one (Fig. 4(a)). This is crucial since a larger orientation of the system along $O^{18} + O^{16}O^{16}$ mode in the ground state will ultimately pave the way for a higher integrated flux for dissociation when the UV is fired.

For dissociating the $O^{16} + O^{16}O^{18}$ channel, similar contour evolution in the ground state only (without firing UV) with initial and optimized IR pulses is shown in Fig. 5. Fig. 5(a) is with the initial pulse and Fig. 5(b) is for the optimized one. Here also we notice that relatively higher build up with the optimized IR pulse (Fig. 5(b)) as compared to the unoptimized one (Fig. 5(a)).

The contour disposition along the two dissociating channels with IR pulses only gives us an idea that the system is more prepared to be dissociated fully along a particular mode. However to established the point categorically, we need to look at what happens to the contours when UV pulses are fired, both with unoptimized (initial) and optimized one and along both channels. To this end, we first look at the scenario for breaking $O^{16}-O^{18}$ bond. Figs. 6(a) and 6(b) show the contour evolutions of the population at excited state with time with the unoptimized and optimized IR and UV hybrid pulses. If we look at the plots at larger times (130 fs and 150 fs), we observe noticeable large orientation along the $r_{O^{16}-O^{18}}$ compared the $r_{O^{16}-O^{16}}$ bond with the optimized hybrid pulse (Fig. 6(b)) than the unoptimized (Fig. 6(a)) one. The two snapshots at 150 fs are a definite indication of the optimizable pulse being considerably better suited to selective bond breaking. Fig. 7 is in a similar vein, with the objective now being to follow the $O^{16} + O^{16}O^{18}$ channel. Again the relative large build up of the system along $r_{O^{16}-O^{16}}$ bond and depletion along the $r_{O^{16}-O^{18}}$ is noticeable. This is even more glaring at later time (150 fs) with the optimized hybrid pulse (Fig. 7(b)) than the unoptimized (Fig. 7(a)) hybrid field.

To summarize our result in a nutshell, we depict the evaluated integrated flux values and the relevant branching ratios in Table III. We again stress on the point that an optimized pulse perturbation is more suited to achieving greater optimal control in selective bond breaking dynamics as opposed to an unoptimized pulse shape. The ratio of the integrated fluxes

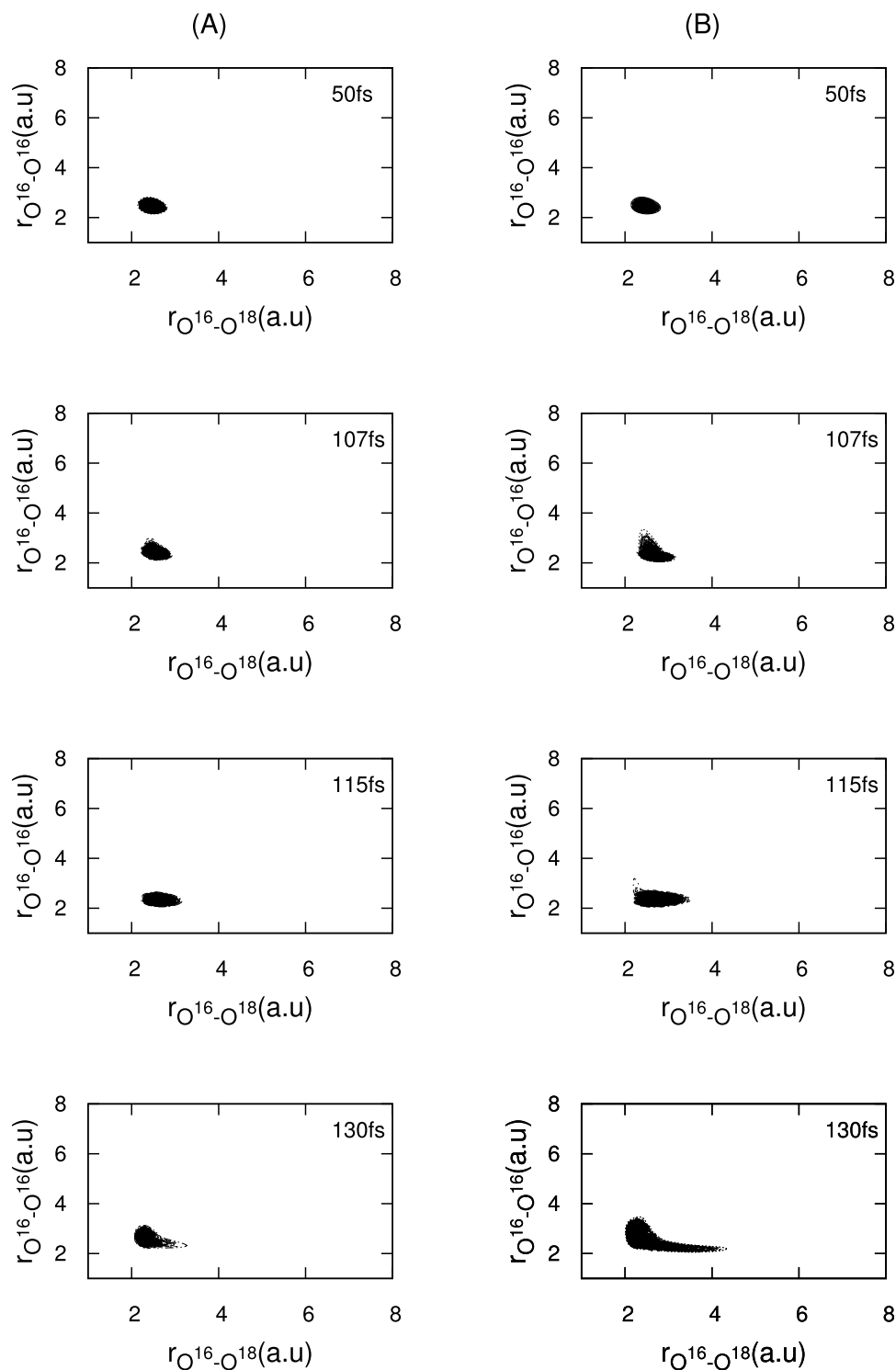


FIG. 4. Snapshot of contours of population in ground state along $r_{O^{16}_O^{18}}$ and $r_{O^{16}_O^{16}}$ at 50 fs, 107 fs, 115 fs, and 130 fs generated with the application of **IR pulse (UV pulse is not fired to generate these plots), while optimization is performed for $J_{O^{18}_+O^{16}_O^{16}}$ mode.** (a) and (b) columns are obtained with initial and optimized pulse parameter, respectively.

are two to three times higher with the optimized pulses than with the unoptimized ones. Having obtained our results with optimized pulses, it is now logical to observe what happens if a monochromatic field is used instead of a linear combination with different frequencies. This examination is initiated by the values of the optimized frequencies in the linearly combined field. It is indeed true that the range of frequencies is a narrow one (Tables I and II). The parameters of the single IR and UV hybrid pulse for the two channels are reported in Table IV for both unoptimized and optimized one. In Table V, we present the individual fluxes in the two channels as well as the ratios

obtained with a monochromatic field. For the optimization along $O^{16} + O^{16}O^{18}$, $J_{O^{16}_+O^{16}O^{18}}$ has a value of 67.62% while the other channel shows a value 4.25%. If we examine the results for the linearly combined field (Table III), the corresponding values are 69.15% and 1.71%. The ratio of the fluxes is also better for the polychromatic field (40.44), while it is 15.91 for the single pulse. When the observed channel is the $O^{18} + O^{16}O^{16}$, the performance is on a similar line. The flux values are 79.3% (polychromatic with six components) and 75.98% (single pulse). The ratios of the two channels show remarkable improvement (74.11) for polychromatic than the

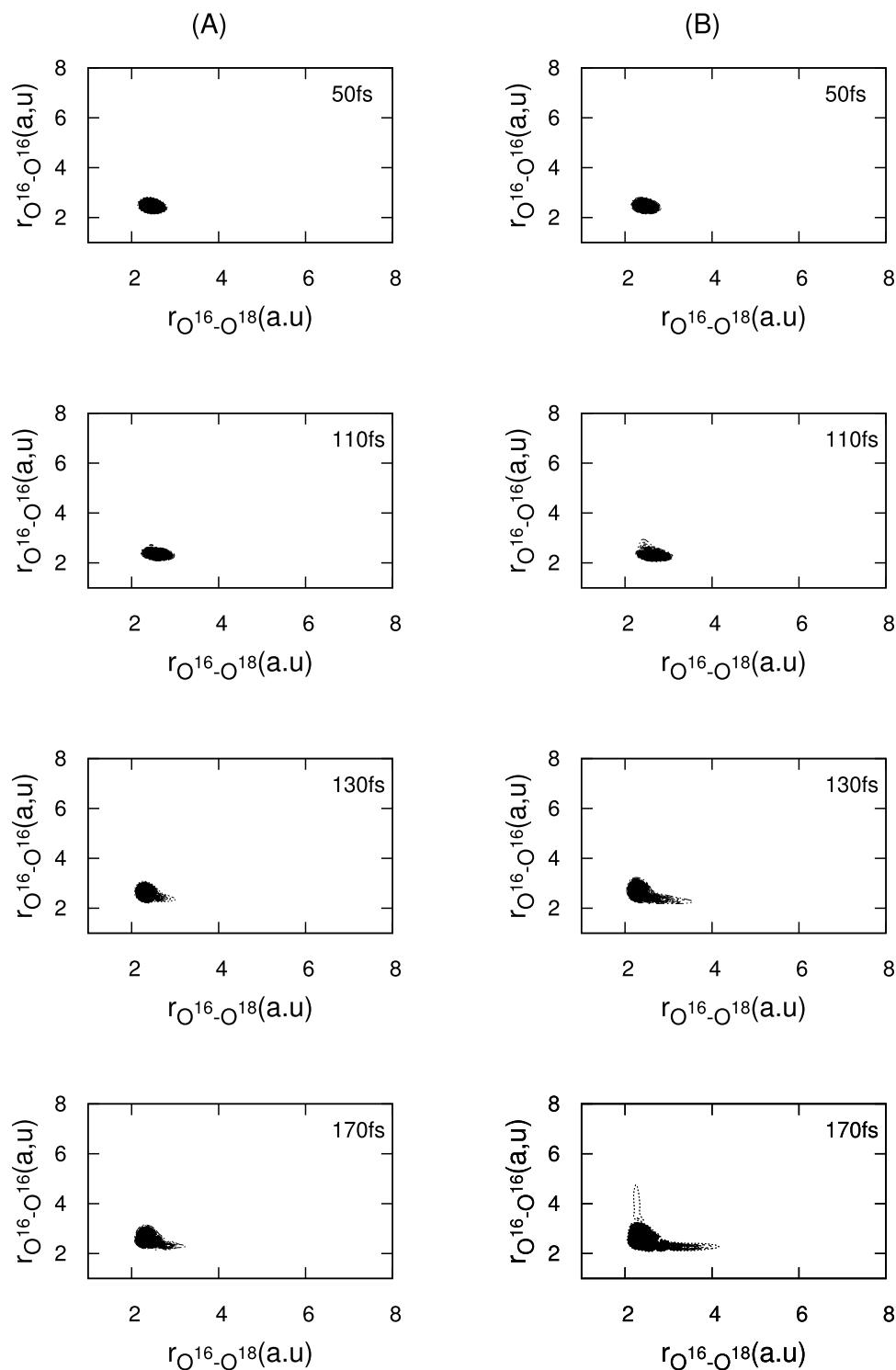


FIG. 5. Snapshot of contours of population in ground state along $r_{O^{16}-O^{18}}$ and $r_{O^{16}-O^{16}}$ at 50 fs, 110 fs, 130 fs, and 170 fs generated with the application of **IR pulse (UV pulse is not fired to generate these plots), while optimization is performed for $J_{O^{16},+O^{16}O^{18}}$ mode.** (a) and (b) columns are obtained with initial and optimized pulse parameter, respectively.

single pulse (21.70). This also establishes an important fact, that the polychromatic field can also reduce the dissociation to an appreciable extent in the channel not under observation better than the single pulse situation. To further study this point we have also tried calculations with a bichromatic situation and also a field which is created with combining four components. These results are also presented in Table V. While the bichromatic situation shows little improvement compared to the monochromatic one, the four component pulse is somewhat more successful with an increase in flux along one of the channels to 77.17% while the corresponding value for

the six component pulse is around 79%. It is worth noting that though in the polychromatic pulse the frequencies are within a narrow range, the polychromatic pulse is more selective in increasing the flux along a specified target channel than the monochromatic one. The results are testimony to this fact.

Having presented our results, one logical question can arise. Since our effort in finding a solution strongly depends on the potency of the optimizer used, it should be made to face a stronger test. If we start from a completely wrong channel, i.e., from a set of pulse parameters which gives a very small

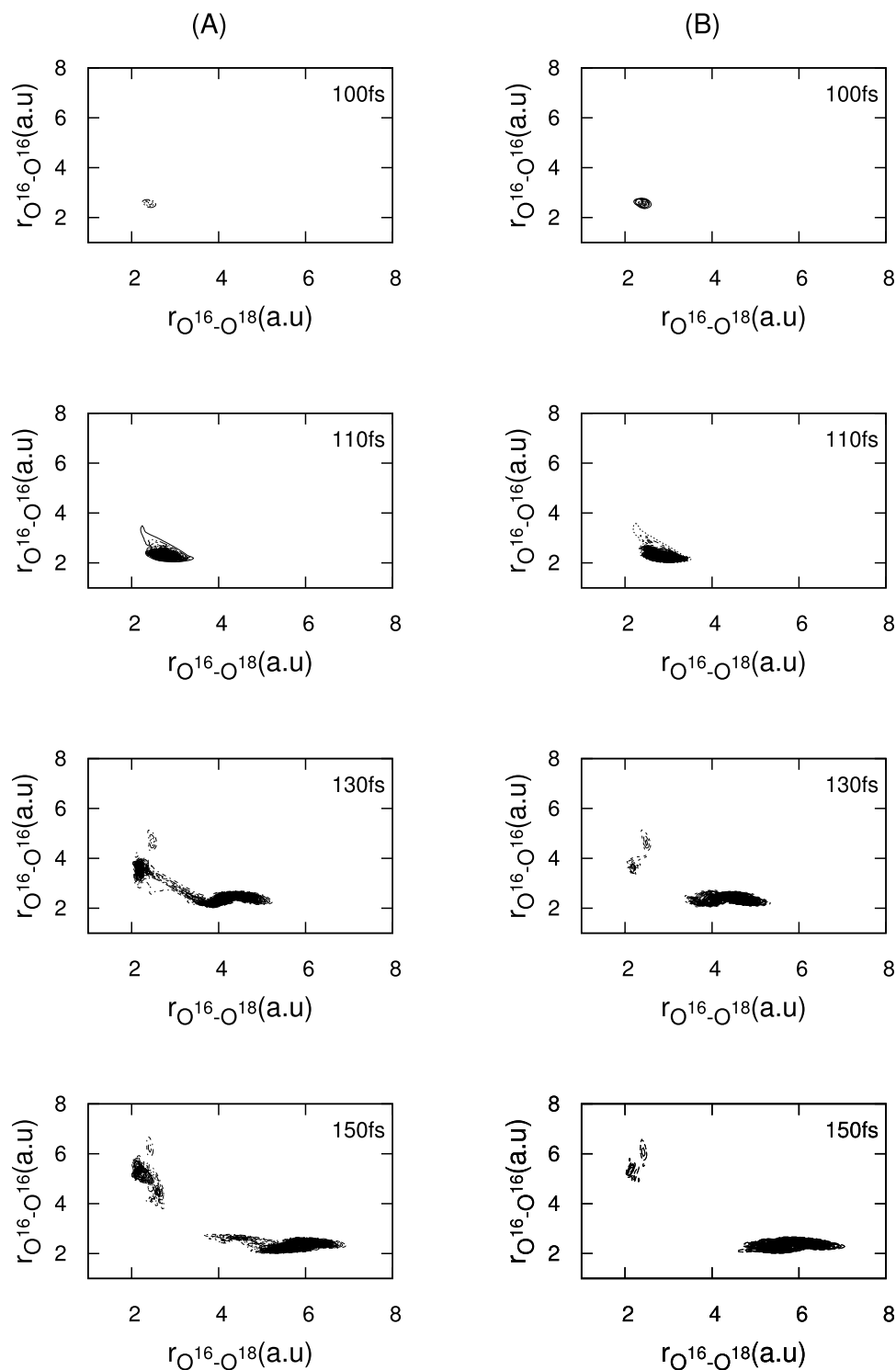


FIG. 6. Snapshot of contours of population in excited state along $r_{O^{16}-O^{18}}$ and $r_{O^{16}-O^{16}}$ at 100 fs, 110 fs, 130 fs, and 150 fs generated with the application of **hybrid pulse (IR and UV)**, while **optimization is performed for $J_{O^{18}+O^{16}O^{16}}$ mode**. (a) and (b) columns are obtained with initial and optimized pulse parameter, respectively.

value of flux in the given target channel under observation, can the optimizer still find out a pulse which ultimately leads to an appreciable flux? This has been studied and the results are presented in Table VI. If the target channel is the $O^{18} + O^{16}O^{16}$ one, an initial flux in this channel which starts at 6.02% finally gets increased to 77.68% at the end of the optimization procedure. For the $O^{16} + O^{16}O^{18}$ channel, the change is from 8.03% (initial) to 69.48% (final). So, we can conclude that the optimization procedure used by us can converge to a solution even when the procedure starts from a space which is far away from the solution.

If we look at the results of Tables III and VI, we see that the results show some deviation. For the dissociation to $O^{18} + O^{16}O^{16}$, the values are 79.30% and 77.68% (starts from wrong channel) while for the $O^{16} + O^{16}O^{18}$ dissociation, they are more closer with the values 69.15% and 69.48%. The small differences are due to the slight difference in the final optimized parameter values for the two SA simulations. These small differences can be farther reduced by doing the simulation for more number of steps but sometimes they remain as a stochastic search procedure can produce different solution in two different running schedules.

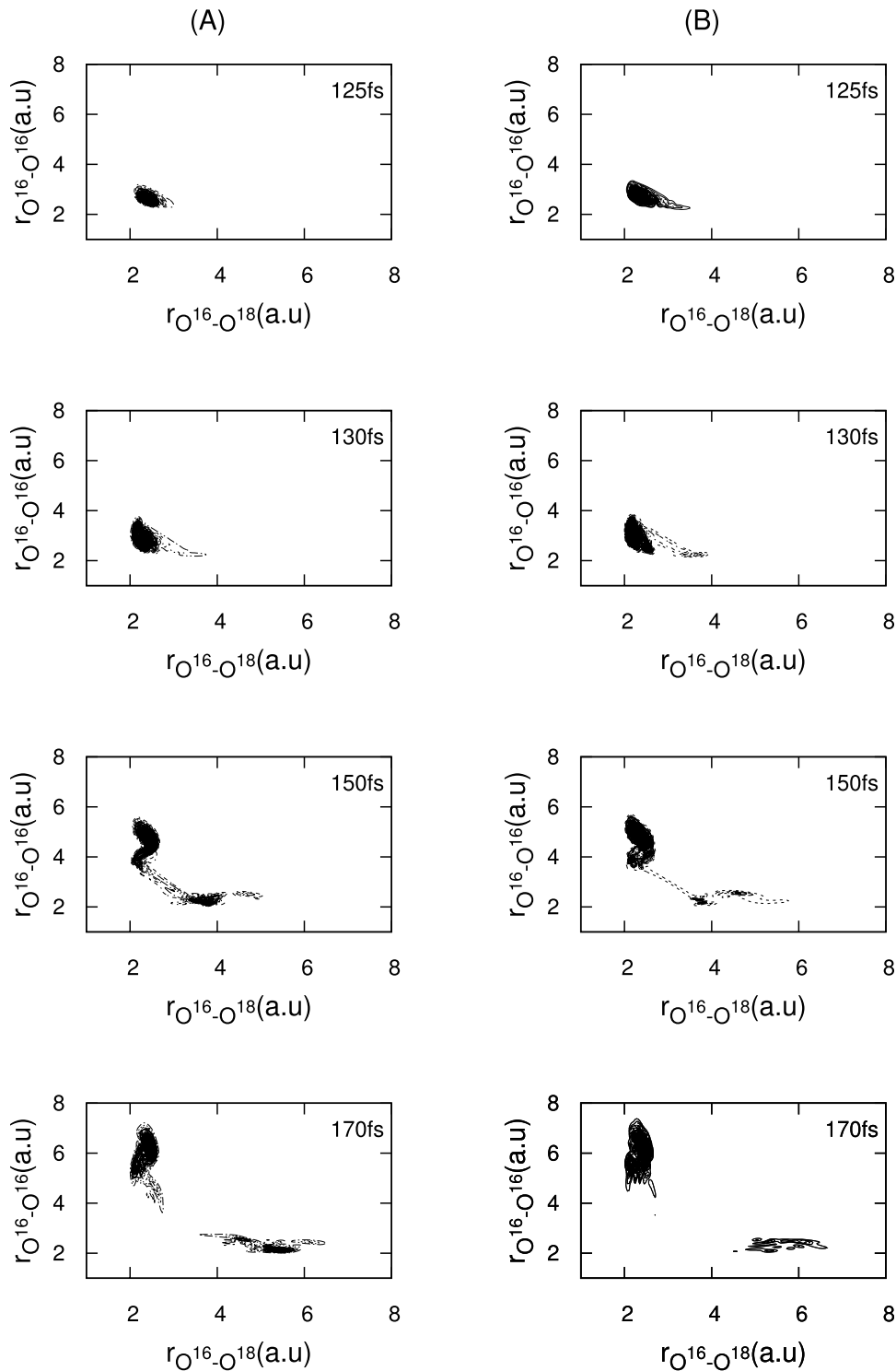


FIG. 7. Snapshot of contours of population in excited state along $r_{O^{16}-O^{18}}$ and $r_{O^{16}-O^{16}}$ at 123 fs, 130 fs, 150 fs, and 170 fs generated with the application of **hybrid pulse (IR and UV), while optimization is performed for $J_{O^{16}+O^{16}O^{18}}$ mode.** (a) and (b) columns are obtained with initial and optimized pulse parameter, respectively.

TABLE III. The initial and optimized fluxes and branching ratios for both $O^{18}+O^{16}O^{16}$ channel and $O^{16}+O^{16}O^{18}$ channel for **polychromatic electromagnetic field of eight components of light.**

Optimization along $O^{18}+O^{16}O^{16}$ channel			Optimization along $O^{16}+O^{16}O^{18}$ channel		
$J_{O^{18}+O^{16}O^{16}}$	int	64.67%	$J_{O^{18}+O^{16}O^{16}}$	int	6.02%
	opt	79.30%		opt	1.71%
$J_{O^{16}+O^{16}O^{18}}$	int	8.03%	$J_{O^{16}+O^{16}O^{18}}$	int	58.94%
	opt	1.07%		opt	69.15%
$J_{O^{18}+O^{16}O^{16}}/J_{O^{16}+O^{16}O^{18}}$	int	8.05	$J_{O^{16}+O^{16}O^{18}}/J_{O^{18}+O^{16}O^{16}}$	int	9.79
	opt	74.11		opt	40.44

TABLE IV. Single IR and UV hybrid pulse parameters for both initial and optimized state for both channels.

Optimization along O ¹⁸ +O ¹⁶ O ¹⁶ channel								
IR pulse parameter	C_{IR}		E_{IR}^0 (a.u.)		ω_{IR} (cm ⁻¹)		FWHM _{IR} (fs)	
	int	opt	int	opt	int	opt	int	opt
	1.0	1.0	0.015	0.0242	957.0	956.64	50.0	60.25
UV pulse parameter	E_{UV}^0 (a.u.)		ω_{UV} (cm ⁻¹)		FWHM _{UV} (fs)		t_{UV}^0 (fs)	
	int	opt	int	opt	int	opt	int	opt
	0.015	0.0204	35 619.0	34 860.95	15.0	14.39	113.0	111.84
Optimization along O ¹⁶ +O ¹⁶ O ¹⁸ channel								
IR pulse parameter	C_{IR}		E_{IR}^0 (a.u.)		ω_{IR} (cm ⁻¹)		FWHM _{IR} (fs)	
	int	opt	int	opt	int	opt	int	opt
	1.0	1.0	0.015	0.0171	957.0	976.605	50.0	61.91
UV pulse parameter	E_{UV}^0 (a.u.)		ω_{UV} (cm ⁻¹)		FWHM _{UV} (fs)		t_{UV}^0 (fs)	
	int	opt	int	opt	int	opt	int	opt
	0.015	0.0153	35 619.0	35 442.27	15.0	14.53	130.0	125.206

TABLE V. The optimized fluxes and branching ratios for both O¹⁸+O¹⁶O¹⁶ channel and O¹⁶+O¹⁶O¹⁸ channel for **monochromatic, bichromatic, and polychromatic (with 4 components) electromagnetic fields.**

	Optimization along O ¹⁸ +O ¹⁶ O ¹⁶ channel			Optimization along O ¹⁶ +O ¹⁶ O ¹⁸ channel		
Monochromatic	$J_{O^{18+O^{16}O^{16}}}$	75.98%	$J_{O^{18+O^{16}O^{16}}}$	4.25%		
	$J_{O^{16+O^{16}O^{18}}}$	3.5%	$J_{O^{16+O^{16}O^{18}}}$	67.62%		
	$J_{O^{18+O^{16}O^{16}}}/J_{O^{16+O^{16}O^{18}}}$	21.70%	$J_{O^{16+O^{16}O^{18}}}/J_{O^{18+O^{16}O^{16}}}$	15.91%		
Bichromatic	$J_{O^{18+O^{16}O^{16}}}$	75.76%	$J_{O^{18+O^{16}O^{16}}}$	2.58%		
	$J_{O^{16+O^{16}O^{18}}}$	2.51%	$J_{O^{16+O^{16}O^{18}}}$	67.58%		
	$J_{O^{18+O^{16}O^{16}}}/J_{O^{16+O^{16}O^{18}}}$	29.36%	$J_{O^{16+O^{16}O^{18}}}/J_{O^{18+O^{16}O^{16}}}$	26.92%		
Polychromatic (4 component)	$J_{O^{18+O^{16}O^{16}}}$	77.17%	$J_{O^{18+O^{16}O^{16}}}$	2.32%		
	$J_{O^{16+O^{16}O^{18}}}$	1.87%	$J_{O^{16+O^{16}O^{18}}}$	67.38%		
	$J_{O^{18+O^{16}O^{16}}}/J_{O^{16+O^{16}O^{18}}}$	41.26%	$J_{O^{16+O^{16}O^{18}}}/J_{O^{18+O^{16}O^{16}}}$	29.04%		

TABLE VI. The initial and optimized fluxes and branching ratios for both O¹⁸+O¹⁶O¹⁶ channel and O¹⁶+O¹⁶O¹⁸ channel for **polychromatic electromagnetic field of eight components of light**, where optimization starts from the **wrong channel** (i.e., the opposite channel than that of the desired one).

	Optimization along O ¹⁸ +O ¹⁶ O ¹⁶ channel			Optimization along O ¹⁶ +O ¹⁶ O ¹⁸ channel		
$J_{O^{18+O^{16}O^{16}}}$	int	6.02%	$J_{O^{18+O^{16}O^{16}}}$	int	64.67%	
	opt	77.68%		opt	1.68%	
$J_{O^{16+O^{16}O^{18}}}$	int	58.94%	$J_{O^{16+O^{16}O^{18}}}$	int	8.03%	
	opt	1.23%		opt	69.48%	
$J_{O^{18+O^{16}O^{16}}}/J_{O^{16+O^{16}O^{18}}}$	int	0.102	$J_{O^{16+O^{16}O^{18}}}/J_{O^{18+O^{16}O^{16}}}$	int	0.124	
	opt	63.15		opt	41.36	

IV. CONCLUSION

We have demonstrated how the strategy of using hybrid pulses, obtained using involved stochastic optimizational procedure, can be a method of choice to selective cleave a bond in a system like O¹⁶O¹⁶O¹⁸, which has inherent complexities

due to strong internal vibrational redistribution as well as strong coupling between the two modes. Our results show that both absolute values of integrated flux along a target mode as well as the ratio of fluxes are obtained at much higher values using the optimized pulse than with an unoptimized pulse. The progress of the dynamics has been shown by depicting how

the contours of populations along the two modes change with time both for the ground as well as the excited state. To further show the efficiency of the procedure, the problem has been also studied when one starts from a completely wrong channel and ultimately reach the desired solution by optimizing and generating the correct perturbation. The recipe used by us to design optimum perturbation by focussing on the laser pulse can be a good approach to follow if greater selectivity and control in bond breaking is the sought after goal.

ACKNOWLEDGMENTS

S.T. would like to thank UGC for granting a senior research fellowship. P.C. acknowledges UGC for the funding through Major Research Project. We dedicate this work to Prof. Kamal Bhattacharya on his 60th birthday.

APPENDIX: CONTINUITY EQUATION AND RELATION OF FLUX WITH PROBABILITY DENSITY FOR $O^{16}O^{16}O^{18}$

The probability density (ρ) is given by

$$\rho = \psi^* \psi, \quad (A1)$$

$$\frac{\partial \rho}{\partial t} = \psi^* \frac{\partial \psi}{\partial t} + \psi \frac{\partial \psi^*}{\partial t}. \quad (A2)$$

The time dependent Schrödinger equation is

$$i\hbar \frac{\partial \psi}{\partial t} = H\psi \quad (A3)$$

$$\Rightarrow \frac{\partial \psi}{\partial t} = \frac{1}{i\hbar} H\psi, \quad (A4)$$

and, the complex conjugate for Eq. (A4) will be

$$\frac{\partial \psi^*}{\partial t} = -\frac{1}{i\hbar} H\psi^*. \quad (A5)$$

For $^{16}O^{16}O^{18}O$,

$$H = \frac{\hat{p}_1^2}{2\mu_1} + \frac{\hat{p}_2^2}{2\mu_2} + \frac{\hat{p}_1 \hat{p}_2}{m(^{16}O)} \cos \theta + V(r_1, r_2). \quad (A6)$$

Now, from Eq. (A4), we get

$$\begin{aligned} \frac{\partial \psi}{\partial t} &= \frac{1}{i\hbar} H\psi \\ &= \frac{1}{i\hbar} \left[\frac{\hat{p}_1^2}{2\mu_1} + \frac{\hat{p}_2^2}{2\mu_2} + \frac{\hat{p}_1 \hat{p}_2}{m(^{16}O)} \cos \theta + V(r_1, r_2) \right] \psi \\ &= \frac{1}{i} \left[\left(-\frac{\hbar}{2\mu_1} \right) \frac{\partial^2 \psi}{\partial r_1^2} + \left(-\frac{\hbar}{2\mu_2} \right) \frac{\partial^2 \psi}{\partial r_2^2} + \left(-\frac{\hbar}{m(^{16}O)} \right) \cos \theta \frac{\partial^2 \psi}{\partial r_1 \partial r_2} + \frac{V}{\hbar} \psi \right] \\ \Rightarrow \psi^* \frac{\partial \psi}{\partial t} &= \frac{1}{i} \left[\left(-\frac{\hbar}{2\mu_1} \right) \psi^* \frac{\partial^2 \psi}{\partial r_1^2} + \left(-\frac{\hbar}{2\mu_2} \right) \psi^* \frac{\partial^2 \psi}{\partial r_2^2} + \left(-\frac{\hbar}{m(^{16}O)} \right) \cos \theta \psi^* \frac{\partial^2 \psi}{\partial r_1 \partial r_2} + \frac{V}{\hbar} \psi^* \psi \right] \end{aligned} \quad (A7)$$

[since V is multiplicative therefore $\psi^* \frac{V}{\hbar} \psi = \frac{V}{\hbar} \psi^* \psi$].

Similarly from Eq. (A5), we get

$$\psi \frac{\partial \psi^*}{\partial t} = \frac{1}{i} \left[\left(\frac{\hbar}{2\mu_1} \right) \psi \frac{\partial^2 \psi^*}{\partial r_1^2} + \left(\frac{\hbar}{2\mu_2} \right) \psi \frac{\partial^2 \psi^*}{\partial r_2^2} + \left(\frac{\hbar}{m(^{16}O)} \right) \cos \theta \psi \frac{\partial^2 \psi^*}{\partial r_1 \partial r_2} - \frac{V}{\hbar} \psi \psi^* \right]. \quad (A8)$$

Thus, Eq. (A2) becomes

$$\begin{aligned} \frac{\partial \rho}{\partial t} &= \frac{1}{i} \left[\left(\frac{\hbar}{2\mu_1} \right) \psi \frac{\partial^2 \psi^*}{\partial r_1^2} + \left(\frac{\hbar}{2\mu_2} \right) \psi \frac{\partial^2 \psi^*}{\partial r_2^2} + \left(\frac{\hbar}{m(^{16}O)} \right) \cos \theta \psi \frac{\partial^2 \psi^*}{\partial r_1 \partial r_2} - \frac{V}{\hbar} \psi \psi^* \right] \\ &\quad + \frac{1}{i} \left[\left(-\frac{\hbar}{2\mu_1} \right) \psi^* \frac{\partial^2 \psi}{\partial r_1^2} + \left(-\frac{\hbar}{2\mu_2} \right) \psi^* \frac{\partial^2 \psi}{\partial r_2^2} + \left(-\frac{\hbar}{m(^{16}O)} \right) \cos \theta \psi^* \frac{\partial^2 \psi}{\partial r_1 \partial r_2} + \frac{V}{\hbar} \psi^* \psi \right] \\ &= \frac{\hbar}{2i\mu_1} \left[\psi \frac{\partial^2 \psi^*}{\partial r_1^2} - \psi^* \frac{\partial^2 \psi}{\partial r_1^2} \right] + \frac{\hbar}{2i\mu_2} \left[\psi \frac{\partial^2 \psi^*}{\partial r_2^2} - \psi^* \frac{\partial^2 \psi}{\partial r_2^2} \right] + \frac{\hbar \cos \theta}{im(^{16}O)} \left[\psi \frac{\partial^2 \psi^*}{\partial r_1 \partial r_2} - \psi^* \frac{\partial^2 \psi}{\partial r_1 \partial r_2} \right] \\ \Rightarrow \frac{\partial \rho}{\partial t} &= T_1 + T_2 + T_3. \end{aligned} \quad (A9)$$

Eq. (A9) can be simplified as follows:

$$\begin{aligned} T_1 &= \frac{\hbar}{2i\mu_1} \left[\psi \frac{\partial^2 \psi^*}{\partial r_1^2} - \psi^* \frac{\partial^2 \psi}{\partial r_1^2} \right] \\ &= \frac{\hbar}{2i\mu_1} \left[\psi \frac{\partial^2 \psi^*}{\partial r_1^2} - \psi^* \frac{\partial^2 \psi}{\partial r_1^2} + \frac{\partial \psi^*}{\partial r_1} \frac{\partial \psi}{\partial r_1} - \frac{\partial \psi^*}{\partial r_1} \frac{\partial \psi}{\partial r_1} \right] \\ &= \frac{\hbar}{2i\mu_1} \left[-\left(\frac{\partial \psi^*}{\partial r_1} \frac{\partial \psi}{\partial r_1} + \psi^* \frac{\partial^2 \psi}{\partial r_1^2} \right) + \left(\frac{\partial \psi}{\partial r_1} \frac{\partial \psi^*}{\partial r_1} + \psi \frac{\partial^2 \psi^*}{\partial r_1^2} \right) \right] \\ &= \frac{\hbar}{2i\mu_1} \left[-\frac{\partial}{\partial r_1} \left(\psi^* \frac{\partial \psi}{\partial r_1} - \psi \frac{\partial \psi^*}{\partial r_1} \right) \right] \\ &= \frac{\hbar}{2i\mu_1} \left[-\frac{\partial}{\partial r_1} j_1 \right], \quad \text{where } j_1 = \left(\psi^* \frac{\partial \psi}{\partial r_1} - \psi \frac{\partial \psi^*}{\partial r_1} \right). \end{aligned} \quad (A10)$$

Similarly,

$$T_2 = \frac{\hbar}{2i\mu_2} \left[-\frac{\partial}{\partial r_2} j_2 \right]. \quad (\text{A11})$$

Finally,

$$\begin{aligned} T_3 &= \frac{\hbar \cos \theta}{im(^{16}\text{O})} \left[\psi \frac{\partial^2 \psi^*}{\partial r_1 \partial r_2} - \psi^* \frac{\partial^2 \psi}{\partial r_1 \partial r_2} \right] \\ &= \frac{\hbar \cos \theta}{2im(^{16}\text{O})} \left[2\psi \frac{\partial^2 \psi^*}{\partial r_1 \partial r_2} - 2\psi^* \frac{\partial^2 \psi}{\partial r_1 \partial r_2} \right] \\ &= \frac{\hbar \cos \theta}{2im(^{16}\text{O})} \left[2\psi \frac{\partial^2 \psi^*}{\partial r_1 \partial r_2} - 2\psi^* \frac{\partial^2 \psi}{\partial r_1 \partial r_2} + \frac{\partial \psi}{\partial r_1} \frac{\partial \psi^*}{\partial r_2} - \frac{\partial \psi}{\partial r_1} \frac{\partial \psi^*}{\partial r_2} + \frac{\partial \psi^*}{\partial r_1} \frac{\partial \psi}{\partial r_2} - \frac{\partial \psi^*}{\partial r_1} \frac{\partial \psi}{\partial r_2} \right] \\ &= \frac{\hbar \cos \theta}{2im(^{16}\text{O})} \left[-\left(\frac{\partial \psi^*}{\partial r_1} \frac{\partial \psi}{\partial r_2} + \psi^* \frac{\partial^2 \psi}{\partial r_1 \partial r_2} \right) + \left(\frac{\partial \psi}{\partial r_1} \frac{\partial \psi^*}{\partial r_2} + \psi \frac{\partial^2 \psi^*}{\partial r_1 \partial r_2} \right) \right. \\ &\quad \left. - \left(\frac{\partial \psi^*}{\partial r_2} \frac{\partial \psi}{\partial r_1} + \psi^* \frac{\partial^2 \psi}{\partial r_2 \partial r_1} \right) + \left(\frac{\partial \psi}{\partial r_2} \frac{\partial \psi^*}{\partial r_1} + \psi \frac{\partial^2 \psi^*}{\partial r_2 \partial r_1} \right) \right] \\ &= \frac{\hbar \cos \theta}{2im(^{16}\text{O})} \left[-\frac{\partial}{\partial r_1} \left(\psi^* \frac{\partial \psi}{\partial r_2} \right) + \frac{\partial}{\partial r_1} \left(\psi \frac{\partial \psi^*}{\partial r_2} \right) - \frac{\partial}{\partial r_2} \left(\psi^* \frac{\partial \psi}{\partial r_1} \right) + \frac{\partial}{\partial r_2} \left(\psi \frac{\partial \psi^*}{\partial r_1} \right) \right] \\ &= \frac{\hbar \cos \theta}{2im(^{16}\text{O})} \left[-\frac{\partial}{\partial r_1} j_2 - \frac{\partial}{\partial r_2} j_1 \right]. \end{aligned} \quad (\text{A12})$$

Therefore, the continuity equation, i.e., Eq. (A9) may now be written as

$$\begin{aligned} \frac{\partial \rho}{\partial t} &= \frac{\hbar}{2i\mu_1} \left[-\frac{\partial}{\partial r_1} j_1 \right] + \frac{\hbar}{2i\mu_2} \left[-\frac{\partial}{\partial r_2} j_2 \right] + \frac{\hbar \cos \theta}{2im(^{16}\text{O})} \left[-\frac{\partial}{\partial r_1} j_2 - \frac{\partial}{\partial r_2} j_1 \right] \\ \Rightarrow \frac{\partial \rho}{\partial t} &= -\frac{\partial}{\partial r_1} \left[\frac{\hbar}{2i\mu_1} j_1 + \frac{\hbar \cos \theta}{2im(^{16}\text{O})} j_2 \right] - \frac{\partial}{\partial r_2} \left[\frac{\hbar}{2i\mu_2} j_2 + \frac{\hbar \cos \theta}{2im(^{16}\text{O})} j_1 \right]. \end{aligned} \quad (\text{A13})$$

Hence, the flux expression in the two directions “1” and “2” (for $^{16}\text{O}^{16}\text{O}^{18}\text{O}$, 1 refers to ^{16}O – ^{18}O and 2 refers to ^{16}O – ^{16}O) should also have additional terms (cross terms) due to the momentum coupling. Integrating Eq. (A13) with $dr_1 dr_2 dt$ with limits $r_1 = 0$ to $r_1 = r_{1d}$, $r_2 = 0$ to $r_2 = r_{2d}$, and $t = 0$ to $t = T$ and since at $r = 0$ flux is zero, we get

$$\begin{aligned} \int_0^{r_{1d}} \int_0^{r_{2d}} \int_0^T \frac{\partial \rho}{\partial t} dr_1 dr_2 dt &= -\int_0^{r_{1d}} \int_0^{r_{2d}} \int_0^T \left[\frac{\partial}{\partial r_1} \left(\frac{\hbar}{2i\mu_1} j_1 + \frac{\hbar \cos \theta}{2im(^{16}\text{O})} j_2 \right) \right. \\ &\quad \left. + \frac{\partial}{\partial r_2} \left(\frac{\hbar}{2i\mu_2} j_2 + \frac{\hbar \cos \theta}{2im(^{16}\text{O})} j_1 \right) \right] dr_1 dr_2 dt \\ \Rightarrow \int_0^{r_{1d}} \int_0^{r_{2d}} (\rho(T) - \rho(0)) dr_1 dr_2 &= -\left[\int_0^{r_{2d}} \int_0^T \left\{ \left(\frac{\hbar}{2i\mu_1} j_1(r_1 = r_{1d}) + \frac{\hbar \cos \theta}{2im(^{16}\text{O})} j_2(r_1 = r_{1d}) \right) \right. \right. \\ &\quad \left. \left. - \left(\frac{\hbar}{2i\mu_1} j_1(r_1 = 0) + \frac{\hbar \cos \theta}{2im(^{16}\text{O})} j_2(r_1 = 0) \right) \right\} dr_2 dt \right. \\ &\quad \left. + \int_0^{r_{1d}} \int_0^T \left\{ \left(\frac{\hbar}{2i\mu_2} j_2(r_2 = r_{2d}) + \frac{\hbar \cos \theta}{2im(^{16}\text{O})} j_1(r_2 = r_{2d}) \right) \right. \right. \\ &\quad \left. \left. - \left(\frac{\hbar}{2i\mu_2} j_2(r_2 = 0) + \frac{\hbar \cos \theta}{2im(^{16}\text{O})} j_1(r_2 = 0) \right) \right\} dr_1 dt \right] \\ \Rightarrow -\int_0^{r_{1d}} \int_0^{r_{2d}} (\rho(0) - \rho(T)) dr_1 dr_2 &= -\left[\int_0^{r_{2d}} \int_0^T \left\{ \left(\frac{\hbar}{2i\mu_1} j_1(r_1 = r_{1d}) + \frac{\hbar \cos \theta}{2im(^{16}\text{O})} j_2(r_1 = r_{1d}) \right) \right\} dr_2 dt \right. \\ &\quad \left. + \int_0^{r_{1d}} \int_0^T \left\{ \left(\frac{\hbar}{2i\mu_2} j_2(r_2 = r_{2d}) + \frac{\hbar \cos \theta}{2im(^{16}\text{O})} j_1(r_2 = r_{2d}) \right) \right\} dr_1 dt \right] \\ \Rightarrow \int_0^{r_{1d}} \int_0^{r_{2d}} (\rho(0) - \rho(T)) dr_1 dr_2 &= J_{\text{O}^{18+\text{O}}^{16}\text{O}^{16}} + J_{\text{O}^{16+\text{O}}^{16}\text{O}^{18}}, \end{aligned} \quad (\text{A14})$$

where

$$J_{\text{O}^{18+\text{O}}^{16}\text{O}^{16}} = \frac{\hbar}{2i} \int_0^{r_{1d}} \int_0^T \left[\frac{1}{\mu_1} j_1(r_1 = r_{1d}) + \frac{\cos \theta}{m(^{16}\text{O})} j_2(r_1 = r_{1d}) \right] dr_2 dt \quad (\text{A15})$$

$$\text{and } J_{\text{O}^{16+\text{O}}^{16}\text{O}^{18}} = \frac{\hbar}{2i} \int_0^{r_{1d}} \int_0^T \left[\frac{1}{\mu_2} j_2(r_2 = r_{2d}) + \frac{\cos \theta}{m(^{16}\text{O})} j_1(r_2 = r_{2d}) \right] dr_1 dt. \quad (\text{A16})$$

- ¹H. Rabitz, *Science* **314**, 264 (2006).
- ²P. Gross, D. Neuhauser, and H. Rabitz, *J. Chem. Phys.* **96**, 2834 (1992).
- ³P. Gross, D. M. Bairagi, M. K. Mishra, and H. Rabitz, *Chem. Phys. Lett.* **223**, 263 (1994).
- ⁴P. Gross, A. K. Gupta, D. M. Bairagi, and M. K. Mishra, *J. Chem. Phys.* **104**, 7045 (1996).
- ⁵K. Vandana and M. K. Mishra, *J. Chem. Phys.* **110**, 5140 (1999).
- ⁶K. Vandana and M. K. Mishra, *J. Chem. Phys.* **113**, 2336 (2000).
- ⁷M. Sarma, S. Adhikari, and M. K. Mishra, *Mol. Phys.* **107**, 939 (2009).
- ⁸S. A. Rice, *Nature* **409**, 422 (2001).
- ⁹D. J. Tannor and S. A. Rice, *Adv. Chem. Phys.* **70**, 441 (1988).
- ¹⁰B. Hartke, J. Manz, and J. Mathis, *Chem. Phys.* **139**, 123 (1989).
- ¹¹C. Kalyanaraman and N. Sathyamurti, *Chem. Phys. Lett.* **209**, 52 (1993).
- ¹²C. Shu, T. Rozgonyi, L. González, and N. E. Henriksen, *J. Chem. Phys.* **136**, 174303 (2012).
- ¹³S. K. Lee, A. G. Suits, H. B. Schlegel, and W. Li, *J. Phys. Chem. Lett.* **3**, 2541 (2012).
- ¹⁴S. K. Lee, H. B. Schlegel, and W. Li, *J. Phys. Chem. A* **117**, 11202 (2013).
- ¹⁵M. E. Corrales, J. González-Vázquez, G. Balardi, I. R. Solá, R. de Nalda, and L. Bañares, *Nat. Chem.* **6**, 785 (2014).
- ¹⁶A. P. Pierce, M. A. Daleh, and H. Rabitz, *Phys. Rev. A* **37**, 4950 (1988).
- ¹⁷M. A. Daleh, A. P. Pierce, and H. Rabitz, *Phys. Rev. A* **42**, 1065 (1990).
- ¹⁸N. Zhu, J. Botina, and H. Rabitz, *J. Chem. Phys.* **108**, 1953 (1998).
- ¹⁹S. Shi, A. Woody, and H. Rabitz, *J. Chem. Phys.* **88**, 6870 (1988).
- ²⁰P. Kumar, S. Sharma, and H. Singh, *J. Theor. Comput. Chem.* **8**, 157 (2009).
- ²¹S. Sharma, P. Sharma, H. Singh, and G. G. Balint-Kurti, *J. Mol. Model.* **15**, 623 (2009).
- ²²W. Jakubetz, E. Kades, and J. Manz, *J. Phys. Chem.* **97**, 12609 (1993).
- ²³S. Sharma, H. Singh, and G. G. Balint-Kurti, *J. Chem. Phys.* **132**, 064108 (2010).
- ²⁴S. Sharma, H. Singh, J. Harvey, and G. G. Balint-Kurti, *J. Chem. Phys.* **133**, 174103 (2010).
- ²⁵B. K. Shandilya, S. Sen, T. Sahoo, S. Talukder, P. Chaudhury, and S. Adhikari, *J. Chem. Phys.* **139**, 034310 (2013).
- ²⁶S. Sen, S. Talukder, and P. Chaudhury, *Indian J. Phys.* **87**, 865 (2013).
- ²⁷S. Ghosh, S. Talukder, S. Sen, and P. Chaudhury, *Chem. Phys.* **425**, 73 (2013).
- ²⁸*Femtosecond Chemistry*, edited by J. Manz and L. Wöst (Verlag Chemie, Weinheim, 1995).
- ²⁹R. Chakrabarti and H. Rabitz, *Int. Rev. Phys. Chem.* **26**, 671 (2007).
- ³⁰M. Shapiro and P. Brumer, *Phys. Rep.* **425**, 195 (2006).
- ³¹M. Shapiro and P. Brumer, *Principles of the Quantum Control of Molecular Processes* (Wiley-Interscience, Hoboken, NJ, 2003).
- ³²P. Brumer and M. Shapiro, *Annu. Rev. Phys. Chem.* **43**, 257 (1992).
- ³³S. A. Rice and M. Zhao, *Optical Control of Molecular Dynamics* (Wiley, New York, 2000).
- ³⁴R. J. Gordon and S. A. Rice, *Annu. Rev. Phys. Chem.* **48**, 601 (1997).
- ³⁵F. F. Crim, *Annu. Rev. Phys. Chem.* **44**, 397 (1993).
- ³⁶F. F. Crim, *J. Phys. Chem.* **100**, 12725 (1996).
- ³⁷R. N. Zare, *Science* **279**, 1875 (1998).
- ³⁸M. J. Bronikowski, W. R. Simpson, and R. N. Zare, *J. Phys. Chem.* **97**, 2194 (1993).
- ³⁹M. J. Bronikowski, W. R. Simpson, and R. N. Zare, *J. Phys. Chem.* **97**, 2204 (1993).
- ⁴⁰D. Goswami, *Phys. Rep.* **374**, 385 (2003).
- ⁴¹A. Assion, T. Baumert, M. Bergt, T. Brixner, B. Kiefer, V. Seyfried, M. Strehle, and G. Gerber, *Science* **282**, 919 (1998).
- ⁴²J. B. Ballard, H. U. Stauffer, Z. Amitay, and S. R. Leone, *J. Chem. Phys.* **116**, 1350 (2002).
- ⁴³B. Friedrich and D. Herschbach, *J. Phys. Chem.* **99**, 15686 (1995).
- ⁴⁴B. Friedrich and D. Herschbach, *Phys. Rev. Lett.* **74**, 4623 (1995).
- ⁴⁵W. Kim and P. M. Felker, *J. Chem. Phys.* **104**, 1147 (1996).
- ⁴⁶W. Kim and P. M. Felker, *J. Chem. Phys.* **107**, 2193 (1997).
- ⁴⁷J. J. Larsen, H. Sakai, C. P. Safvan, I. Wendt-Larsen, and H. Stapelfeldt, *J. Chem. Phys.* **111**, 7774 (1999).
- ⁴⁸H. Sakai, C. P. Safvan, J. J. Larsen, K. M. Hilligsoe, K. Hald, and H. Stapelfeldt, *J. Chem. Phys.* **110**, 10235 (1999).
- ⁴⁹J. J. Larsen, K. Hald, N. Bjerre, H. Stapelfeldt, and T. Seideman, *Phys. Rev. Lett.* **85**, 2470 (2000).
- ⁵⁰T. Seideman, *J. Chem. Phys.* **103**, 7887 (1995).
- ⁵¹J. H. Posthumus, J. Plumridge, M. K. Thomas, K. Codling, L. J. Frasinski, A. J. Langley, and P. F. Taday, *J. Phys. B* **31**, L553 (1998).
- ⁵²C. Ellert and P. B. Corkum, *Phys. Rev. A* **59**, R3170 (1999).
- ⁵³M. Comstock, V. A. Senekerimyan, and M. Dantus, *J. Phys. Chem. A* **107**, 8271 (2003).
- ⁵⁴K. Yamanouchi, *Science* **295**, 1659 (2002).
- ⁵⁵D. M. Villeneuve, S. A. Aseyev, P. Dietrich, M. Spanner, M. Y. Ivanov, and P. B. Corkum, *Phys. Rev. Lett.* **85**, 542 (2000).
- ⁵⁶A. Ashkin, J. M. Dziedzic, J. E. Bjorkholm, and S. Chu, *Opt. Lett.* **11**, 288 (1986).
- ⁵⁷A. Ashkin, J. M. Dziedzic, and T. Yamane, *Nature* **330**, 769 (1987).
- ⁵⁸A. Ashkin and J. M. Dziedzic, *Science* **235**, 1517 (1987).
- ⁵⁹A. Ashkin and J. M. Dziedzic, *Proc. Natl. Acad. Sci. U. S. A.* **86**, 7914 (1989).
- ⁶⁰M. F. DeCamp, D. A. Reis, P. H. Bucksbaum, and R. Merlin, *Phys. Rev. B* **64**, 092301 (2001).
- ⁶¹C. J. Bardeen, V. V. Yakovlev, K. R. Wilson, S. D. Carpenter, P. M. Weber, and W. S. Warren, *Chem. Phys. Lett.* **280**, 151 (1997).
- ⁶²R. S. Judson and H. Rabitz, *Phys. Rev. Lett.* **68**, 1500 (1992).
- ⁶³T. Hornung, R. Meier, D. Zeidler, K. L. Kompa, D. Proch, and M. Motzkus, *Appl. Phys. B* **71**, 277 (2000).
- ⁶⁴P. Ranitovic, C. W. Hogle, P. Rivière, A. Palacios, X. Tong, N. Toshima, A. González-Castrillo, L. Martin, F. Martín, M. M. Murnane, and H. Kapteyn, *Proc. Natl. Acad. Sci. U. S. A.* **111**, 912 (2014).
- ⁶⁵P. F. Zittel and D. D. Little, *J. Chem. Phys.* **72**, 5900 (1980).
- ⁶⁶P. F. Zittel and D. E. Masturzo, *J. Chem. Phys.* **85**, 4362 (1986).
- ⁶⁷H. L. Berghout, S. S. Brown, R. Delgado, and F. F. Crim, *J. Chem. Phys.* **109**, 2257 (1998).
- ⁶⁸N. Shafer, S. Satyapal, and R. J. Bersohn, *J. Chem. Phys.* **90**, 6807 (1989).
- ⁶⁹R. L. Vanderwal, J. L. Scott, and F. F. Crim, *J. Chem. Phys.* **92**, 803 (1990).
- ⁷⁰I. Bar, Y. Cohen, D. David, S. Rosenwaks, and J. J. Valentini, *J. Chem. Phys.* **93**, 2146 (1990).
- ⁷¹M. J. Bronikowski, W. R. Simpson, B. Girard, and R. N. Zare, *J. Chem. Phys.* **95**, 8647 (1991).
- ⁷²R. B. Metz, J. D. Thoemke, J. M. Pfeiffer, and F. F. Crim, *J. Chem. Phys.* **99**, 1744 (1993).
- ⁷³J. H. Gutow, D. Klenerman, and R. N. Zare, *J. Phys. Chem.* **92**, 172–177 (1988).
- ⁷⁴J. Zhang, C. W. Riehn, M. Dulligan, and C. Wittig, *J. Chem. Phys.* **103**, 6815 (1995).
- ⁷⁵J. D. Thoemke, J. M. Pfeiffer, R. B. Metz, and F. F. Crim, *J. Phys. Chem.* **99**, 13748 (1995).
- ⁷⁶S. S. Brown, H. L. Berghout, and F. F. Crim, *J. Chem. Phys.* **102**, 8440 (1995).
- ⁷⁷S. S. Brown, R. B. Metz, H. L. Berghout, and F. F. Crim, *J. Chem. Phys.* **105**, 6293 (1996).
- ⁷⁸H. L. Berghout, S. Hsieh, and F. F. Crim, *J. Chem. Phys.* **114**, 10835 (2001).
- ⁷⁹L. J. Butler, E. J. Hints, S. F. Shane, and Y. T. Lee, *J. Chem. Phys.* **86**, 2051 (1987).
- ⁸⁰D. G. Abrashkevich, M. Shapiro, and P. Brumer, *J. Chem. Phys.* **116**, 5584 (2002).
- ⁸¹K. Liu, H. Zhao, C. Wang, A. Zhang, S. Ma, and Z. Li, *J. Chem. Phys.* **122**, 044310 (2005).
- ⁸²N. Elghobashi, P. Krause, J. Manz, and M. Oppel, *Phys. Chem. Chem. Phys.* **5**, 4806 (2003).
- ⁸³B. Amstrup and N. E. Henriksen, *J. Chem. Phys.* **97**, 8285 (1992).
- ⁸⁴N. E. Henriksen, K. B. Møller, and V. Engel, *J. Chem. Phys.* **122**, 204320 (2005).
- ⁸⁵J. Zhang and D. G. Imre, *Chem. Phys. Lett.* **149**, 233 (1988).
- ⁸⁶D. G. Imre and J. Zhang, *Chem. Phys.* **139**, 89 (1989).
- ⁸⁷M. G. Sheppard and R. B. Walker, *J. Chem. Phys.* **78**, 7191 (1983).
- ⁸⁸S. M. Alder-Golden, S. R. Langhoff, C. W. Bauschlicher, and G. D. Carney, *J. Chem. Phys.* **83**, 255 (1985).
- ⁸⁹C. Leforestier, F. LeQuéré, K. Yamashita, and K. Morokuma, *J. Chem. Phys.* **101**, 3806 (1994).
- ⁹⁰B. Amstrup and N. E. Henriksen, *J. Chem. Phys.* **105**, 9115 (1996).
- ⁹¹S. Kirkpatrick, C. D. Gelatt, Jr., and M. P. Vecchi, *Science* **220**, 671 (1983).
- ⁹²S. R. Wilson and W. L. Cui, *Biopolymers* **29**, 225 (1990).
- ⁹³I. Andricioaei and J. E. Straub, *Phys. Rev. E* **53**, R3055 (1996).
- ⁹⁴J. Zhang, *J. Mol. Model.* **17**, 173 (2011).
- ⁹⁵M. J. van Setten, W. Lohstroh, and M. Fichtner, *J. Mater. Chem.* **19**, 7081 (2009).
- ⁹⁶E. Onbasoglu and L. Özdamar, *J. Global Optim.* **19**, 27 (2001).
- ⁹⁷M. J. Field, *J. Chem. Phys.* **103**, 3621 (1995).
- ⁹⁸P. Dutta, D. Majumdar, and S. P. Bhattacharyya, *Chem. Phys. Lett.* **181**, 293 (1999).

- ⁹⁹S. K. Biring and P. Chaudhury, *Chem. Phys.* **377**, 46 (2010).
- ¹⁰⁰S. Guha, S. Roy, and P. Chaudhury, *Struct. Chem.* **22**, 1007 (2011).
- ¹⁰¹S. Talukder, P. Chaudhury, R. Metzler, and S. K. Banik, *J. Chem. Phys.* **135**, 165103 (2011).
- ¹⁰²S. Talukder, S. Sen, R. Sharma, S. K. Banik, and P. Chaudhury, *Chem. Phys.* **431-432**, 5 (2014).
- ¹⁰³C. Leforestier, R. Bisseling, C. Cerjan, M. D. Feit, R. Friesner, A. Guldberg, A. Hammerich, G. Jolicard, W. Karrlein, H.-D. Meyer, N. Lipkin, O. Roncero, and R. Kosloff, *J. Comput. Phys.* **59**, 59 (1991).
- ¹⁰⁴R. Siebert, P. Fleurat-Lessard, and R. Schinke, *J. Chem. Phys.* **116**, 9749 (2002).
- ¹⁰⁵I. Barth and J. Manz, "Quantum switching of magnetic fields by circularly polarized re-optimized laser pulses: From one-electron atomic ions to molecules," in *Progress in Ultrafast Intense Laser Science VI* (Springer, New York, 2010), Chap. 2.
- ¹⁰⁶B. Friedrich and D. Herschbach, *J. Phys. Chem. A* **103**, 10280 (1999).
- ¹⁰⁷H. Stapelfeldt and T. Seideman, *Rev. Mod. Phys.* **75**, 543 (2003).
- ¹⁰⁸M. Machholm and N. E. Henriksen, *Phys. Rev. Lett.* **87**, 193001 (2001).
- ¹⁰⁹D. Kosloff and R. Kosloff, *J. Comput. Phys.* **52**, 35 (1983).

Selective bond breaking mediated by state specific vibrational excitation in model HOD molecule through optimized femtosecond IR pulse: A simulated annealing based approach

Cite as: J. Chem. Phys. **139**, 034310 (2013); <https://doi.org/10.1063/1.4813127>

Submitted: 03 January 2013 . Accepted: 24 June 2013 . Published Online: 17 July 2013

Bhavesh K. Shandilya, Shrabani Sen, Tapas Sahoo, Srijeeta Talukder, Pinaki Chaudhury, and Satrajit Adhikari



View Online



Export Citation



CrossMark

ARTICLES YOU MAY BE INTERESTED IN

Enhancing the branching ratios in the dissociation channels for $O^{16}O^{16}O^{18}$ molecule by designing optimum laser pulses: A study using stochastic optimization

The Journal of Chemical Physics **143**, 144109 (2015); <https://doi.org/10.1063/1.4932333>

Non-resonant vibrational excitation of HOD and selective bond breaking

The Journal of Chemical Physics **148**, 234307 (2018); <https://doi.org/10.1063/1.5029548>

Selective breaking of bonds in water with intense, 2-cycle, infrared laser pulses

The Journal of Chemical Physics **143**, 244310 (2015); <https://doi.org/10.1063/1.4938500>

Lock-in Amplifiers

Find out more today



Zurich
Instruments



Selective bond breaking mediated by state specific vibrational excitation in model HOD molecule through optimized femtosecond IR pulse: A simulated annealing based approach

Bhaves K. Shandilya,^{1,2} Shrabani Sen,³ Tapas Sahoo,¹ Srijeeta Talukder,³ Pinaki Chaudhury,³ and Satrajit Adhikari^{1,a)}

¹Department of Physical Chemistry, Indian Association for the Cultivation of Science, Jadavpur, Kolkata 700 032, India

²Department of Chemistry, Indian Institute of Technology Bombay, Powai, Mumbai 400 076, India

³Department of Chemistry, University of Calcutta, 92, A. P. C. Road, Kolkata 700 009, India

(Received 3 January 2013; accepted 24 June 2013; published online 17 July 2013)

The selective control of O–H/O–D bond dissociation in reduced dimensionality model of HOD molecule has been explored through IR+UV femtosecond pulses. The IR pulse has been optimized using simulated annealing stochastic approach to maximize population of a desired low quanta vibrational state. Since those vibrational wavefunctions of the ground electronic states are preferentially localized either along the O–H or O–D mode, the femtosecond UV pulse is used only to transfer vibrationally excited molecule to the repulsive upper surface to cleave specific bond, O–H or O–D. While transferring from the ground electronic state to the repulsive one, the optimization of the UV pulse is not necessarily required except specific case. The results so obtained are analyzed with respect to time integrated flux along with contours of time evolution of probability density on excited potential energy surface. After preferential excitation from $|0, 0\rangle$ ($|m, n\rangle$ stands for the state having m and n quanta of excitations in O–H and O–D mode, respectively) vibrational level of the ground electronic state to its specific low quanta vibrational state ($|1, 0\rangle$ or $|0, 1\rangle$ or $|2, 0\rangle$ or $|0, 2\rangle$) by using optimized IR pulse, the dissociation of O–D or O–H bond through the excited potential energy surface by UV laser pulse appears quite high namely, 88% (O–H ; $|1, 0\rangle$) or 58% (O–D ; $|0, 1\rangle$) or 85% (O–H ; $|2, 0\rangle$) or 59% (O–D ; $|0, 2\rangle$). Such selectivity of the bond breaking by UV pulse (if required, optimized) together with optimized IR one is encouraging compared to the normal pulses. © 2013 AIP Publishing LLC. [<http://dx.doi.org/10.1063/1.4813127>]

I. INTRODUCTION

Controlling chemical events in a desired manner has been, and will always be a much sought after endeavour of any chemist, be it an experimentalist or a theoretician. However, the traditional way of studying reactions is mostly thermal, but unfortunately, the thermal way is not a prudent choice for channelizing or dictating a reaction to go in a desired specific direction. On the contrary, if light is used to control and to follow chemical transformations, a high degree of control can be achieved like dissociating a particular bond selectively in a polyatomic molecule. Specifically, a time dependent perturbation induced by an external radiation field with a properly designed pulse shape can, to a high degree of specificity, generate the desired results in a chemical transformation.^{1–15} There are many examples^{12–15} in which different standard pulse shape functions such as Gaussian, triangular, saw-toothed, sine squared, etc., have been used to follow target excitations in vibrational levels with high accuracy and specificity.

The problem of state specific vibrational excitation or maximizing the dissociation probability in simple diatomic molecules, modelled by Morse potentials, though intellectu-

ally illuminating and allowing the user to develop the necessary theoretical tools, is rather academic or pedagogic from the point of view of contemporary research in the field. On the contrary, the low quanta vibrational excitation to specific level of the ground electronic state and dissociation of a desired bond of a triatomic molecule through repulsive surface are the nontrivial attempts for controlling chemical reaction both by experimental technique as well as theoretical methodology. The HOD molecule is a model system to test different theoretical approaches to state selective vibrational excitation^{14,15} or selective cleaving of bond^{16–39} due to availability of accurate potential energy surfaces^{19,40,41} and dipole moment functions.^{21,27} Since the stretching frequencies of O–H and O–D in HOD are far apart,^{14,19,21,22,27} the preferential accumulation of wavefunction in H+O–D or H–O+D channel can be achieved by IR pulse with carrier frequency corresponding to those of O–H or O–D stretches, respectively.^{19,21,22,27,36} On the other hand, as the first excited electronic state is purely repulsive one with a saddle point barrier which separates the H+O–D and H–O+D channels,^{40,41} while transferring the vibrationally excited molecule to the upper surface by UV pulse, the barrier height of repulsive surface prevents crossover from one channel to the other and thereby, the desired bond breaks selectively.^{18–20,23} The photodissociation of HOD utilizing IR pulse to excite

^{a)} Author to whom correspondence should be addressed. Electronic mail: pcsa@iacs.res.in

either fundamental or low quanta overtone of O–H/O–D mode followed by appropriate UV field has there been reported experimentally,^{20,23–26,30} which was termed as *vibrationally mediated photochemistry*.⁴² The preferential dissociation of O–H bond has been proposed^{17–19,21,22,25,27} and realized experimentally using the ground vibrational state and low/high overtone excitation of the O–H bond by many groups.^{20,23–26} The Time Dependent Wave Packet (TDWP) calculations^{19,20} predict three (3) or more quanta of excitation in O–D mode is necessary for preferential breaking of O–D mode, whereas only one quanta of excitation is required in case of O–H mode to enhance selectivity. These TDWP calculations show that there is no preferential dissociation of O–D bond with one quanta of excitation in O–D mode and is supported by experiment.²⁶ The remarkable preferential dissociation in O–D mode has been shown experimentally mediated by (5) five quanta of excitation in O–D mode.³⁶ Indeed, these predictions were based on semiclassical TDWP calculations employing δ -function type pulses. Since even a moderately intense IR pulse distributes population in combination of excited vibrational states not in pure O–H/O–D overtone,^{27,39} theoretical calculations employing those vibrationally excited states as the initial state to pump the probability density to the upper repulsive surface by UV pulse for selective bond dissociation may not be experimentally realizable. The state selective vibrational excitation^{12–15} mechanism for model OH and HOD system has been proposed using analytical and numerical pulse shapes under the framework of optimal control theory (OCT) as well, but in all those calculations, the target vibrational states are much higher. However, several attempts^{29,35,38} have also been reported for selective bond dissociation of same system (HOD) using simple as well as OCT optimized UV pulses under various constrains over pulse parameters.

An interesting and important problem is how to selectively cleave a particular bond in a molecule, leaving the rest of the molecule as it is, by using optimally designed laser pulse shapes. It is our purpose to investigate selective bond breaking in reduced dimensionality model of HOD molecule through lower quanta vibrational excitation using optimized field attributes. Since the lower quanta vibrational wavefunctions are preferentially localized along O–H or O–D mode, selective vibrational IR excitation can efficiently help to dissociate O–H or O–D bond while pumping either by a simple or an optimized (if required) UV pulse. Therefore, optimization of the IR pulse is much more important for selective dissociation than the UV one in our two step mechanism for the increase of time integrated flux. The optimization of the pulse fields has been performed by using a stochastic approach called simulated annealing (SA), where the profile of the IR and UV pulse field are optimized by maximizing the population of a targeted vibrational state and the flux in a desired mode, respectively. The dissociation of the HOD molecule in a specific channel is to explore the validity of simulated annealing stochastic approach for optimization of IR pulse to selectively populate lower vibrational levels and then, to pump on the upper electronic state with simple or optimized UV pulse.

Section II deals with details of the Hamiltonian and laser field profile and is followed by section on stochastic approach and a section on initialization, time propagation, and flux

analysis. A discussion of prominent results and summary of main findings conclude this article.

II. THE HAMILTONIAN AND THE LASER FIELD PROFILE

We consider two-dimensional model Hamiltonian for the triatomic molecule HOD, neglecting bending and rotation mode,^{17,27} where r_1 and r_2 refer the O–H and O–D stretches, respectively. The conjugate momenta are denoted by p_1 (O–H) and p_2 (O–D). The kinetic energy operator is given by

$$\hat{T} = \frac{\hat{p}_1^2}{2\mu_1} + \frac{\hat{p}_2^2}{2\mu_2} + \frac{\hat{p}_1\hat{p}_2}{m_O} \cos\theta, \quad (1)$$

where

$$\begin{aligned} \hat{p}_j &= \frac{\hbar}{i} \frac{\partial}{\partial r_j}, \quad j = 1, 2, \\ \mu_1 &= m_H m_O / (m_H + m_O), \\ \mu_2 &= m_O m_D / (m_O + m_D), \end{aligned} \quad (2)$$

and θ is the fixed (equilibrium) bending angle of 104.52° for HOD.

We consider two electronic states of the molecule (HOD) in our calculation, namely, the electronic ground state and the first electronically excited state. A laser in the infrared (ir) region and another one in the ultraviolet (uv) region are allowed to interact with the molecule. The time evolution associated with the nuclear motion can then be calculated from the time-dependent Schrödinger equation,

$$i\hbar \frac{\partial}{\partial t} \begin{pmatrix} \psi_g \\ \psi_e \end{pmatrix} = \begin{pmatrix} \hat{H}_g + \hat{H}_{ir}(t) & \hat{H}_{uv}(t) \\ \hat{H}_{uv}(t) & \hat{H}_e \end{pmatrix} \begin{pmatrix} \psi_g \\ \psi_e \end{pmatrix}, \quad (3)$$

where the wavefunctions associated with nuclear motion on the ground and the excited electronic state are $\psi_g \equiv \psi_g(r_1, r_2, t)$ and $\psi_e \equiv \psi_e(r_1, r_2, t)$, respectively. The nuclear Hamiltonians for the two states are described by $\hat{H}_g = \hat{T} + V_g$ and $\hat{H}_e = \hat{T} + V_e$. $\hat{H}_{ir}(t)$ and $\hat{H}_{uv}(t)$ are the interaction between the molecule with IR and UV laser, respectively.

At this point, we specify the details of the Hamiltonian in Eq. (3) for HOD molecule, where two Morse oscillators and a coupling term^{19,43} are taken to represent the potential energy surface associated with the electronic ground state,

$$\begin{aligned} V_g(r_1, r_2) &= D[1 - e^{-\alpha(r_1-r_0)}]^2 + D[1 - e^{-\alpha(r_2-r_0)}]^2 \\ &\quad + f_{12}(r_1 - r_0)(r_2 - r_0) \\ f_{12} &= \frac{F_{12}}{1 + e^{\beta[(r_1-r_0)+(r_2-r_0)]}}, \end{aligned} \quad (4)$$

with $D = 0.2092$ hartree, $\alpha = 1.13 a_0^{-1}$, $r_0 = 1.81 a_0$, $\beta = 1.0 a_0^{-1}$, and $F_{12} = -6.76 \times 10^{-3}$ hartree/ a_0^2 .

The potential energy surface of the first electronically excited state, V_e , was obtained from the fitting of *ab initio* data^{40,41} with the following analytic expression as suggested

originally by Sorbie and Murrell:^{44,45}

$$\begin{aligned} V_e &= V_e^{fit}(r_1, r_2, r_3) \\ &= V_{OH}(r_1)\chi(r_2, r_3) + V_{OH}(r_3)\chi(r_1, r_2) + V_I(r_1, r_2, r_3), \end{aligned} \quad (5)$$

with H–O, O–D, and D–H separations as r_1 , r_2 , and r_3 , respectively. V_{OH} is a Morse potential,

$$V_{OH}(r_1) = D_{OH}\{1 - \exp[-\beta_{OH}(r_1 - r_{OH})]\}^2 - D_{OH} \quad (6)$$

and

$$\chi(r_i, r_j) = [1 - \exp(-\delta r_i^2)][1 - \exp(-\delta r_j^2)], \quad (7)$$

is a cutoff function. The three-body term has the form:

$$V_I(r_1, r_2, r_3) = \sum_{i=1}^{50} c_i P_i(S_1, S_2, S_3) \times \prod_{j=1}^3 (1 - \tanh \alpha_j S_j), \quad (8)$$

where P_i refers polynomial up to sixth order with three variables, $S_j = r_j - 1 \text{ \AA}$ ($j = 1, 2, 3$). The parameters c_i , α_j , and δ together with the polynomials P_i and the Morse parameters are given in Table I of Ref.40.

The interaction with the laser field can be written as

$$\hat{H}_{ir}(t) = -\vec{\mu}_g(\mathbf{r}_1, \mathbf{r}_2) \cdot \vec{S}^{ir}(t) = -\mu_g(r_1, r_2) E_0^{ir} a(t) \cos \omega^{ir} t, \quad (9)$$

where $a(t)$ is the envelope of the pulse, ω^{ir} is the carrier frequency, and E_0^{ir} denotes the maximum amplitude of the IR pulse. We consider a Gaussian pulse,

$$a(t) = \left(\frac{8\gamma t_l^2}{\pi}\right)^{1/4} \exp[-\gamma(t - t^{ir})^2], \quad (10)$$

where t_l gives the pulse length and t^{ir} is the peak time for the maximum amplitude of the IR pulse. The pulse width of the Gaussian pulse is defined as the full width at half-maximum (FWHM) [FWHM = $\sqrt{4\ln 2/\gamma}$].

The electric dipole moment function of the electronic ground state is given by,⁴⁶

$$\vec{\mu}_g(\mathbf{r}_1, \mathbf{r}_2) = \mathbf{r}_1 \mu_0 \exp(-r_1/r^*) + \mathbf{r}_2 \mu_0 \exp(-r_2/r^*), \quad (11)$$

where $\mu_0 = 7.85 \text{ D/\AA}$ and $r^* = 0.6 \text{ \AA}$. The plane XZ is molecular plane of HOD with Z axis as bisector. If X polarized electric field of the exciting IR laser is considered, the interaction of the IR field and molecule is given by

$$\hat{H}_{ir}(t) = [\mu_1(r_1) - \mu_2(r_2)] A_0 a(t) \cos \omega^{ir} t, \quad (12)$$

where

$$\begin{aligned} \mu_j(r_j) &= \mu_0 r_j \exp(-r_j/r^*), \quad j = 1, 2 \\ A_0 &= E_0 \cos \phi \end{aligned} \quad (13)$$

and

$$\phi = (\pi - \theta)/2.$$

The transition dipole function was calculated by *ab initio* methods only within a small region ($r_1, r_2 \leq 2.6a_0$) and has been fitted to the expression,^{21,27}

$$\mu_{ge} = \frac{2.225}{1 + e^{\beta(r_1 - r_0)}} + \frac{2.225}{1 + e^{\beta(r_2 - r_0)}}. \quad (14)$$

The transition dipole moment vector, μ_{ge} , is perpendicular to the molecular plane,⁴⁰ and the electric field vector of the UV-laser field is considered as parallel to the dipole moment vector. Thus, the interaction with the UV laser would be,

$$\hat{H}_{uv}(t) = -\vec{\mu}_{ge}(\mathbf{r}_1, \mathbf{r}_2) \cdot \vec{S}^{uv}(t) = -\mu_{ge}(r_1, r_2) E_0 a(t) \cos \omega^{uv} t, \quad (15)$$

where we consider a Gaussian pulse shape,

$$a(t) = \exp[-\gamma(t - t^{uv})^2], \quad (16)$$

with ω^{uv} is the pumping frequency from ground to the upper electronic state and E_0^{uv} denotes the maximum amplitude of the UV pulse.

III. PULSE OPTIMIZATION: A SIMULATED ANNEALING BASED STOCHASTIC APPROACH

We explore the idea of designing optimized pulses, especially, those for the IR excitation to selected low quanta vibrational levels in the ground electronic state and then, for UV pumping generally by simple pulses from the ground state to the excited one of the HOD molecule. The IR pulse to be optimized could be expressed as a linear combination of individual Gaussian pulses:

$$S^{ir}(t) = \sum c_i^{ir} S_i^{ir}(E_{0,i}^{ir}, \omega_i^{ir}, \gamma_i^{ir}, t), \quad (17)$$

where

$$\begin{aligned} S_i^{ir}(E_{0,i}^{ir}, \omega_i^{ir}, \gamma_i^{ir}, t) \\ = E_{0,i}^{ir} \left(\frac{8\gamma_i^{ir} t_l^2}{\pi}\right)^{1/4} \exp[-\gamma_i^{ir}(t - t^{ir})^2] \cos \omega_i^{ir} t. \end{aligned} \quad (18)$$

The parameters $E_{0,i}^{ir}$, ω_i^{ir} , and γ_i^{ir} represent the i th pulse shape of the hybrid pulse to be designed and c_i^{ir} is the associated combining coefficient. So, in essence, the idea is to find out the optimum values of the quantities c_i^{ir} , $E_{0,i}^{ir}$, ω_i^{ir} , and γ_i^{ir} , a total of 32 parameters, where the summation in Eq. (17) is over eight individual pulse shape. This optimized IR pulse shape function is used as part of the time dependent potential energy term of the Hamiltonian (see Eqs. (9) and (12)) for the selective lower quanta vibrational excitation from $|0, 0\rangle$ level to either $|1, 0\rangle$ or $|0, 1\rangle$ or $|2, 0\rangle$ or $|0, 2\rangle$ of the ground electronic state. The initial and optimized parameters of the IR pulse are presented in Tables I–IV. Since the lower quanta vibrational wavefunctions are preferentially localized along O–H or O–D mode, selective vibrational IR excitation can efficiently help to dissociate O–H or O–D mode while pumping by a simple UV pulse. Therefore, optimization of the IR pulse is much more important for selective dissociation than the UV one in our two step proposed mechanism to increase the time integrated flux. If required, we optimize a single UV pulse rather than a linear combination of pulses, where the trial form of the UV pulse is taken as

$$S^{uv}(t) = \sum c_i^{uv} S_i^{uv}(E_{0,i}^{uv}, \omega_i^{uv}, \gamma_i^{uv}, t), \quad (19)$$

where

$$S_i^{uv}(E_{0,i}^{uv}, \omega_i^{uv}, \gamma_i^{uv}, t) = E_{0,i}^{uv} \exp[-\gamma_i^{uv}(t - t^{uv})^2] \cos \omega_i^{uv} t. \quad (20)$$

TABLE I. The initial and optimized parameters associated with the eight Gaussian IR pulses for $|1, 0\rangle$ as target vibrational state.

Gaussian	1	2	3	4	5	6	7	8
C^{ir} (int)	1.000	1.000	1.000	1.000	1.000	1.000	1.000	1.000
C^{ir} (opt)	1.000	0.977	1.000	1.000	0.982	1.027	1.021	0.968
E_0^{ir} (int)/a.u.	0.00900	0.01000	0.01500	0.02000	0.02500	0.01300	0.01800	0.02200
E_0^{ir} (opt)/a.u.	0.00899	0.00997	0.01507	0.01991	0.02500	0.01296	0.01799	0.02201
ω^{ir} (int)/ cm^{-1}	3556.00	3606.00	3656.00	3706.00	3756.00	3806.00	3856.00	3906.00
ω^{ir} (opt)/ cm^{-1}	3598.96	3539.81	3656.00	3738.58	3763.74	3805.78	3781.14	3899.99
FWHM (int)/fs	55.00	60.00	65.00	70.00	75.00	80.00	85.00	90.00
FWHM (opt)/fs	54.78	60.61	64.95	71.90	75.00	80.00	81.65	90.48

TABLE II. The initial and optimized parameters associated with the eight Gaussian IR pulses for $|0, 1\rangle$ as target vibrational state.

Gaussian	1	2	3	4	5	6	7	8
C^{ir} (int)	1.000	1.000	1.000	1.000	1.000	1.000	1.000	1.000
C^{ir} (opt)	0.980	0.964	1.000	0.991	0.986	1.015	1.000	1.006
E_0^{ir} (int)/a.u.	0.00900	0.01000	0.01500	0.02000	0.02500	0.01300	0.01800	0.02200
E_0^{ir} (opt)/a.u.	0.00899	0.01000	0.01508	0.02009	0.02484	0.01304	0.01810	0.02189
ω^{ir} (int)/ cm^{-1}	2577.00	2627.00	2677.00	2727.00	2777.00	2827.00	2877.00	2927.00
ω^{ir} (opt)/ cm^{-1}	2598.69	2620.25	2674.89	2769.20	2786.25	2816.66	2820.26	2877.93
FWHM (int)/fs	55.00	60.00	65.00	70.00	75.00	80.00	85.00	90.00
FWHM (opt)/fs	54.96	60.59	65.76	69.44	73.61	80.38	86.37	87.51

TABLE III. The initial and optimized parameters associated with the eight Gaussian IR pulses for $|2, 0\rangle$ as target vibrational state.

Gaussian	1	2	3	4	5	6	7	8
C^{ir} (int)	1.000	1.000	1.000	1.000	1.000	1.000	1.000	1.000
C^{ir} (opt)	1.027	1.000	1.014	1.001	1.000	0.972	1.002	1.017
E_0^{ir} (int)/a.u.	0.00900	0.01000	0.01500	0.02000	0.02500	0.01300	0.01800	0.02200
E_0^{ir} (opt)/a.u.	0.00899	0.01000	0.01499	0.02007	0.02497	0.01294	0.01791	0.02200
ω^{ir} (int)/ cm^{-1}	3556.00	3606.00	3656.00	3706.00	3756.00	3806.00	3856.00	3906.00
ω^{ir} (opt)/ cm^{-1}	3617.53	3727.23	3737.89	3737.87	3721.73	3794.64	3852.75	3945.14
FWHM (int)/fs	55.00	60.00	65.00	70.00	75.00	80.00	85.00	90.00
FWHM (opt)/fs	53.83	59.64	64.38	71.43	76.33	80.00	88.69	91.67

TABLE IV. The initial and optimized parameters associated with the eight Gaussian IR pulses for $|0, 2\rangle$ as target vibrational state.

Gaussian	1	2	3	4	5	6	7	8
C^{ir} (int)	1.000	1.000	1.000	1.000	1.000	1.000	1.000	1.000
C^{ir} (opt)	1.016	1.013	0.967	0.961	0.983	1.008	1.020	1.010
E_0^{ir} (int)/a.u.	0.00900	0.01000	0.01500	0.02000	0.02500	0.01300	0.01800	0.02200
E_0^{ir} (opt)/a.u.	0.00903	0.01006	0.01484	0.02006	0.02501	0.01299	0.01808	0.02176
ω^{ir} (int)/ cm^{-1}	2577.00	2627.00	2677.00	2727.00	2777.00	2827.00	2877.00	2927.00
ω^{ir} (opt)/ cm^{-1}	2543.29	2652.18	2785.85	2742.12	2784.74	2784.52	2830.63	2966.78
FWHM (int)/fs	55.00	60.00	65.00	70.00	75.00	80.00	85.00	90.00
FWHM (opt)/fs	56.29	60.33	67.87	68.39	76.42	81.47	84.73	90.28

TABLE V. Initial UV pulse parameters used to pump from various target states, where the optimized UV pulse parameters for $|0, 1\rangle$ case are given in parenthesis.

State	$ 1, 0\rangle$	$ 0, 1\rangle$ (opt)	$ 2, 0\rangle$	$ 0, 2\rangle$
E_0^{uv} /a.u.	0.09	0.09 (0.09365)	0.09	0.09
ω^{uv} / cm^{-1}	56 155.00	59 703.00 (60 045.17)	52 449.00	54 372.00
FWHM/fs	50.00	50.00 (42.452)	50.00	50.00

The parameters $E_{0,i}^{uv}$, ω_i^{uv} , γ_i^{uv} , and c_i^{uv} represent intensity, frequency, width, and combining coefficient, respectively, of the i th UV pulse. At present case, we keep only one of the combining coefficient to maximize the dissociative flux, where the parameters of the UV pulse (see Table V) are optimized by using simulated annealing technique to pump from the ground electronic state to the excited repulsive surface. It appears that we need to optimize the UV pulse parameters only when the molecule is transferred from vibrationally excited $|0, 1\rangle$ level to the repulsive surface.

The process of finding the optimized pulse parameters is a non-trivial task. An initially chosen set of parameters and the optimized ones too are obviously be such that the corresponding pulse should be experimentally realizable. Optimizers can be both deterministic or stochastic. Deterministic optimizers are in general not real global optimizers, i.e., if there is a possibility of multiple solutions to be found out, it will always seek out the one which is nearest to the initially chosen trial solution. On the other hand, stochastic optimizers are truly global, use concepts of random walk and Markov chains, and are able to find out the correct global or best solution independent of the starting point. We will use a stochastic optimization based search to generate the pulse shape, which will be fed into the time dependent Schrödinger equation.

IV. INITIALIZATION, TIME PROPAGATION, FLUX ANALYSIS, AND OPTIMIZATION

We solve Eq. (3) numerically on two-dimensional grid with the initial condition ($t = 0$), where ψ_g is the vibrational wavefunction of the ground electronic state of HOD molecule,

$$\psi_g(r_1, r_2, t = 0) = \langle r_1, r_2 | \chi \rangle \quad (21)$$

and $\psi_e = 0$. The vibrational eigenstates ($|\chi_i\rangle$) are obtained employing two-dimensional Fourier grid Hamiltonian method.⁴⁷ The kinetic energy operator of the Hamiltonian is effected using two-dimensional fast Fourier transform (FFT) algorithm⁴⁸ and the time propagation is performed using the Lanczos scheme.⁴⁹ A linear imaginary potential is used asymptotically on both the modes to avoid unphysical reflection from the boundary. The functional form of the imaginary potential is:

$$V_{img} = V_{max} \frac{(r - r^d)}{(r^{max} - r^d)}, \quad (22)$$

where $V_{max} = 0.6$ a.u., $r^{max} = 10$ a₀, and $r^d = 7.5$ a₀. The parameters are adjusted with the convergence profile of time integrated flux in both the channels. The time integrated total flux in the channels, H + O–D and H–O + D are given by

$$J_{H+O-D} = \frac{\hbar}{2i} \int_0^{r_2^d} \int_0^T \left[\frac{1}{\mu_1} j_1(r_1 = r_1^d) + \frac{\cos \theta}{m_o} j_2(r_1 = r_1^d) \right] dr_2 dt \quad (23)$$

and

$$J_{H-O+D} = \frac{\hbar}{2i} \int_0^{r_1^d} \int_0^T \left[\frac{1}{\mu_2} j_2(r_2 = r_2^d) + \frac{\cos \theta}{m_o} j_1(r_2 = r_2^d) \right] dr_1 dt, \quad (24)$$

where $j_i = (\psi^* \frac{\partial \psi}{\partial r_i} - \psi \frac{\partial \psi^*}{\partial r_i})$. μ_i and r_i^d are the reduced mass, and a grid point in the asymptotic region of the i th channel (O–H/O–D).

In order to transfer maximum population from $|0, 0\rangle$ to low quanta vibrational levels of the ground electronic state and to pump from the lower state to the repulsive one for selective OH/OD bond dissociation, we need to optimize the IR pulse and if necessary, the UV pulse by using Simulated Annealing technique. While employing SA as stochastic technique, an objective function (also called as cost function) is defined as: $\text{cost} = (X_{pop} - 1)^2$, where $X_{pop} (= |\langle \chi_i | \psi_g(t) \rangle|^2$, χ_i is the eigenstate of \hat{H}_g) is the population in the i th target vibrational level of the ground electronic state of the molecule HOD after certain period of time propagation employing the attributes of the linear combination of eight Gaussian IR pulses as an input to the dynamics code (see Eq. (9) or (12)). In case of UV pulse optimization, the cost function can be expressed as: $\text{cost} = (X_{flux} - 1)^2$, where $X_{flux} (= J_{H+O-D}/H-O+D$, see Eqs. (23) and (24)) is the time integrated flux in the desired O–H or O–D mode.

SA is a stochastic, global search algorithm which mimics the process of annealing in metallurgy. SA uses a “temperature” like dimensionless quantity in the simulation procedure, which is kept high to begin with. A high “temperature” has the effect of inducing large thermal fluctuations, which is necessary for surmounting any optimizational barrier, if the search has led the system to be trapped in any local minimum. SA, since its proposition as a method, back in 1983, has been used extensively as a serious optimization tool in solving problems of chemistry and physics.^{50–59}

In this SA algorithm, the cost function is evaluated at each SA step. If cost function decreases, the move is accepted right away. Whereas, if cost function increases, even then SA algorithm does not allow the move to be rejected instead forward this move to Metropolis test as briefly presented here. If the change in the value of the cost function in two consecutive SA steps is positive, the probability of accepting the move is determined by the function $F = \exp(-\Delta/T)$, where Δ is the change in the value of the cost function in two consecutive steps and T is “temperature” like quantity. For $\Delta > 0$, F is always between 0 and 1. A random number “rand” between 0 and 1 is invoked for each evaluation of F . If $F > \text{rand}$, the move is accepted otherwise not. It is to be mentioned that at high value of T , F will be close to 1 and thus, almost all move will be accepted. At this very high value of T , larger region of the search space will be sampled. As the simulation proceeds, T is decreased according to the annealing schedule, where lower the value of T , lower will be the number of moves that qualify the Metropolis test.

V. RESULTS AND DISCUSSION

The initial and optimized values of the parameters of the hybrid IR pulse for different target vibrational levels of the ground electronic state are shown in Tables I–IV. The linear combining coefficients of the initial pulses (Eq. (17)) are assigned with equal weightage and those coefficients undergo changes while optimization processes, but normalization of the coefficients is enforced to be unity. As initial choice, the values of the other parameters (intensity, frequency, and FWHM) are taken as steadily increasing ones with the number of Gaussian pulses of the linear combining field attribute. At this point, it is important to note that in principle, SA is a global optimizer with “infinity” number of iteration for any arbitrary choice of initial values of the parameters, but such choices could lead the SA as practically inefficient approach reaching to local solution within finite number of iteration. We have explored the optimization of the hybrid pulse with different sets of initial values of the parameters (increasing, decreasing, or both with respect to each other), but all other sets except the presented ones in Tables I–IV apparently reach to the local solutions, i.e., low population in the target vibrational level. We are not claiming that the initial sets of the values of the parameters given in Tables I–IV are the best ones to reach the global solutions, but those are either close to the global solutions or nearby of it.

When the HOD molecule is allowed to interact with a single initial Gaussian IR pulse and the frequency of the laser is in resonance between $|0, 0\rangle$ and target level ($|1, 0\rangle$ or $|0, 1\rangle$ or $|2, 0\rangle$ or $|0, 2\rangle$) of the ground electronic state, the molecule does not reach substantially to the target state but to other levels including lower/higher quanta vibrational states and thereby, selectivity of dissociation for OH or OD bond could not be achieved. On the contrary, when we initialize the wavefunction at $|0, 0\rangle$ and target at $|1, 0\rangle$ level of the ground electronic state, optimal population in $|1, 0\rangle$ state become $\approx 86\%$ after 90 SA steps of optimization of IR pulse as shown in Fig. 1(a). The IR pulse has been optimized with respect to the field attributes such as FWHM, intensity, carrier frequency, and combining coefficients for each individual pulse. The initial and optimized hybrid pulses are plotted together in Fig. 1(b). Even though the initial one is a combination of eight closely overlapping pulses, it appears as two color with asymmetrically shaped (in time) overlapping amplitude peaked at around 75 and 110 fs. On the other hand, the optimized one does not remain two color but remain asymmetric shaped in time. The Fourier transform of the initial (time dependent) field profile shows two peaks in the energy domain, where one of them dominates over the other but this domination magnifies with the optimization of the pulse parameters (see the inset in Fig. 1(b)) and smaller peak disappears, i.e., narrower band in energy domain which is required for selective vibrational excitation. Similarly, if the target vibrational state is either $|0, 1\rangle$ or $|2, 0\rangle$ or $|0, 2\rangle$ of the ground electronic state, such state accumulates the optimum population 67% or 81% or 55% after 200 or 145 or 296 SA steps of optimization of IR pulse. The optimal population and the corresponding IR pulse for the target state either $|0, 1\rangle$ or $|2, 0\rangle$ or $|0, 2\rangle$ are presented in Figs. 2(a) and 2(b) or 3(a) and 3(b) or 4(a) and 4(b).

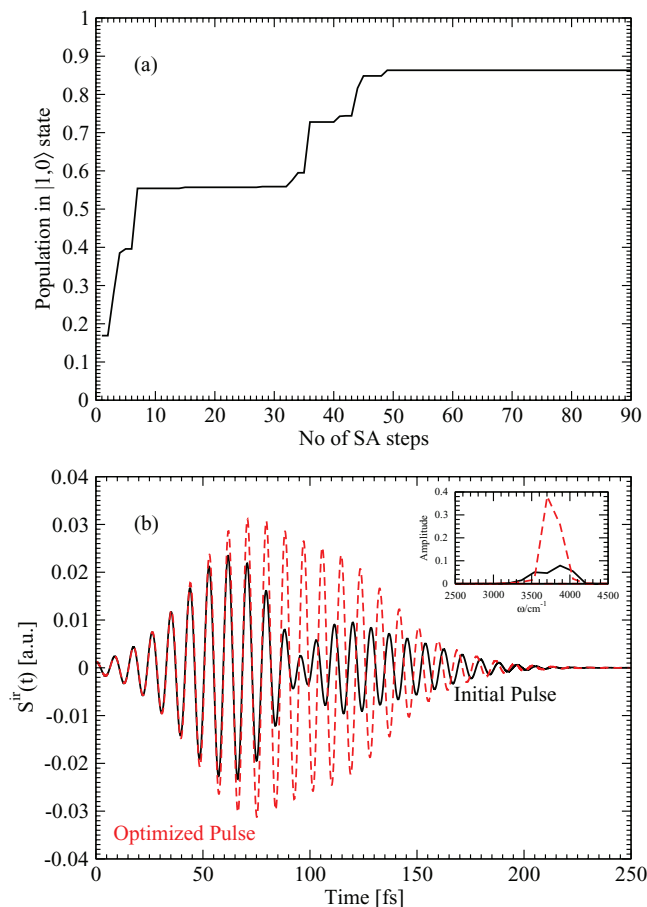
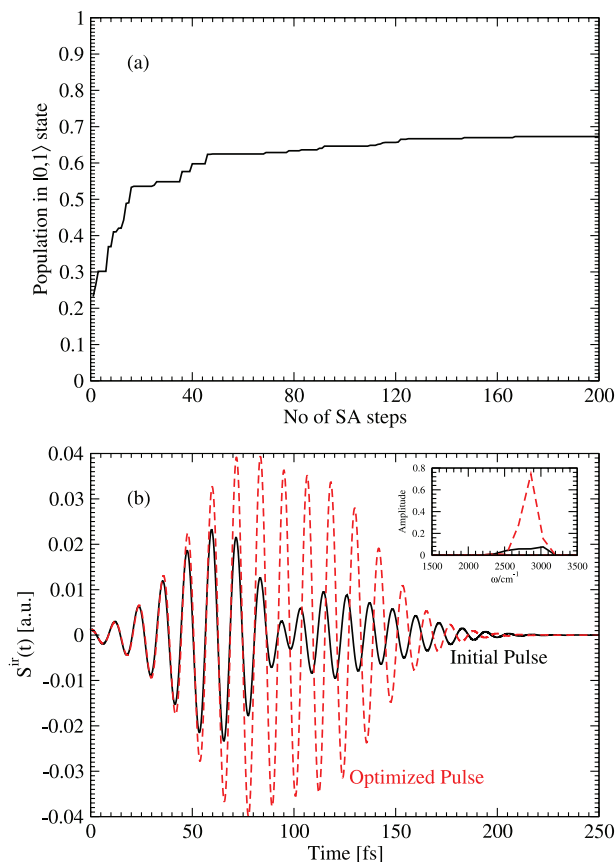
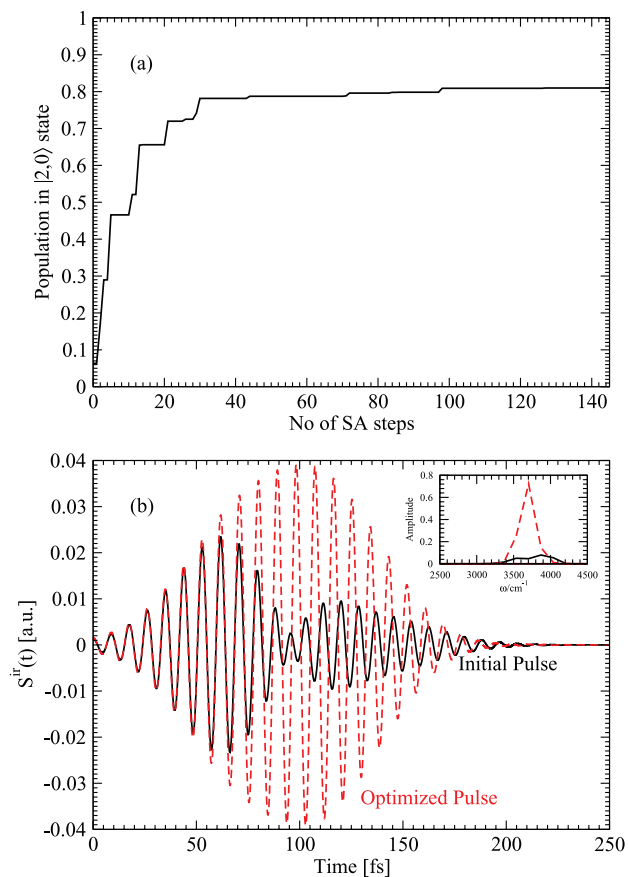
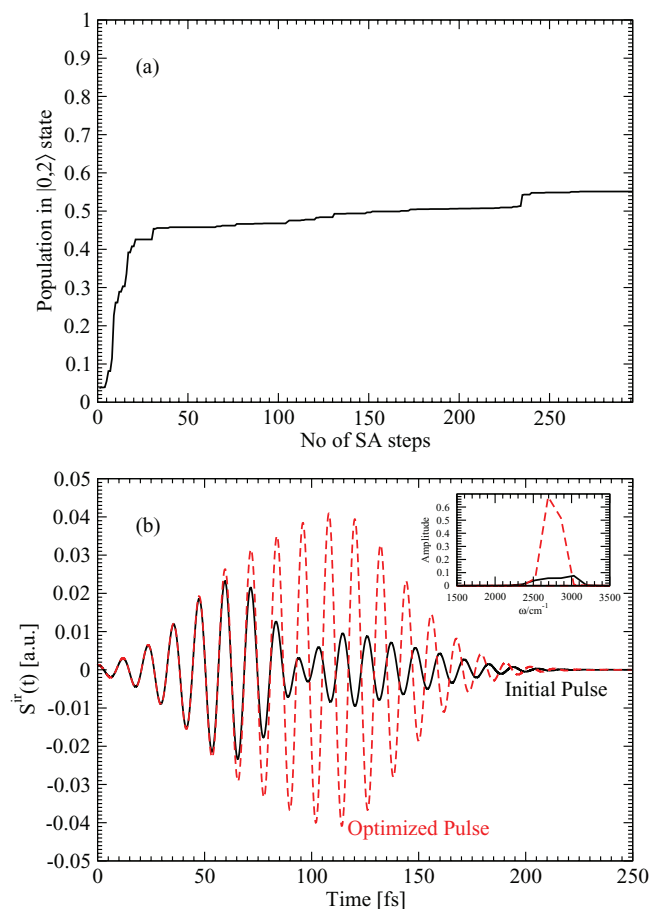


FIG. 1. (a) Population in $|1, 0\rangle$ vs. number of simulated annealing (SA) steps and (b) the corresponding initial and optimized hybrid pulse along with their Fourier transform as inset.

In all cases, we start with initial IR pulse composed of eight closely overlapping ones essentially showing two color with asymmetrically shaped (in time) amplitude peaked at around 75 and 110 fs and such IR pulse after optimization shows a single peak at different time. Though the Fourier transform of the initial (time dependent) hybrid IR pulse parameters clearly shows two peaks in energy domain, after optimization one peak is clearly magnified with respect to other one. Even in two cases ($|1, 0\rangle$, $|2, 0\rangle$), smaller peak is essentially vanished (see the inset in Figs. 2(b), 3(b), and 4(b)).

The optimized hybrid field attribute for each of the target levels ($|1, 0\rangle$ or $|0, 1\rangle$ or $|2, 0\rangle$ or $|0, 2\rangle$) is fed in the Hamiltonian and the corresponding quantum dynamics has been performed for 500 fs, where the optimized IR pulse is on up to 250 fs and then, the UV pulse is active for the remaining 250 fs. When the target state is $|1, 0\rangle$, the resulting population distribution due to initial and optimized values of the IR pulse parameters (see Table I) in various vibrational state is mapped in Figs. 5(a) and 5(b), respectively. These figures depict that with the initial choice on the values of the pulse parameters, the population is evenly spread over many low quanta vibrational levels, namely, 76% in $|0, 0\rangle$, 17% $|1, 0\rangle$, and the rest 7% population is spread over higher overtones such as $|2, 0\rangle$ and $|3, 0\rangle$, whereas the optimized values of the pulse parameters create about 86% population in

FIG. 2. (a) and (b) same as Figs. 1(a) and 1(b) except target state is $|0, 1\rangle$.FIG. 3. (a) and (b) same as Figs. 1(a) and 1(b) except target state is $|2, 0\rangle$.FIG. 4. (a) and (b) same as Figs. 1(a) and 1(b) except target state is $|0, 2\rangle$.

$|1, 0\rangle$ state and only 14% population is spread over its higher overtones such as $|2, 0\rangle$ and $|3, 0\rangle$. When optimized IR pulse is employed, the contour plots of the probability density are at $t = 25, 75, 175,$ and 225 fs as shown in Fig. 5(c). Since the initial wavepacket for $|0, 0\rangle$ state is perfectly symmetric with respect to O–H and O–D bonds and the wavepacket for the target state $|1, 0\rangle$ is known to be preferentially localized along O–H bond with a single node, the probability density is slightly stretched at 25 fs along the O–H bond, become prominent at 75 fs, and finally turned into a wavepacket very much close to $|1, 0\rangle$ state. Similarly, when the $|0, 0\rangle$ state wavepacket is propagated to populate the target state $|0, 1\rangle$ or $|2, 0\rangle$ or $|0, 2\rangle$ by using the corresponding pulse constructed by the initial choice on the values of the parameters, Figs. 6(a), 7(a), and 8(a) show that the population is dominantly distributed over many low quanta vibrational levels including the target state. On the contrary, with the optimized laser pulse for the corresponding target state, namely, $|0, 1\rangle$ or $|2, 0\rangle$ or $|0, 2\rangle$, we can achieve a population on that level about 67% or 81% or 55% as depicted in Figs. 6(b), 7(b), and 8(b) where rest of the population is distributed over lower and higher overtones of the target state. For all the above cases ($|0, 1\rangle, |2, 0\rangle,$ and $|0, 2\rangle$), the probability density due to optimized pulse show only slight loss of symmetry either along O–H or O–D bond at $t = 25$ fs, then the wavepackets spread at 75 fs and finally, become close to the target state either

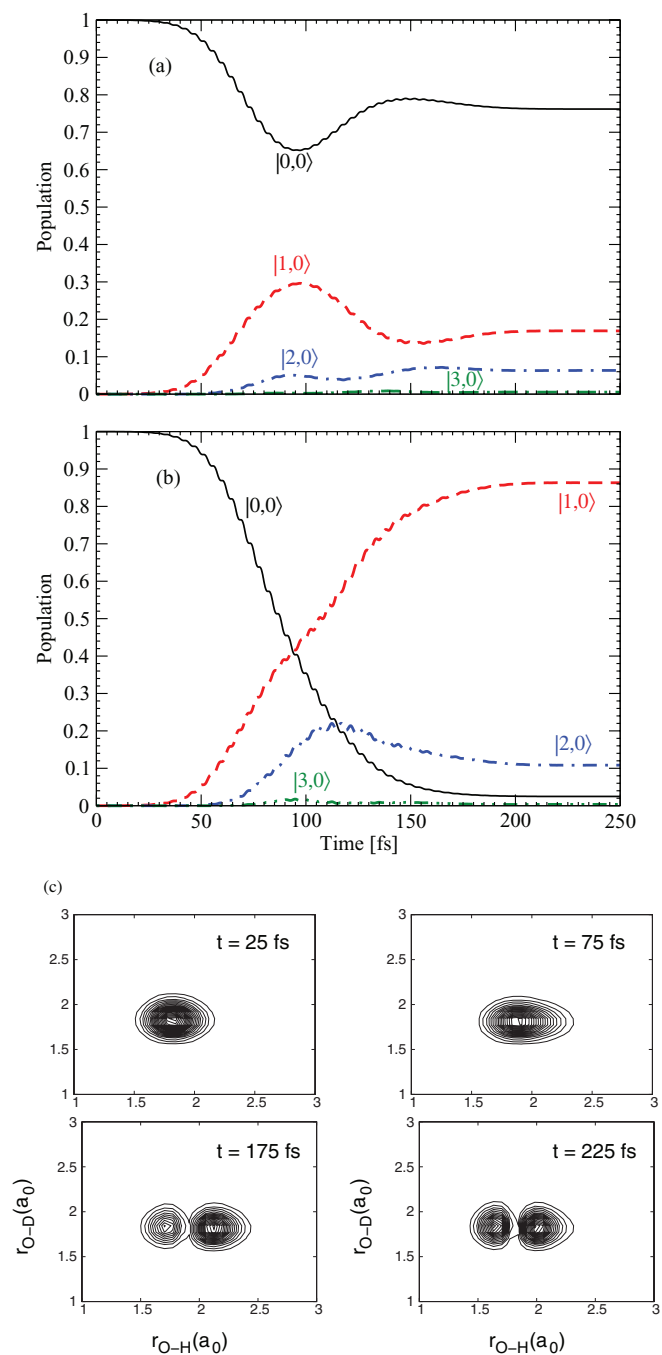


FIG. 5. Distribution of population in the vibrational levels of ground electronic state with (a) initial and (b) optimized pulse attributes. (c) Contour of time evolution of $|0, 0\rangle$ wavepacket fired with optimized IR laser pulse at $t = 25, 75, 175,$ and 225 fs.

with a single or two node(s) as shown in Figs. 6(c), 7(c), and 8(c).

When the UV laser pulse with appropriate carrier frequency (Table V) builds up at 250 fs after the low quanta vibrational excitation from $|0, 0\rangle$ to $|1, 0\rangle$ in the ground electronic state with the use of initial and optimized hybrid IR laser pulse to pump on the excited repulsive state, the population and flux analysis are shown in Figs. 9(a) and 9(b), respectively. Figure 9(a) displays that the ground state (GS) population starts decreasing as soon as UV pulse sets on

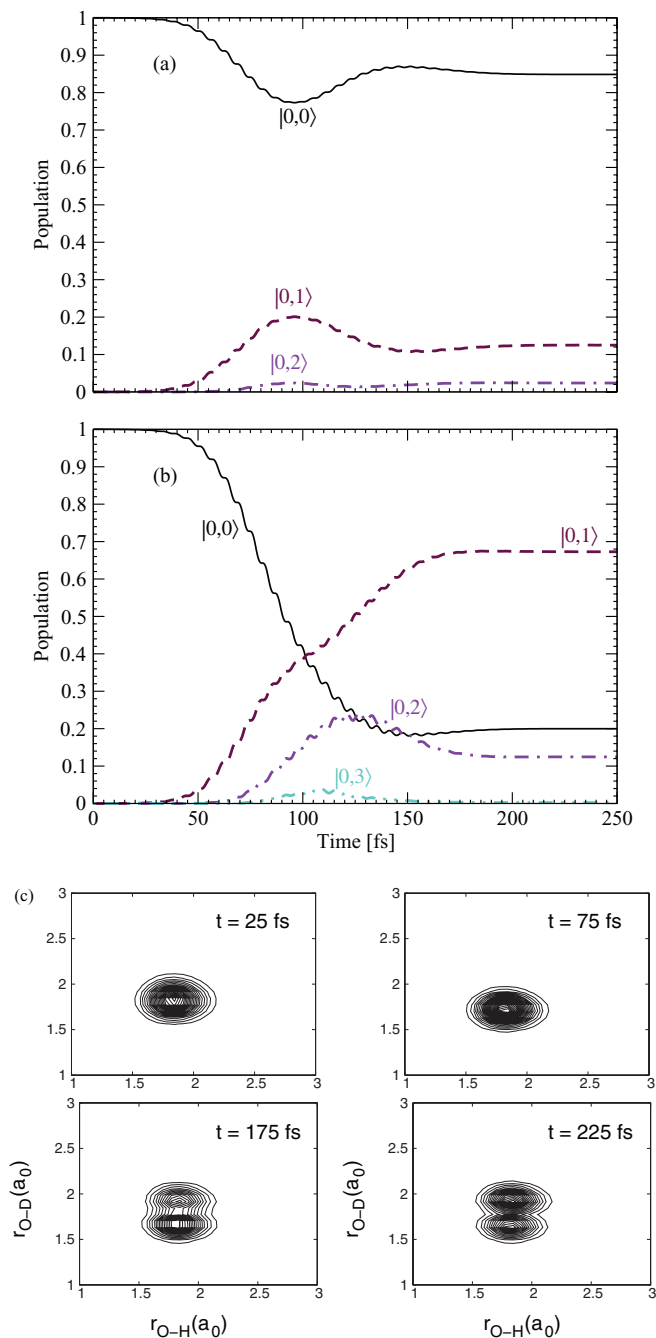
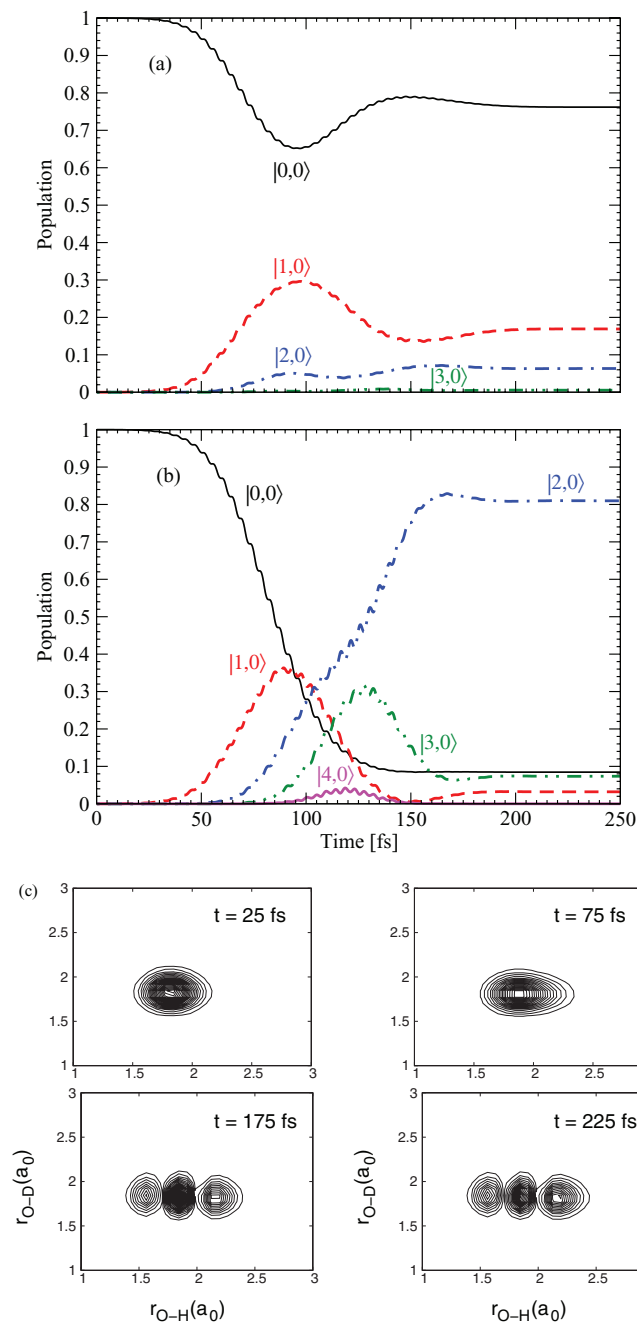
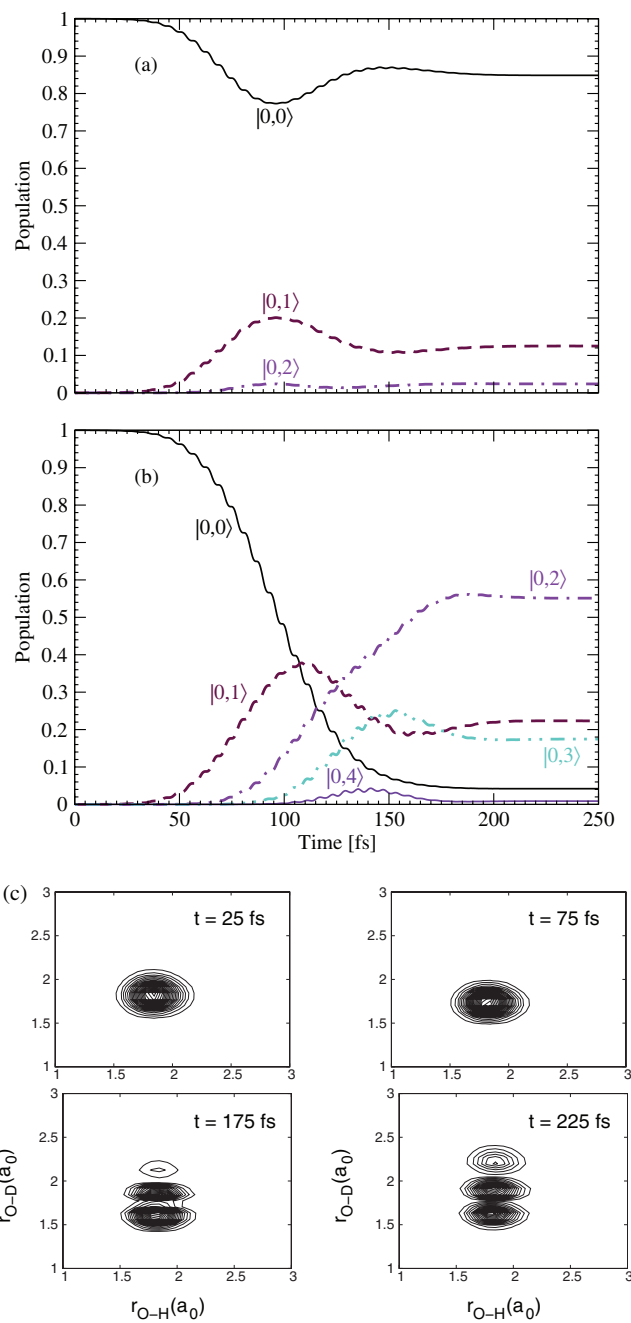


FIG. 6. (a)–(c) same as Figs. 5(a)–5(c) except target state is $|0, 1\rangle$.

and the population in excited state (ES) rises up to around 320 fs, but then, the excited state population decreases with a kick of flux flow through the O–H mode, i.e., with the absorption of wavefunction at the boundary. When the vibrational excitation is carried out with the initial choice on the values of the hybrid IR pulse parameters, the population is not even completely transferred to the excited state with the onset of UV laser pulse and the corresponding flux for the OH bond breaking grows only up to 21%. On the contrary, if the hybrid IR pulse parameters are optimized to obtain highly populated vibrationally excited molecule and then, the UV pulse sets on, both the ground and excited states population ultimately decays to zero, so that the flux on the

FIG. 7. (a)–(c) same as Figs. 5(a)–5(c) except target state is $|2, 0\rangle$.

OH channel increases up to 88% leading to absorption of the wavefunction on the boundary. The population on the excited state and its movement either on OH or OD channel (flux) can be visualized by contour plots of the probability density in Fig. 9(c), where the UV laser pulse pumps the vibrationally excited molecule from the ground electronic state to the repulsive one and the vibrational excitation in the ground electronic state is obtained by employing the optimized IR laser pulse. This figure shows that there is only small probability density transfer from ground to the excited state at 275 fs, where with the sufficient transfer of wavefunction, the density starts flowing in O–H channel on the excited state at 325 fs. Similarly, when the vibrationally excited molecule either at $|0, 1\rangle$ or $|2, 0\rangle$ or $|0, 2\rangle$ from $|0, 0\rangle$ due to the use

FIG. 8. (a)–(c) same as Figs. 5(a)–5(c) except target state is $|0, 2\rangle$.

of initial and optimized hybrid IR pulse is pumped by the UV pulse having appropriate carrier frequency (Table V), the population and flux analysis are shown in Figs. 10(a) and 10(b) or 11(a) and 11(b) or 12(a) and 12(b), respectively. Figures 10(a), 11(a), and 12(a) depict the decay and growth of the ground and excited state population up to 320 fs, but as soon as the population in the excited state starts decaying, the corresponding flux grows as shown in Figs. 10(b), 11(b), and 12(b). The UV pulse is peaked at 350 fs with the FWHM 50 fs. As long as the pulse is active, the ground and excited states interact with each other and thereby, a part of the wavefunction is delayed to reach the asymptotic channels to increase the time integrated flux. On the other hand, as soon as the UV pulse is died off, the wavefunction moves relatively

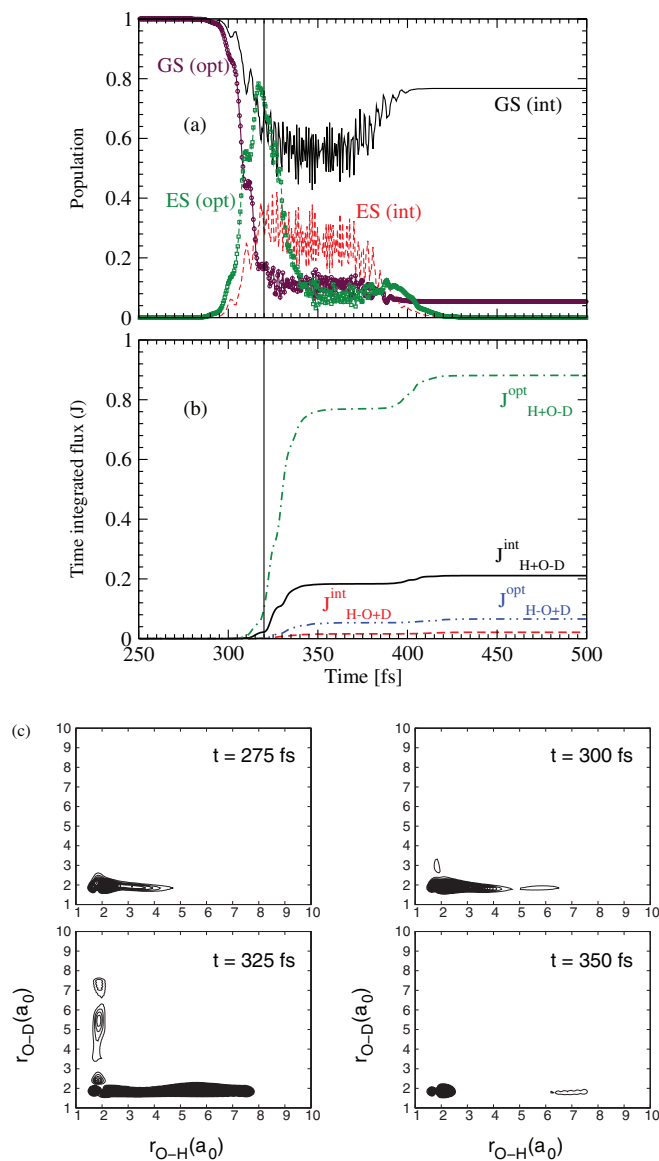


FIG. 9. The UV pulse is fired to pump the molecule from $|1, 0\rangle$ vibrational level of the ground electronic state to the excited one. (a) Population vs. time for initial and optimized IR pulse attributes, (b) Time integrated flux vs. time for initial and optimized hybrid IR pulse, and (c) Contours of time evolution of the wavepacket on the excited potential energy surface at $t = 275$, 300, 325, and 350 fs. The GS(int) and ES(int) stand for ground and excited electronic state population profile due to the initial choice of the IR/UV laser pulse field parameters, where GS(opt) and ES(opt) define the same with optimized parameters.

fast to those channels and the flux increases very sharply in a stepwise manner. If we use the initial hybrid IR laser pulse, the ground state population is not even fully transferred to the excited state during the time span of the UV pulse as depicted in Figs. 10(a), 11(a), and 12(a). On the contrary, when we use the optimized hybrid IR laser pulse, the population is completely transferred from the ground to the excited one due to the UV pulse and then, the excited state population decays after 320 fs with the growth of flux either on the OH or OD channel. The movement of the population on the excited state either in OH or OD channel are shown as probability density plots in Figs. 10(c), 11(c), and 12(c), when the vibrationally excited molecule either in $|0, 1\rangle$ or $|2, 0\rangle$ or $|0, 2\rangle$ is pumped

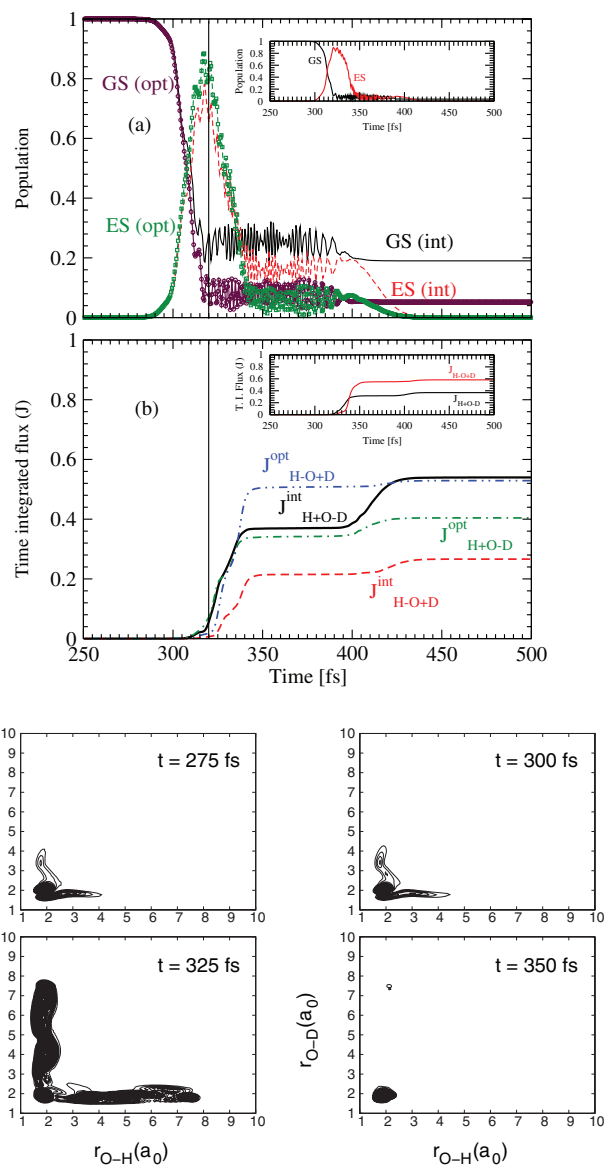


FIG. 10. (a)–(c) same as Figs. 9(a)–9(c) except the population is pumped from $|0, 1\rangle$ state. [Inset (a) shows population profile of ground and excited states vs time and (b) depicts time integrated flux vs. time when both IR and UV pulse were optimized].

by the corresponding UV pulse (see Table V). Those probability densities on the excited state at 275 fs are very little and then, grows on the same surface at 300 fs followed by a decay at 325 fs due to absorption of the wavefunction on the boundary. As the population in the low quanta vibrational levels $|1, 0\rangle$ or $|2, 0\rangle$ or $|0, 2\rangle$ due to state specific optimized hybrid IR pulse and the corresponding dissociation/flux either along OH or OD bond on the repulsive surface by UV pulse is so close, the optimization of the UV pulse is not required. On the contrary, since the difference between the population in $|0, 1\rangle$ due to the use of optimized hybrid IR pulse and its dissociation on repulsive surface by simple UV pulse is so much, we intend to optimize the UV pulse parameters (see Table V), and find different population profile (see inset of Fig. 10(a)) and higher flux (58%) than the simple UV one (55%) (see inset of Fig. 10(b)). At this point, we wish to

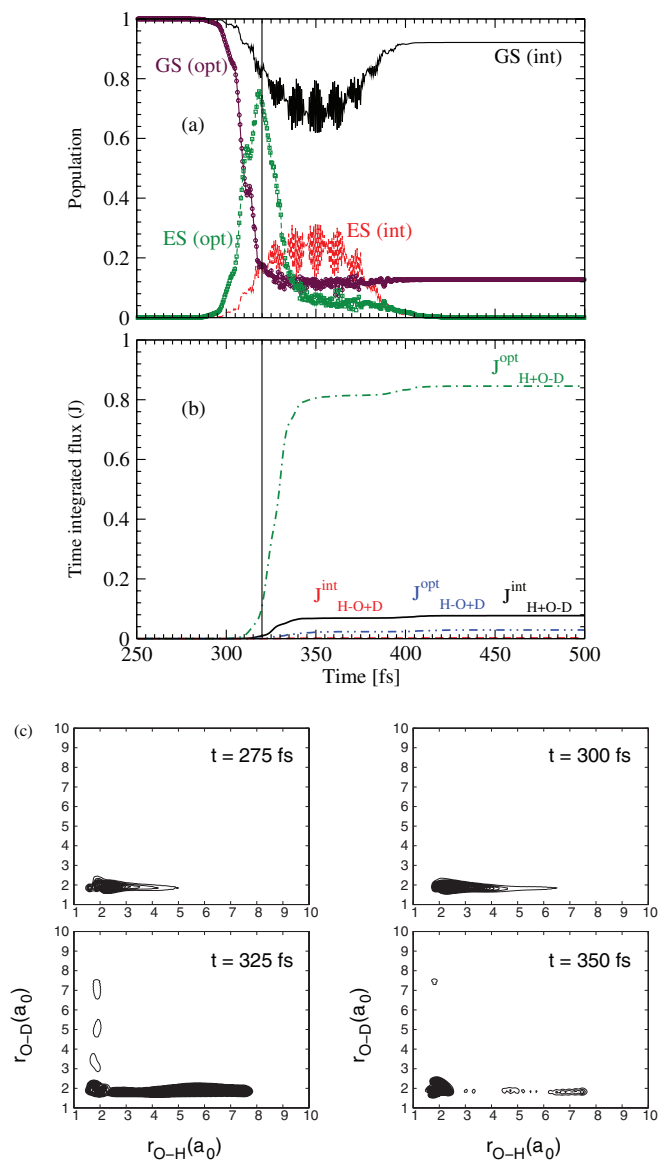


FIG. 11. (a)–(c) same as Figs. 9(a)–9(c) except the population is pumped from $|2, 0\rangle$ state.

mention the optimization of hybrid IR pulse for $|0, 1\rangle$ state followed by with or without optimized UV pulse could have produced higher flux with better initial choice on the parameters of the IR and UV pulses. Finally, we wish to explore the asymptotic ($t \rightarrow \infty$) value of time integrated flux as a function of maximum amplitude of different IR pulses, when the UV pulse parameters for specific state remain unchanged. Operationally, this is performed by optimizing parameters of the pulse ($E_{0,i}^{ir}$, ω_i^{ir} , γ_i^{ir} , and c_i^{ir}) under the constrain of a maximum value of the pulse amplitude, S_{max}^{ir} . Figures 13(a)–13(d) display the asymptotic time integrated flux $[J_{H+O-D}(t \rightarrow \infty) / J_{H+O-D}(t \rightarrow \infty)]$ as a function of maximum values of the IR pulse amplitude with and without optimizing the pulse parameters, when the initial wavefunction is located either on $|1, 0\rangle$ or $|2, 0\rangle$ or $|0, 1\rangle$ or $|0, 2\rangle$ state. Those figures clearly show that the quantity, $J_{H+O-D}(t \rightarrow \infty) / J_{H+O-D}(t \rightarrow \infty)$, decreases as the magnitude of the maximum pulse amplitude become less than 0.03 a.u. and thereby, the workability of the

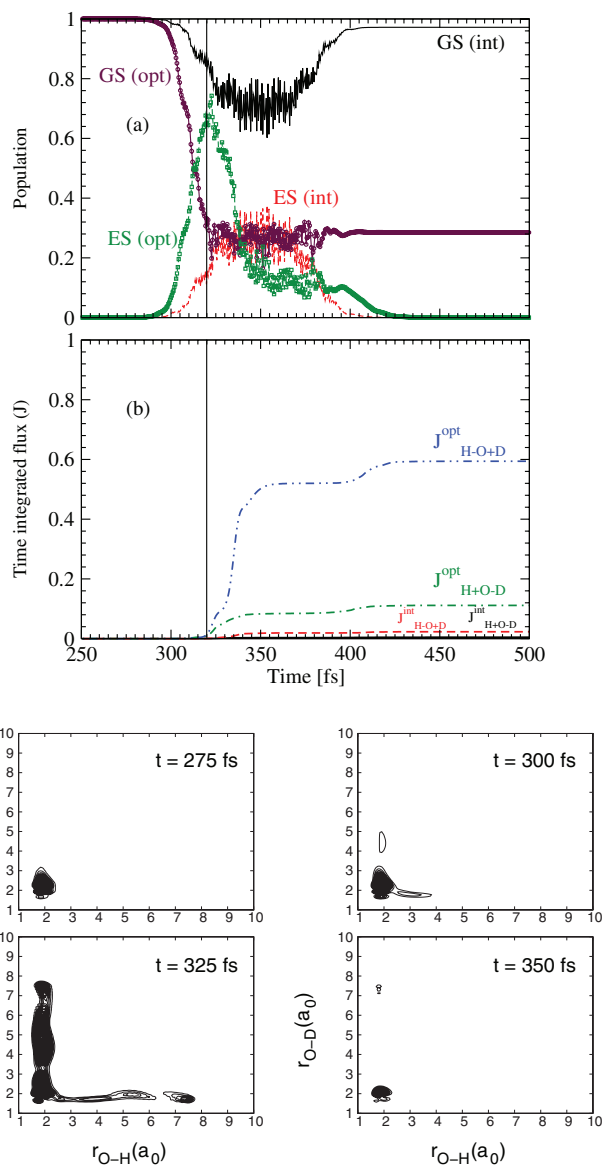


FIG. 12. (a)–(c) same as Figs. 9(a)–9(c) except the population is pumped from $|0, 2\rangle$ state.

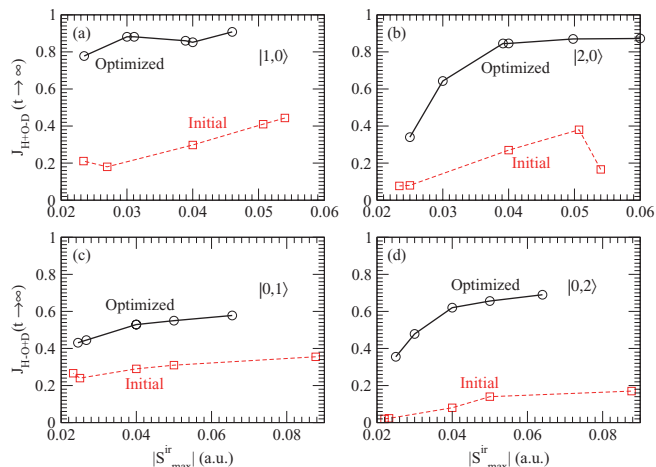


FIG. 13. Asymptotic time integrated flux, $J_{H+O-D}(t \rightarrow \infty)$ and $J_{H+O-D}(t \rightarrow \infty)$ for O–H and O–D channel, respectively, vs. maximum IR field amplitude, $|S_{max}^{ir}|$, when (a) $|1, 0\rangle$, (b) $|2, 0\rangle$, (c) $|0, 1\rangle$, and (d) $|0, 2\rangle$ as initial states.

optimized parameters for the pulses decreases significantly. At this point, we wish to mention the peak intensities for the corresponding maximum pulse amplitudes are taken from 12 to 94 TW/cm² in our calculations, where such intensities are not really far away from several experimental^{20,23} and theoretical^{27,29,34} studies on such systems.

VI. CONCLUDING REMARKS

When the quantum dynamics for selective bond dissociation of a triatomic molecule in presence of IR and UV laser field is interfaced with a stochastic optimizer, namely, simulated annealing, it is possible to obtain maximum population in a desired low quanta vibrational level through the optimization of various parameters of the hybrid IR pulse and then, quite high flux for the dissociation of a desired bond using simple/optimized UV pulse field. In order to demonstrate the workability of such a compound scheme (dynamics + optimization), we consider the HOD molecule as model system, choose $|0, 0\rangle$ vibrational state as the initial one and selectively populate either $|1, 0\rangle$ or $|0, 1\rangle$ or $|2, 0\rangle$ or $|0, 2\rangle$ of the ground electronic state to pump on the repulsive one by the UV field for desired bond dissociation either on OH or OD mode. We have performed quantum dynamics for 500 fs, where the optimization of the IR pulse is carried out for 250 fs before we apply the UV pulse for the maximum dissociation of a specific bond. This scheme has been done repeatedly until the maximum population in the target vibrational state either at $|1, 0\rangle$ or $|0, 1\rangle$ or $|2, 0\rangle$ or $|0, 2\rangle$ saturates to 86% or 67% or 81% or 55%, respectively. Finally, the molecule is pumped by UV pulse to the repulsive excited state, which leads to preferential breaking of O–H or O–D bond according to prior excitation in respective mode. Selective breaking of O–H appears as 88% from $|1, 0\rangle$ and 85% from $|2, 0\rangle$, where the preferential breaking of O–D is marked about 58% from $|0, 1\rangle$ and 59% from $|0, 2\rangle$.

We compare the results between with and without optimized hybrid IR laser pulse and found widely different populations at specific target vibrational level. On the contrary, when the optimized hybrid IR pulse is used to populate a specific target state and then, the UV pulse is allowed to interact for dissociation, the difference between the population at that vibrational level of the ground electronic state and the corresponding flux/dissociation through the repulsive surface is very small. If there is a difference between them like O–D dissociation through $|0, 1\rangle$ state, the optimization of the UV pulse has been done to reduce such problem. In this specific case, the difference arises probably due to the initial choice on the values of the hybrid IR parameters that leads to local solution by SA technique instead of reaching to the global one.

These results are quite encouraging for this lower level stochastic optimizer (SA). To get more population in the desired vibrational level, we would like to use higher level multi-temperature variant of SA and genetic algorithm (GA). On the other hand, this type of soft computing for the optimization of pulse could be interfaced in an experimental setup, where the IR or even UV laser pulse shape may be modulated through stochastic algorithm.

ACKNOWLEDGMENTS

This research has been supported by grants from Board of Research in Nuclear Sciences (BRNS) (Project No. 2009/37/42/BRNS/2265) under Department of Atomic Energy (DAE), Government of India. P.C. thanks UGC for a major research project. S.A. thanks Professor Manoj K. Mishra, Department of Chemistry, Indian Institute of Technology Bombay, Mumbai, India for stimulating discussion on equation of continuity. B.K.S. acknowledges support from CSIR, India (SRF, F. No. 09/087(0485)/2007-EMR-I) for fellowship. S.S. would like to acknowledge D. S. Kothari fellowship from UGC. T.S. and S.T. acknowledge fellowship from CSIR and UGC, respectively.

APPENDIX: CONTINUITY EQUATION AND RELATION OF FLUX WITH PROBABILITY DENSITY FOR HOD MOLECULE

The probability density (ρ) is given by

$$\rho = \psi^* \psi \quad (\text{A1})$$

$$\frac{\partial \rho}{\partial t} = \psi^* \frac{\partial \psi}{\partial t} + \psi \frac{\partial \psi^*}{\partial t}.$$

Considering the Hamiltonian of the HOD molecule and employing the time dependent Schrödinger equation, Eq. (A1) can be written as

$$\begin{aligned} \psi^* \frac{\partial \psi}{\partial t} &= \frac{1}{i\hbar} \psi^* H \psi \\ &= \frac{1}{i\hbar} \psi^* \left[\frac{\hat{p}_1^2}{2\mu_1} + \frac{\hat{p}_2^2}{2\mu_2} + \frac{\hat{p}_1 \hat{p}_2}{m_o} \cos \theta + V(r_1, r_2) \right] \psi \\ &= -\frac{1}{i} \left[\left(\frac{\hbar}{2\mu_1} \right) \psi^* \frac{\partial^2 \psi}{\partial r_1^2} + \left(\frac{\hbar}{2\mu_2} \right) \psi^* \frac{\partial^2 \psi}{\partial r_2^2} + \left(\frac{\hbar}{m_o} \right) \right. \\ &\quad \left. \times \cos \theta \psi^* \frac{\partial^2 \psi}{\partial r_1 \partial r_2} + \frac{V}{\hbar} \psi^* \psi \right]. \end{aligned} \quad (\text{A2})$$

Similarly,

$$\begin{aligned} \psi \frac{\partial \psi^*}{\partial t} &= \frac{1}{i} \left[\left(\frac{\hbar}{2\mu_1} \right) \psi \frac{\partial^2 \psi^*}{\partial r_1^2} + \left(\frac{\hbar}{2\mu_2} \right) \psi \frac{\partial^2 \psi^*}{\partial r_2^2} + \left(\frac{\hbar}{m_o} \right) \right. \\ &\quad \left. \times \cos \theta \psi \frac{\partial^2 \psi^*}{\partial r_1 \partial r_2} - \frac{V}{\hbar} \psi \psi^* \right]. \end{aligned} \quad (\text{A3})$$

On substituting Eqs. (A2) and (A3), Eq. (A1) becomes:

$$\begin{aligned} \frac{\partial \rho}{\partial t} &= \frac{\hbar}{2i\mu_1} \left[\psi \frac{\partial^2 \psi^*}{\partial r_1^2} - \psi^* \frac{\partial^2 \psi}{\partial r_1^2} \right] \\ &\quad + \frac{\hbar}{2i\mu_2} \left[\psi \frac{\partial^2 \psi^*}{\partial r_2^2} - \psi^* \frac{\partial^2 \psi}{\partial r_2^2} \right] \\ &\quad + \frac{\hbar \cos \theta}{im_o} \left[\psi \frac{\partial^2 \psi^*}{\partial r_1 \partial r_2} - \psi^* \frac{\partial^2 \psi}{\partial r_1 \partial r_2} \right] \\ &= -\frac{\hbar}{2i\mu_1} \left[\frac{\partial}{\partial r_1} j_1 \right] - \frac{\hbar}{2i\mu_2} \left[\frac{\partial}{\partial r_2} j_2 \right] \\ &\quad - \frac{\hbar \cos \theta}{2im_o} \left[\frac{\partial}{\partial r_1} j_2 + \frac{\partial}{\partial r_2} j_1 \right], \end{aligned} \quad (\text{A4})$$

where $j_1 = (\psi^* \frac{\partial \psi}{\partial r_1} - \psi \frac{\partial \psi^*}{\partial r_1})$ and $j_2 = (\psi^* \frac{\partial \psi}{\partial r_2} - \psi \frac{\partial \psi^*}{\partial r_2})$. Therefore, the continuity equation [Eq. (A4)] may now be written as

$$\begin{aligned} \frac{\partial \rho}{\partial t} = & -\frac{\partial}{\partial r_1} \left[\frac{\hbar}{2i\mu_1} j_1 + \frac{\hbar \cos \theta}{2im_o} j_2 \right] \\ & - \frac{\partial}{\partial r_2} \left[\frac{\hbar}{2i\mu_2} j_2 + \frac{\hbar \cos \theta}{2im_o} j_1 \right]. \end{aligned} \quad (\text{A5})$$

Hence, the flux expressions for O–H and O–D dissociation have additional terms (cross terms) due to the momentum coupling.

Integrating Eq. (A5) with the volume element, $dr_1 dr_2 dt$ and the limits ($r_1 = 0 - r_1^d$, $r_2 = 0 - r_2^d$, and $t = 0 - T$) and assuming flux is zero at $r = 0$, we get,

$$\begin{aligned} & \int_0^{r_1^d} \int_0^{r_2^d} \int_0^T \frac{\partial \rho}{\partial t} dr_1 dr_2 dt \\ &= - \int_0^{r_1^d} \int_0^{r_2^d} \int_0^T \left[\frac{\partial}{\partial r_1} \left(\frac{\hbar}{2i\mu_1} j_1 + \frac{\hbar \cos \theta}{2im_o} j_2 \right) \right. \\ & \quad \left. + \frac{\partial}{\partial r_2} \left(\frac{\hbar}{2i\mu_2} j_2 + \frac{\hbar \cos \theta}{2im_o} j_1 \right) \right] dr_1 dr_2 dt \\ &\Rightarrow \int_0^{r_1^d} \int_0^{r_2^d} \left(\rho(0) - \rho(T) \right) dr_1 dr_2 \\ &= \left[\int_0^{r_1^d} \int_0^T \left\{ \left(\frac{\hbar}{2i\mu_1} j_1(r_1 = r_1^d) \right. \right. \right. \\ & \quad \left. \left. + \frac{\hbar \cos \theta}{2im_o} j_2(r_1 = r_1^d) \right) \right\} dr_2 dt \\ & \quad + \int_0^{r_1^d} \int_0^T \left\{ \left(\frac{\hbar}{2i\mu_2} j_2(r_2 = r_2^d) \right. \right. \\ & \quad \left. \left. + \frac{\hbar \cos \theta}{2im_o} j_1(r_2 = r_2^d) \right) \right\} dr_1 dt \right] \\ &\Rightarrow \int_0^{r_1^d} \int_0^{r_2^d} \left(\rho(0) - \rho(T) \right) dr_1 dr_2 \\ &= J_{\text{H+O-D}} + J_{\text{H-O+D}}, \end{aligned} \quad (\text{A6})$$

where,

$$\begin{aligned} J_{\text{H+O-D}} = & \frac{\hbar}{2i} \int_0^{r_1^d} \int_0^T \left[\frac{1}{\mu_1} j_1(r_1 = r_1^d) \right. \\ & \left. + \frac{\cos \theta}{m_o} j_2(r_1 = r_1^d) \right] dr_2 dt \end{aligned} \quad (\text{A7})$$

and

$$\begin{aligned} J_{\text{H-O+D}} = & \frac{\hbar}{2i} \int_0^{r_1^d} \int_0^T \left[\frac{1}{\mu_2} j_2(r_2 = r_2^d) \right. \\ & \left. + \frac{\cos \theta}{m_o} j_1(r_2 = r_2^d) \right] dr_1 dt. \end{aligned} \quad (\text{A8})$$

Thus Eqs. (A7) and (A8) show that we need to perform time integration for calculating the flux as a function of time and the integration over the other mode(s) for evaluating the flux for a particular mode.

- ¹K. Moore and H. Rabitz, *Nat. Chem.* **4**, 72 (2012).
- ²V. V. Lozovoy, X. Zhu, T. C. Gunaratne, D. A. Harris, J. C. Shane, and M. Dantus, *J. Phys. Chem. A* **112**, 3789 (2008).
- ³R. Chakrabarti and H. Rabitz, *Int. Rev. Phys. Chem.* **26**, 671 (2007).
- ⁴H. Rabitz, *Science* **314**, 264 (2006).
- ⁵M. Shapiro and P. Brumer, *Phys. Rep.* **425**, 195 (2006).
- ⁶M. Shapiro and P. Brumer, *Principles of the Quantum Control of Molecular Processes* (Wiley, New York, 2003).
- ⁷N. E. Henriksen, *Chem. Soc. Rev.* **31**, 37 (2002).
- ⁸J. L. Herek, W. Wohleben, R. J. Cogdell, D. Zeidler, and M. Motzkus, *Nature (London)* **417**, 533 (2002).
- ⁹S. A. Rice, *Nature (London)* **409**, 422 (2001).
- ¹⁰S. A. Rice and M. Zhao, *Optical Control of Molecular Dynamics* (Wiley, New York, 2000).
- ¹¹*Femtosecond Chemistry*, edited by J. Manz and L. Wöste (Verlag Chemie, Weinheim, 1995).
- ¹²B. Just, J. Manz, and I. Trisca, *Chem. Phys. Lett.* **193**, 423 (1992).
- ¹³B. Just, J. Manz, and G. K. Paramonov, *Chem. Phys. Lett.* **193**, 429 (1992).
- ¹⁴J. Manz and G. K. Paramonov, *J. Phys. Chem.* **97**, 12625 (1993).
- ¹⁵W. Jakubetz, E. Kades, and J. Manz, *J. Phys. Chem.* **97**, 12609 (1993).
- ¹⁶E. Segev and M. Shapiro, *J. Chem. Phys.* **77**, 5604 (1982).
- ¹⁷V. Engel and R. Schinke, *J. Chem. Phys.* **88**, 6831 (1988).
- ¹⁸J. Zhang and D. G. Imre, *Chem. Phys. Lett.* **149**, 233 (1988).
- ¹⁹J. Zhang, D. G. Imre, and J. H. Frederick, *J. Phys. Chem.* **93**, 1840 (1989).
- ²⁰N. Shafer, S. Satyapal, and R. Bersohn, *J. Chem. Phys.* **90**, 6807 (1989).
- ²¹D. G. Imre and J. Zhang, *Chem. Phys.* **139**, 89 (1989).
- ²²B. Hartke, J. Manz, and J. Mathis, *Chem. Phys.* **139**, 123 (1989).
- ²³R. L. Vander Wal, J. L. Scott, and F. F. Crim, *J. Chem. Phys.* **92**, 803 (1990).
- ²⁴I. Bar, Y. Cohen, D. David, S. Rosenwaks, and J. J. Valentini, *J. Chem. Phys.* **93**, 2146 (1990).
- ²⁵R. L. Vander Wal, J. L. Scott, F. F. Crim, K. Weide, and R. Schinke, *J. Chem. Phys.* **94**, 3548 (1991).
- ²⁶I. Bar, Y. Cohen, D. David, T. Arusi-Parper, S. Rosenwaks, and J. J. Valentini, *J. Chem. Phys.* **95**, 3341 (1991).
- ²⁷B. Amstrup and N. E. Henriksen, *J. Chem. Phys.* **97**, 8285 (1992).
- ²⁸M. Shapiro and P. Brumer, *J. Chem. Phys.* **98**, 201 (1993).
- ²⁹N. E. Henriksen and B. Amstrup, *Chem. Phys. Lett.* **213**, 65 (1993).
- ³⁰Y. Cohen, I. Bar, and N. Rosenwaks, *J. Chem. Phys.* **102**, 3612 (1995).
- ³¹M. Brouard and S. R. Langford, *J. Chem. Phys.* **106**, 6354 (1997).
- ³²G. Campolieti and P. Brumer, *J. Chem. Phys.* **107**, 791 (1997).
- ³³S. Meyer and V. Engel, *J. Phys. Chem. A* **101**, 7749 (1997).
- ³⁴N. Elghobashi, P. Krause, J. Manz, and M. Ooppel, *Phys. Chem. Chem. Phys.* **5**, 4806 (2003).
- ³⁵N. E. Henriksen, K. B. Møller, and V. Engel, *J. Chem. Phys.* **122**, 204320 (2005).
- ³⁶H. Akagi, H. Fukazawa, K. Yokoyama, and A. Yokoyama, *J. Chem. Phys.* **123**, 184305 (2005).
- ³⁷K. B. Møller, H. C. Westtoft, and N. E. Henriksen, *Chem. Phys. Lett.* **419**, 65 (2006).
- ³⁸A. K. Tiwari, K. B. Møller, and N. E. Henriksen, *Phys. Rev. A* **78**, 065402 (2008).
- ³⁹M. Sarma, S. Adhikari, and M. K. Mishra, *Mol. Phys.* **107**, 939 (2009).
- ⁴⁰V. Engel, R. Schinke, and V. Staemmler, *J. Chem. Phys.* **88**, 129 (1988).
- ⁴¹V. Staemmler and A. Palma, *Chem. Phys.* **93**, 63 (1985).
- ⁴²M. D. Lika, J. E. Baggott, A. Sinha, R. L. Vander Wal, and F. F. Crim, *J. Chem. Soc., Faraday Trans. 2* **84**, 1483 (1988).
- ⁴³J. R. Reimers and R. O. Watts, *Mol. Phys.* **52**, 357 (1984).
- ⁴⁴K. S. Sorbie and J. N. Murrell, *Mol. Phys.* **29**, 1387 (1975).
- ⁴⁵K. S. Sorbie and J. N. Murrell, *Mol. Phys.* **31**, 905 (1976).
- ⁴⁶R. T. Lawton and M. S. Child, *Mol. Phys.* **40**, 773 (1980).
- ⁴⁷P. Dutta, S. Adhikari, and S. P. Bhattacharyya, *Chem. Phys. Lett.* **212**, 677 (1993).

- ⁴⁸D. Kosloff and R. Kosloff, *J. Comput. Phys.* **52**, 35 (1983).
- ⁴⁹C. Leforestier, R. Bisseling, C. Cerjan, M. D. Feit, R. Friesner, A. Guldberg, A. Hammerich, G. Jolicard, W. Karrlein, H.-D. Meyer, N. Lipkin, O. Roncero, and R. Kosloff, *J. Comput. Phys.* **94**, 59 (1991).
- ⁵⁰S. Kirkpatrick, J. C. D. Gelatt, and M. P. Vecchi, *Science* **220**, 671 (1983).
- ⁵¹S. R. Wilson and W. L. Cui, *Biopolymers* **29**, 225 (1990).
- ⁵²I. Andricioaei and J. E. Straub, *Phys. Rev. E* **53**, R3055 (1996).
- ⁵³J. Zhang, *J. Mol. Model.* **17**, 173 (2011).
- ⁵⁴M. J. van Setten, W. Lohstroh, and M. Fichtner, *J. Mater. Chem.* **19**, 7081 (2009).
- ⁵⁵E. Onbasoglu and L. Özdamar, *J. Global Optim.* **19**, 27 (2001).
- ⁵⁶M. J. Field, *J. Chem. Phys.* **103**, 3621 (1995).
- ⁵⁷P. Dutta, D. Majumdar, and S. P. Bhattacharyya, *Chem. Phys. Lett.* **181**, 293 (1991).
- ⁵⁸S. K. Biring and P. Chaudhury, *Chem. Phys.* **377**, 46 (2010).
- ⁵⁹S. Guha, S. Roy, and P. Chaudhury, *Struct. Chem.* **22**, 1007 (2011).

Optimal designing of polychromatic field for maximum dissociation of LiH molecule

S Sen, S Talukder and P Chaudhury*

Department of Chemistry, University of Calcutta, 92, A.P.C. Road, Kolkata 700 009, India

Received: 10 January 2013 / Accepted: 30 April 2013

Abstract: We present a strategy for enhancing the dissociation probability of a diatomic molecule, namely LiH, by designing optimal laser pulse. Dissociation dynamics is followed by solving time-dependent Schrödinger equation using time-dependent Fourier Grid Hamiltonian technique with optimal laser pulse function, generated by using the stochastic optimization technique of simulated annealing. We show that as we increase number of variable parameters while designing the optimal time dependent perturbation, higher dissociation is obtained. The step-wise increase in dissociation probability with the increase in complexity of designed pulse is clearly shown.

Keywords: Simulated annealing; TDFGH; Pulse shape; Dissociation probability

PACS Nos.: 82.37.Np; 05.40.-a; 02.60.Lj; 42.60.Pk

1. Introduction

The study of quantum dynamics in atomic and molecular systems under influence of ultrashort laser light has been a popular field of research in the last two decades [1–11]. During the last few years, these studies have gradually shifted their attention from the observation of system dynamics to their control and manipulation. In this regard, optimal control theory (OCT) provides a systematic tool to design fields for manipulation of molecular motion. A general aim is to steer the intramolecular dynamics to desired physical objectives, e.g., selective bond breaking through infrared excitation, control of curve-crossing reactions, selective rotational excitation as well as state selective vibrational excitation [12–36]. Several authors [5, 6] have controlled the duration of propagation of a wavepacket on an excited-state electronic potential energy surface to manipulate selective influence of product formation. Amstrup et al. [7] have treated effects of pulse shaping for Tannor-Rice scheme and applied to simple diatomic molecules. They have modulated the product yield in the photo-dissociation of a diatomic molecule by controlling the delay between pump and dump pulses. Jakubetz et al. and Manz et al. [23, 24] have proposed an

approach to control the population dynamics with ultra-short infrared pulses and applied it to a two-dimensional model of the HOD (deuterated hydrogen) stretching vibrations in the electronic ground state. They have controlled the molecular dynamics with properly chosen optimal laser fields.

Controlling a chemical event with properly designed external radiation is thus a challenging and much sought after area of work in contemporary chemical physics. Strategies adopted by workers have been varied [5–7, 12–31], but with the ultimate goal of achieving specificity and selectivity in controlling a chemical event. Even if a simple analytical pulse shape function is used, the objective of achieving high target excitations in higher vibrational levels can be achieved to some extent by using chirped pulses [14, 15], in which the variation in external frequency is incorporated in such a way that excitation in a bunch of anharmonic levels with gradually decreasing vibrational energy gap is properly achieved. Attempts have also been made to use multiphoton excitations with continuous wave lasers to achieve higher target excitation [12]. There has been substantive work on the construction of a Lagrangian based objective functional containing the principle term which maximizes the population of the target excited states, along with the constraints as regard to the amount of pulse energy transferred as well as a proper check on the fact that the Schrödinger equation should be obeyed at every point in time [37]. Several works [18–20, 23, 24]

*Corresponding author, E-mail: pinakc@rediffmail.com

deserve special attention in this regard with applications to study state selective vibrational excitation in simple anharmonic diatomic potentials, triatomic systems and rather complicated systems like adenine or adenine-thymine base pairs [28]. The strategy, one can use in designing an optimum time-dependent perturbation can be many-fold. Lagrangian based method [37], involving proper constraints is one and is widely used. An alternative strategy can focus on other parameters of time-dependent perturbation leaving the pulse shape as it is. An optimal perturbation, written down as a combination of terms having different optimal non-resonant frequencies, intensities as well as phase angles can be an alternative approach [12]. The idea would be then to use some kind of optimization scheme to find out the optimal values for the frequencies, intensities and phase angles. The obvious check that one must keep while varying values of these parameters is to keep the evaluated magnitudes of the intensities within acceptable and permitted subthreshold limits.

With these aforementioned literature in mind we have focused our attention to solving time dependent Schrödinger Equation (TDSE) in a diatomic Morse oscillator. Among several methods available in the literature in solving TDSEs we have used time dependent Fourier Grid Hamiltonian (TDFGH) method. Time-dependent part of the Fourier Grid Hamiltonian method has been proposed by Adhikari et al. [38, 39], whereas time independent part has been formerly proposed by Marston and Balint Kutti [40]. This is a special case of the so called discrete variable representation (DVR) method. Recently Ghosh et al. [12] and Guha et al. [13] have used this method of solving SE followed by coupling with some stochastic optimization techniques to explore the dependence of photo-dissociation rate on frequencies of the applied polychromatic field. The solution of SE is then allowed to interact with an external radiation field. Photo-dissociation takes place when the energy eigen-states reached by the photo absorption are in the continuum. The laser pulse shape function and time width of the pulse, which determines time of interaction of the external field with the molecule, are two important parameters of the radiation field in governing the dynamics of the system. In addition to the shape and time width two other important parameters are the intensity and the frequency of the external radiation. In order to achieve maximum dissociation probability we have stochastically optimized the polychromatic pulse. The stochastic optimization technique we have used here is Simulated Annealing (SA) [41, 42]. The inspiration for the method lies in the experimental observations on crystal formation from a melt. At temperatures above the melting point, the species that constitute the system in the melt are free to move but as the temperature is reduced, they tend to

crystallize into a solid. If the cooling is too rapid then crystals with defects are formed i.e. with metastable locally optimal structures. Such defects cost energy. With the enormous number of possible configurations with defects, the energy landscape of the cooled solid becomes very complicated with numerous local minima. A slow gradual decrease in temperature, instead of cooling rapidly, stands for a better chance of forming a perfect crystal which can be termed the global minimum energy configuration of the system and to free the system of any residual defects the idea of annealing, i.e. repeating the previous process after raising the temperature of the system to a high value again leads to the formation of a single crystal free from all defects. This natural technique of driving a thermodynamic system to the global minimum may be grafted into an optimization algorithm which then works on a simulated thermodynamic system. Although, temperature of a physical system has no relevance to the system to be optimized, one can introduce an effective temperature to transcribe the system into a simulated thermodynamic one and then search for the global minimum energy configuration of the system. SA has been effectively used in quantum mechanical calculations, especially in the optimization of parameters of wave functions [43]. SA has also been applied for solving SE for various potentials using Discretized Generator Coordinate method [44], with the use of unoptimized as well as optimized basis to generate the effective Hamiltonians [45, 46]. SA has also been used as an efficient optimization tool in several physical problems e.g. searching global geometry of atomic and molecular clusters [47], tracing out the so called Minimum Energy Path (MEP) [48] for cluster transformations on going from one stable geometry to another through a transition state (TS), in basis set optimization [43, 49] and finding optimum wave functions, in biological problems like DNA breathing dynamics [50] etc.

2. Methodology

2.1. The TDFGH formulation

The TDFGH method is quite easy and natural way for solving time dependent problems in quantum mechanics. The following section describes salient features in the method. Main aim is to solve TDSE for a given pulsed morse oscillator. TDSE can be written in the form

$$i\hbar \frac{\partial \psi}{\partial t} = H\psi \quad (1)$$

where

$$H = \frac{p^2}{2m} + V^0(x) + V'(x, t) \quad (2)$$

In Eq. (2), $V(x)$ is the morse potential and $V'(x, t)$ contains time dependent interaction of the pulse with the molecule.

$$V'(x, t) = x\epsilon(t) \sin(\omega t) = xs(t, t_p)\epsilon_0 \sin(\omega t) \quad (3)$$

where $s(t, t_p) = \sin^2(\frac{\pi t}{t_p})$ with t_p signifying single pulse width. Since at $t = 0$, the pulse shape function $s(t, t_p) = 0$, the system can be described by unperturbed Hamiltonian (H_0) at $t = 0$.

It is possible to invoke Fourier Grid Hamiltonian method for calculating the eigen functions and eigen values of H_0 ;

$$H_0|\phi_i^0(x)\rangle = \epsilon_i^0|\phi_i^0(x)\rangle, \quad i = 1, 2, \dots, N \quad (4)$$

where N is number of grid points used for presenting $|\phi_i^0\rangle$:

$$|\phi_i^0\rangle = \sum_i^N |x_i\rangle \Delta x w_i^0 \quad (5)$$

In Eq. (5), w_i^0 is values of coordinate representative of state function $|\phi_i^0\rangle$ on the corresponding grid points. Standard variational techniques are used for obtaining w_i^0 s. In TDFGH method, we represent $|\psi(x, t)\rangle$ on a uniform discretized grid with time dependent grid point amplitudes as follows:

$$|\psi(x, t)\rangle = \sum_i^n |x_i\rangle \Delta x w_i(t) \quad (6)$$

with the orthogonality condition on the grid specified as

$$\langle x_i | x_j \rangle = \delta(x_i - x_j) \quad (7)$$

Application of Dirac Frenkle variational theorem then leads to evolution equation of the grid point amplitudes $w_i(t)$ as follows:

$$\dot{w}_j = \frac{1}{\hbar} \sum_i [\langle x_j | H_0 | x_i \rangle + \langle x_j | V'(x, t) | x_i \rangle] w_i(t) \quad (8)$$

These set of N coupled differential equations can be numerically computed once values of w_j ($t = 0$) are provided. The matrix element of H_0 and V' on the right hand side can be evaluated by invoking FGH representation

$$\langle x_i | H_0 | x_j \rangle = \frac{1}{\Delta x} \left(\sum_{l=-n}^n \frac{\exp(\frac{2\pi i l (i-j)}{n})}{N} \right) T_l + V(x_i) \delta(x_i - x_j), \quad (9)$$

where $T_l = \frac{\hbar^2}{2m} (l\Delta k)^2$, $\Delta k = \frac{2\pi}{n\Delta x}$, $2n = N$.

Next we project $\psi(x, t)$ on the eigen states of H_0 to generate time dependent overlap amplitudes that describe the dynamics of time evolution of the system in terms of the eigen-states of H_0 . Assuming that the system was initially in the i th eigenstate of H at $t = 0$, the probability of finding the perturbed system in the i th state at a time t after perturbation is switched on and ψ is allowed to evolve, is given by

$$S_i(t) = |\langle \phi_i^0 | \psi(x, t) \rangle|^2, \quad i = 1, 2, \dots, N \quad (10)$$

The dissociation probability at time t with n_b number of bound states is given by

$$P_d(t) = 1 - \sum_{i=0}^{n_b} S_i(t) \quad (11)$$

2.2. SA method used for optimization

Our intention here is to cast our problem as one of optimization, such that we can solve it with the help of our stochastic global optimizer, in this case, SA method. One could well have used standard deterministic methods Newton Raphson and others, but attainment of the best possible (global) solution can only be unequivocally guaranteed by using a stochastic one. SA is one of the many stochastic search methods in common use. It is simple, easy to understand intuitively but at the same time a very potent technique. A schematic representation of the algorithm is shown in Fig. 1.

The main objective in our study is to increase the dissociation probability of LiH molecule, described by Morse potential. For any optimization technique to function, one must design a proper objective functional or sometimes referred to as the cost functional. Extremization (maximization/minimization) of this functional by properly tuning the parameter set (variables on which magnitude of the cost functional depends) is the ultimate goal of the search. For this problem, the cost functional is defined as

$$F = 1 - P_d(t) \quad (12)$$

where $P_d(t)$ is the dissociation probability at time 't'.

Though in this case our target is to achieve maximum dissociation, we can also control the extent of dissociation by manipulating cost function. As an example if the target dissociation is $x\%$ then Eq. (12) can be rewritten as

$$F = \left| \frac{x}{100} - P_d(t) \right| \quad (13)$$

SA or its variants use Monte Carlo random walks to simulate the process of metallurgical annealing. The sampling of the search space at a given temperature 'T' is done by using metropolis algorithm.

We now describe, how the process of SA is used and implemented in the problem being used. For doing a pulse

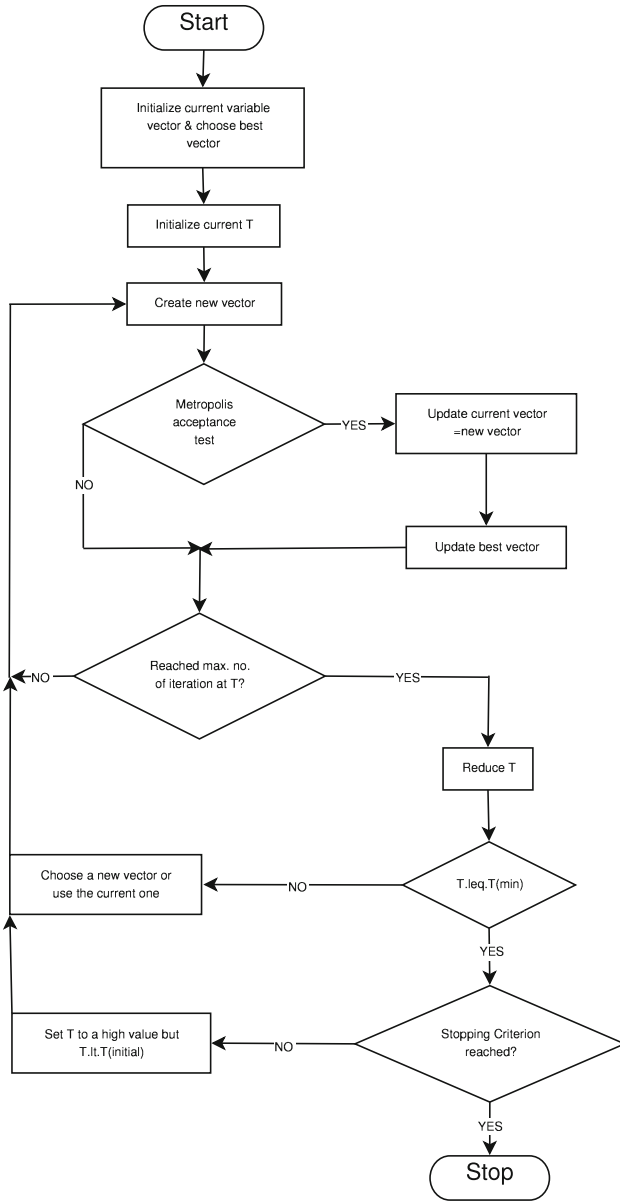


Fig. 1 Flowchart of simulated annealing technique

optimization, time dependent perturbation can be written down in terms of a set of parameters x_i , where the parameters for a given study can be six frequencies (ω_i), six pulse widths (t_p^i), six intensity terms (ϵ_0^i) and six associated coefficients (c_i). The details of such a perturbation is given in the next section.

So an algorithmic progression for solving the problem is as follows:

- (i) Start from an initial guess state x_i^{st} and calculate the values of the corresponding cost F^{st} .
- (ii) Select randomly a given parameter x_j from the set and change it or perturb it by a random amount $x_j' = x_j \pm \Delta$ (Δ is randomly generated).

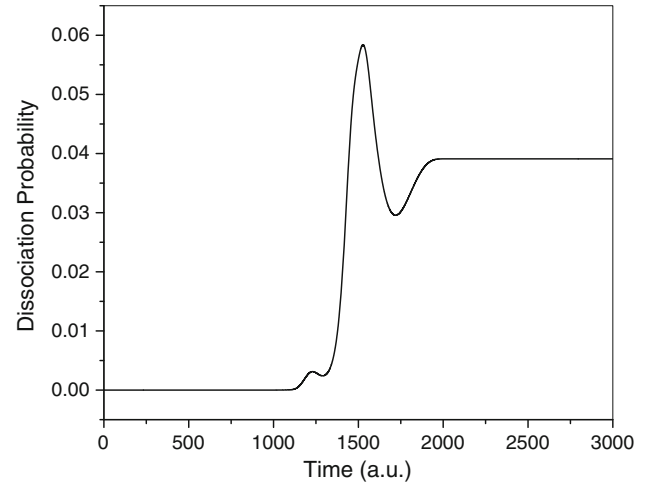


Fig. 2 Dissociation probability using 48 fs single laser pulse

- (iii) Using new set of parameters (of which one has been changed from x_j to x_j') calculate the new cost F' .
- (iv) If $F' < F$, then accept the new set as a better set as it has caused as improvement in optimization or the cost has decreased in magnitude.
- (v) If $F' > F$, do not discard the move straight away, but subject to metropolis test. In a SA simulation a simulation temperature T_{at} is assigned, which is large to begin with. With this T_{at} calculate a sampling probability term $P = \exp\left(\frac{-\Delta F}{T_{at}}\right)$, where $\Delta F = F' - F$. So ' P ' has a value between zero and one. Now call a random number (r) between 0 and 1. If $P > r$, then accept the move, even though cost has gone up. The finite chance that some moves where the cost function has increased in values needs to be accepted if optimization process has to be a truly stochastic one. If the simulation is trapped in a locally attractive basin, the system has to initially climb-up hill, surmount the barrier and proceed towards the global solution. When T_{at} is large, P is close to 1 and most moves pass the metropolis test. So the simulation temperature T_{at} controls magnitude of thermal fluctuation and helps in crossing barriers if trapped locally.
- (vi) Now to begin the next iteration step, start from the best solution so far, decrease T_{at} by a pre-assigned factor (known as annealing schedule) and continue steps (i)-(iv) till a minimum value of cost function is found. In subsequent steps T_{at} is decreased because once the optimizer finds the correct route towards the global solution, the importance of thermal fluctuation diminishes. At the later stage of search, a smooth down-hill passage in which cost function gradually decreases is enough to find the correct solution. Optimized set of parameters $\{x\}_i^{opt}$ corresponding to the minimum cost function value gives us the solution.

Table 1 Optimized frequencies and intensities (12 parameters) in order to achieve maximum dissociation

ϵ_0^i (a.u)	ω_i (a.u)
6.68178×10^{-2}	7.9999404×10^{-3}
6.52750×10^{-2}	7.9999914×10^{-3}
6.78191×10^{-2}	7.9999784×10^{-3}
6.754299×10^{-2}	7.9999988×10^{-3}
6.218782×10^{-2}	7.9999922×10^{-3}
6.743699×10^{-2}	7.9999870×10^{-3}

Table 2 Optimised pulse shape (12 parameters) in order to achieve maximum dissociation

$c_i s \times \sqrt{6}$	t_p^i (fs)
0.99951184	63.1812
1.0001756	63.1881
0.9999823	63.2119
1.0002528	63.2532
0.9997136	63.2642
1.0003610	63.1041

3. Results and discussion

We have designed a time dependent laser pulse which results increased dissociation of a diatomic Morse oscillator, in our case the LiH molecule. We have examined effect of designed perturbation at various levels of complexity with regard to

number of parameters. The parameters for Morse potential used are $D_0 = 0.9244$ a.u., $\alpha = 0.7121$ a.u., $m = 1604.87$ a.u and $x_{eq} = 3.075$ a.u. The form of potential being

$$V(x) = D_0 \{1 - \exp[-\alpha(x - x_{eq})]\}^2 \quad (14)$$

We have solved TDSE where the grid length used is 20 a.u and number of points used to describe the system on the

Fig. 3 (a) Cost function profile obtained from SA optimizing intensities (ϵ_0) and frequencies (ω), (b) Dissociation probability obtained from TDFGH method using optimized frequencies (ω) and intensities (ϵ_0), (c) Evolution profile for intensities, (d) Evolution profile for frequencies, (e) Optimized pulse shape in comparison with initial pulse

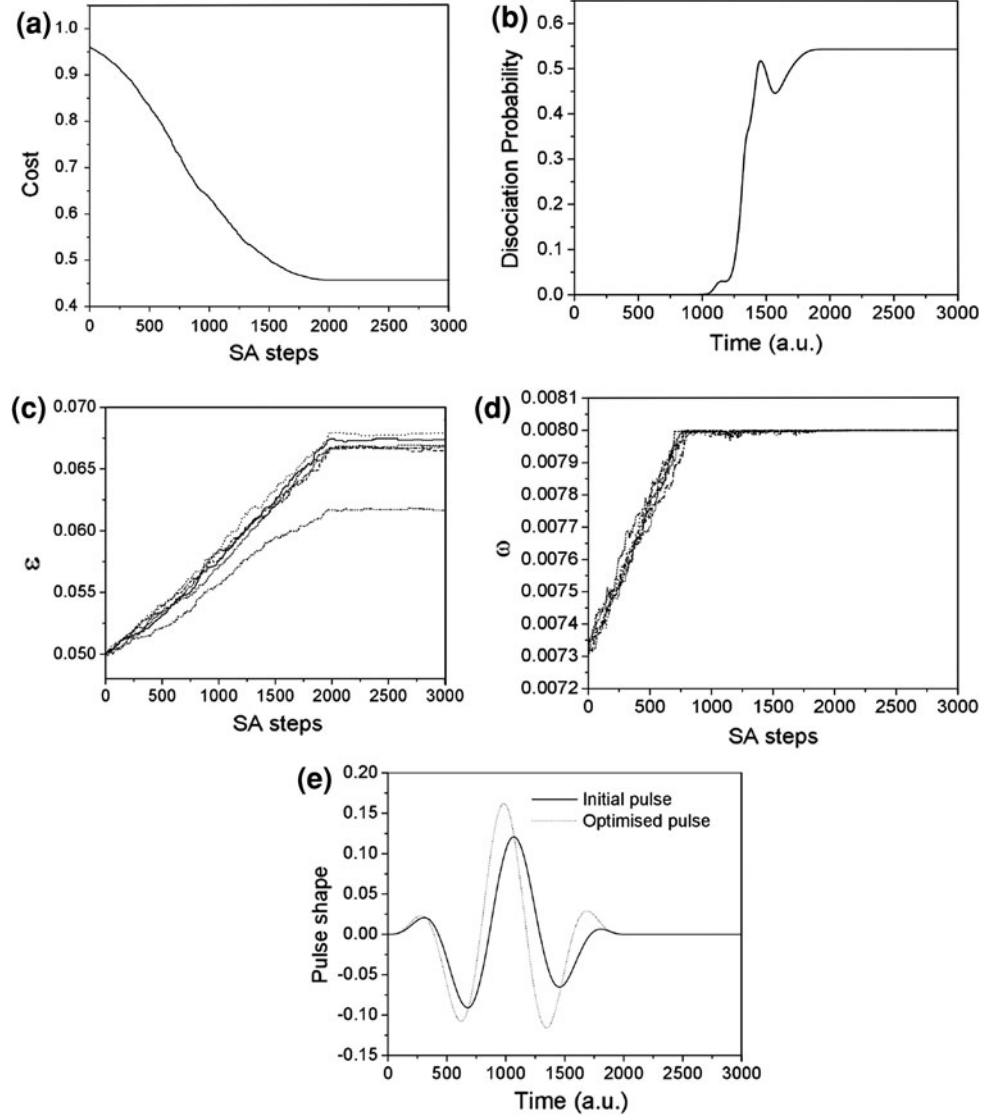


Fig. 4 (a) Dissociation probability obtained from TDFGH method using optimised pulse shape (Using 12 parameters), (b) Optimised pulse shape in comparison with initial pulse

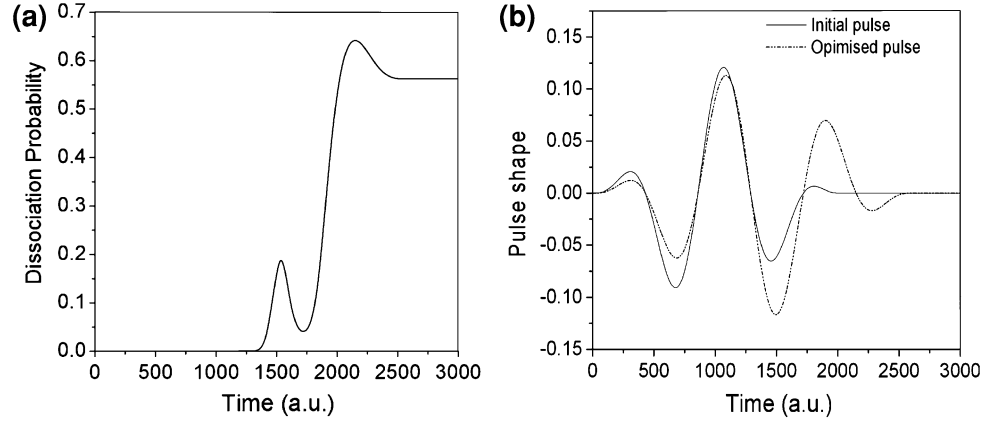


Table 3 Optimised parameters (24 parameters) in order to achieve maximum dissociation

ϵ_0^i (a.u)	ω_i (a.u)	$c_i s \times \sqrt{6}$	t_p^i (fs)
0.057776	7.9243×10^{-3}	0.963847	62.5692
0.060283	7.8213×10^{-3}	0.965654	63.8639
0.061636	7.8556×10^{-3}	1.015017	64.6005
0.058662	7.8366×10^{-3}	1.013498	62.81693
0.0631051	7.8801×10^{-3}	1.051416	64.8628
0.059481	7.8105×10^{-3}	0.9877151	63.6915

grid is 131. The form of the FGH formulation which has been used for the present work demands the use of odd number of points.

Time evolution of the system has been studied at four different levels of the form of perturbation generated by interaction of the system with the external radiation. First, we have used a very simple form of the perturbation

$$V(x, t) = x\epsilon_0 \sin(\omega t) \sin^2(\pi t/t_p) \quad (15)$$

Magnitude of the parameters being $\epsilon_0 = 0.05$ (a.u), $\omega = 0.0073$ (a.u) and the pulse width $t_p = 48$ fs. This monoharmonic, single pulse width pulse is not very effective in dissociating the molecule to a substantial extent, with the final dissociation probability obtained being 3.9 %. Fig. 2 depicts evolution of the dissociation probability with time, till the end of the pulsed perturbation.

As the next step towards designing an improved perturbation we design it as a combination of six frequencies (ω_i) and six intensities (ϵ_0^i). The usual pulse shape is also a part of perturbation. The form of perturbation now being

$$V(x, t) = \sum_i x\epsilon_0^i \sin(\omega_i t) \sin^2(\pi t/t_p) \quad (16)$$

Using this form of perturbation we use SA to optimally find out magnitude of the six ω_i s and ϵ_0^i s. The width of the pulse (t_p) is being kept at 48fs. Values of the optimal ω_i s

and ϵ_0^i s are given in Table 1. The decrease of cost function (objective function) during optimization process is shown in Fig. 3(a) and evolution of the dissociation probability till attainment of a steady value using optimized perturbation is presented in Fig. 3(b). The steady dissociation reached using this procedure is much larger with the value being 54.28 %. A probable reason for this increase in dissociation probability as compared to the earlier case is that our global optimizer finds out right frequencies which aids the vibrational dissociation process. The parameter evolution profiles of ϵ_0^i s and ω_i s obtained during optimization are presented in Fig. 3(c) and 3(d). Figure 3(e) represents the variation in optimal pulse shape with respect to the initial one.

We have used SA to design a pulse, which can aid dissociation process. Here the frequencies and the intensities are kept the same and are not allowed to vary. The perturbation is designed by combining six different sine squared pulses with varying pulse widths t_p^i . The form of perturbation used is thus

$$V(x, t) = \sum_i x\epsilon_0 \sin(\omega t) c_i \sin^2(\pi t/t_p^i) \quad (17)$$

The c_i s are coefficient parameters attached to each individual pulse shape. This gives the extent of contribution of each individual pulse shape towards dynamics. SA is used to find optimal values of six c_i s and six t_p^i s for which a steady dissociation probability is found. The optimized values of these parameters are shown in Table 2. Fig. 4(a) shows evolution of the dissociation probability with time, till a steady final dissociation value is found. The final dissociation reached is quite impressive with value being 56.24 %. Corresponding initial and final pulse shapes are shown in Fig. 4(b). This shows that an effective pulse shape generated by SA can influence the dissociation dynamics to a great extent. At this point we can safely come to the conclusion that varying the pulse widths has a better effect on the dynamics as compared to variations in

Fig. 5 (a) Dissociation probability obtained from TDFGH method using optimized pulse shape (using 24 parameters), (b) Optimized pulse shape in comparison with initial pulse

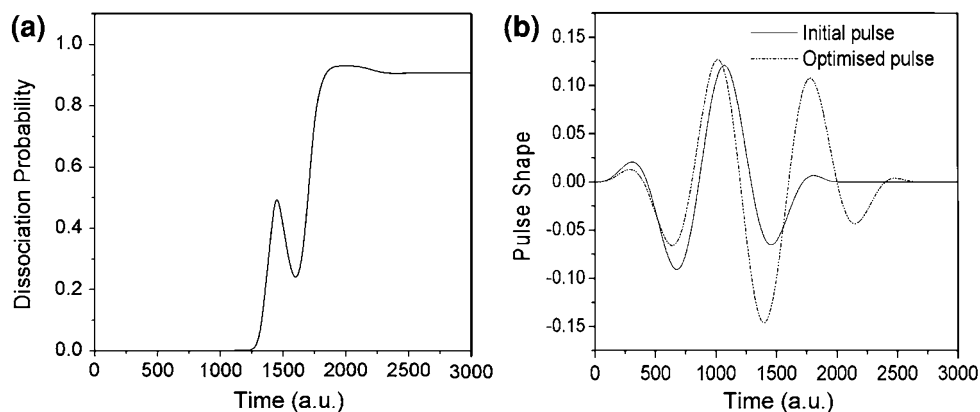


Table 4 Summary of result of optimisation

Method	Dissociation probability's (%)
Single monochromatic laser pulse (48 fs)	3.9
Optimising 6 intensities (ϵ_i s) and 6 frequencies (ω_i s) with single laser pulse (48 fs)	54.28
Optimising 6 pulsewidths (6 c_i s and 6 t_p s) with fixed frequency and intensity	56.24
Optimising 6 ϵ_i s, 6 ω_i s, 6 c_i s and 6 t_p s	90.68

frequencies and intensities. Even the intensities are kept small (0.05 a.u.), we obtain better dissociation by varying the pulse widths.

Having individually seen effects of varying the intensities and frequencies in one attempt and using an hybrid pulse shape, we examine if a time dependent perturbation involving the designing of 24 parameters, six c_i s, t_p^i s, ω_i s and ϵ_0^i s lead to even greater dissociation or not. The form of perturbation used is thus

$$V(x, t) = \sum_i x \epsilon_0^i \sin(\omega_i t) c_i \sin^2(\pi t / t_p^i) \quad (18)$$

SA is involved to find optimal values of the 24 parameters, which are shown in Table 3. Figure 5(a) shows evolution profile for the dissociation probability using the optimized parameters. Here we achieved a final steady dissociation of 90.68 %. Figure 5(b) shows the effective pulse shape found out by SA and how it differs from initial pulse.

4. Conclusions

We thus come to the conclusion that the best dissociation is achieved if the variables in the perturbing term are kept as large as possible and optimal values of those are found by some technique, which is SA in our attempt. The final dissociation probabilities obtained by the four different forms of perturbation are shown in Table 4.

Acknowledgments S. S. thanks UGC, New Delhi for granting a D. S. Kothari post-doctoral fellowship. S. T. acknowledges the financial support from UGC, New Delhi, for granting a senior Research Fellowship. P. C. thanks UGC for the award of a major research project.

References

- [1] S Shi and H Rabitz *Comp. Phys. Com.* **63** 71 (1991)
- [2] T Goswami, D K Das, S K Karthick Kumar and D Goswami *Indian J. Phys.* **86** 181 (2012)
- [3] S Shi and H. Rabitz *J. Chem. Phys.* **92** 364 (1990)
- [4] S Ghosh, B K Paul, A Chakraborty, D N Nath and N Guchhait *Indian J. Phys.* **86** 219 (2012)
- [5] D J Tannor and S A Rice *J. Chem. Phys.* **83** 5013 (1985)
- [6] D J Tannor, R Kosloff, S A Rice *J. Chem. Phys.* **85** 5805 (1986)
- [7] B Amstrup, R J Carlson, A Matro and S A Rice *J. Phys. Chem.* **95** 8091 (1991)
- [8] S Shi, A Woody and H Rabitz *Chem. Phys.* **88** 6870 (1988)
- [9] Z Y Liu, H C Du, S H Sun, L Li, L L Ma and B T Hu *Indian J. Phys.* **86** 647 (2012)
- [10] M A Mahmoud and Y E E Gamal *Indian J. Phys.* **86** 659 (2012)
- [11] S Mitra, M M Hossain, B Ray and Pradip N Ghosh *Indian J. Phys.* **84** 969 (2010)
- [12] S Ghosh, K Maji, R Sharma and S P Bhattacharyya *J. Chem. Science* **121** 757 (2009)
- [13] S Guha, N Mukherjee and P Chaudhury *Indian J. Phys.* **86** 245 (2012)
- [14] M Ghosh, R Sharma and S P Bhattacharyya *Chem. Phys. Lett.* **449** 165 (2007)
- [15] B Dahiya, D Munjal and V Prasad *Indian J. Phys.* **85** 1721 (2011)
- [16] S Sharma, H Singh and G G Balint-kurti *J. Chem. Sc.* **24** 99 (2012)
- [17] S Sharma and H Singh *Chem. Phys.* **390** 68 (2011)
- [18] S Sharma, H Singh, J Harvey and G G Balint-kurti *J. Chem. Phys.* **133** 174103 (2010)
- [19] S Sharma, H Singh and G G Balint-kurti *J. Chem. Phys.* **132** 064108 (2010)
- [20] P Kumar, S Sharma and H Singh *J. Theo. Comp. Chem.* **8** 157 (2009)
- [21] H Rabitz and W S Zhu *Acc. Chem. Res.* **33** 572 (2000)
- [22] J Botina, H Rabitz and N Rehman *J. Chem. Phys.* **102** 226 (1995)
- [23] W Jakubetz, E Kades and J. Manz *J. Phys. Chem.* **97** 12609 (1993)
- [24] J Manz and G K Paramanov *J. Phys. Chem.* **97** 12625 (1993)

-
- [25] A Mitra and H Rabitz *J. Chem. Phys.* **120** 044112 (2008)
- [26] S Shi and H Rabitz *Chem. Phys.* **139** 185 (1989)
- [27] J G B Beumee and H Rabitz *J. Math. Phys.* **31** 1235 (1990)
- [28] H Singh, S Sharma, P Kumar, N H Jeremy and G G Balint-kurty *Lect. Notes Comp. Sci.* **5102** 387 (2008)
- [29] A Kaiser and V May *Chem. Phys.* **320** 95 (2006)
- [30] O Atabek, C M Dion and A B H Yedderi *J. Phys. B* **36** 4667 (2003)
- [31] H. Rabitz *Science* **314** 264 (2006)
- [32] R S Judson and H Rabitz *Phys. Rev. Lett.* **68** 1500 (1992)
- [33] C G Elles and F F Crim *Ann. Rev. Phys. Chem.* **57** 273 (2006)
- [34] M Shapio and P Brumer *Principles of the Quantum Control of Molecular Processes* (New York, USA : Wiley) (2003)
- [35] N E Henriksen *Chem. Soc. Rev* **31** 37 (2002)
- [36] S A Rice *Nature(London)* **409** 422 (2001)
- [37] M V Korolkov, J Manz, G K Paramonov and B Schmidt *Chem. Phys. Lett.* **260** 604 (1996)
- [38] S Adhikari and S P Bhattacharyya, *Phys. Lett. A* **172** 155 (1992)
- [39] S Adhikari, P Dutta and S P Bhattacharyya *Chem. Phys. Lett.* **199** 574 (1992)
- [40] C C Marston and G G Balint-kurty *J. Chem. Phys.* **91** 3571 (1989)
- [41] S Kirkpatrick, C D Gelatt and M P Vecchi *Science* **220** 671 (1983)
- [42] S Kirkpatrick *J. Stat. Phys.* **34** 975 (1984)
- [43] P Chaudhury and S P Bhattacharyya *Inter. J. Quant. Chem.* **74** 153 (1999)
- [44] P Chaudhury and S P Bhattacharyya *Chem. Phys. Lett* **262** 764 (1996)
- [45] P Dutta and S P Bhattacharyya *Chem. Phys. Lett.* **167** 309 (1990)
- [46] S Nandi, P Chaudhury, R Sharma and S P Bhattacharyya *J. Theo. Comp. Chem.* **7** 977 (2008)
- [47] P Chaudhury, R Saha and S P Bhattacharyya *Phys. Lett. A* **291** 397 (2001)
- [48] S K Biring and P Chaudhury *Chem. Phys.* **400** 198 (2012)
- [49] S Nandi, P Chaudhury and S P Bhattacharyya *Adv. Comput. Intell.* **61** 259 (2009)
- [50] P Chaudhury, R Metzler and S K Banik *J. Phys. A* **42** 335101 (2009)



Coherent destruction of tunneling with optimally designed polychromatic external field



Subhasree Ghosh^{a,*}, Srijeeta Talukder^b, Shrabani Sen^b, Pinaki Chaudhury^b

^a Department of Chemistry, Serampore College, Hooghly, India

^b Department of Chemistry, University of Calcutta, 92 APC Road, Kolkata 700 009, India

ARTICLE INFO

Article history:

Received 27 May 2013

In final form 31 July 2013

Available online 13 August 2013

Keywords:

Coherent destruction of tunneling

Floquet theory

TDFGH method

Stochastic optimization

ABSTRACT

A suitably designed polychromatic field with a very low field strength and low frequency ($\sim 10^{-5}$ atomic unit) can bring about coherent destruction of tunneling (CDT) in a symmetric double well system. It is analyzed that in the presence of an external perturbation the difference of energy between the two lowest quasi-energy states may increase or decrease depending on the spatial and temporal nature of the perturbation. We have designed sets of polychromatic fields both spatially symmetric and antisymmetric, which cause CDT in symmetric double well system. A stochastic optimizer (Simulated Annealing) has been used to design such a polychromatic field periodic in time. Both spatial symmetry preserving or symmetry breaking perturbations may cause CDT for a symmetric double well potential.

© 2013 Elsevier B.V. All rights reserved.

1. Introduction

Tunneling is a pure quantum mechanical phenomenon which pervades all areas of chemistry and physics. Tunneling, by definition is the process which involves underbarrier transition or overbarrier reflection. Signature of tunneling is often recognized in rate constant data, where tunneling plays a crucial role in establishing the mechanism of a reaction [1–5]. Study of electron tunneling in condensed matter physics has led to the discovery of Josephson effect [6,7]. Symmetric double well potential has been used to model many physical and chemical systems and to study the effect of tunneling in the processes of interest. In molecular phenomena, double well potential functions as level splitting of tunneling. Resonant tunneling through symmetric double well has been investigated by several authors [8–10]. There are many well known systems like inversion of ammonia, proton transfer in tropolone which involve symmetric double well potentials [11,12]. Coherent control of tunneling dynamics by time dependent fields has been a well studied area of modern research [13–15]. Periodically driven double wells are also very important in contemporary research [16,17], where the destruction of classical stochasticity is suppressed due to quantum interface. Chaos assisted tunneling (CAT) is also a subject of intense scientific interest [18] and has been experimentally established in cold Cs atoms [19].

It has been experimentally realized that quantum tunneling can be controlled by external perturbations based on optimal control theory. Control of tunneling rate in a symmetric double well

system has been a subject of research during recent years. Grossman et al. [20,21] showed that for a specific monochromatic driving, tunneling can be completely suppressed and a particle will be localized in any one well of the bistable potential. This phenomenon was termed as coherent destruction of tunneling (CDT). It was reported that for some specific ratio of the field strength and frequency of the monochromatic driving, the two lowest quasi energy states of the system have exact crossing among themselves which lead to CDT. Also bichromatic fields with frequency ratio (1:2) has been used for coherent control of tunneling [22]. Bavli and Metiu [23] showed that CDT can also be achieved by applying a semi-infinite monochromatic driving. In a recent publication Kar et al. [24] showed that tunneling rate can be controlled by regulating the frequency ratio and spatial nature of the field. Coherent control of single particle tunneling in a strongly driven system was directly experimentally observed by Kierig et al. [15]. Nonlinear dynamics of a Bose–Einstein condensate also shows similar effects. Analytical and numerical result supports those experimental realizations. Lin and Ballentine reported that the tunneling rate is increased due to periodic modulation associated with chaos [25]. Researches have been carried out to compare between coherent destruction of tunneling and dynamical localization [26]. Lu et al. [16] showed that the phase lag between the two components of a bichromatic field also plays a crucial role in controlling tunneling rate. They have also shown that CDT occurs only for symmetric intense driving and the ratio of intensity and frequency ($\frac{I}{\omega}$) plays a significant role for monochromatic and symmetric two-frequency field. Their observation includes significant increase in tunneling rate for asymmetric driving. Our study mainly includes very low intensity, low frequency driving including both dipole

* Corresponding author. Tel.: +91 9674563079.

E-mail address: subhasree81@gmail.com (S. Ghosh).

interaction and quadruple interaction. Suppression of tunneling can be related to classical chaos and this connection was demonstrated by many authors [14–16,24,27–29]. In general, quantum localization is thought to be associated with the termination of classical diffusion. “Quantum localization” is a result of suppression of diffusion in the quantum region and the study of the mechanism of dynamics localization is a field of intense scientific motivation. The connection between quantum mechanical tunneling and classical chaos and their correspondence are of vital importance in this regard.

In this paper we have focused on the designing of a polychromatic field which causes CDT by driving the quasi-energy of the two lowest Floquet states to have an exact crossing. Now, exact crossing of two Floquet states leads to lowering of the tunneling rate even to such an extent that CDT may be achieved. Indeed, the exact crossing of Floquet states do not guarantee CDT, it gives an indication about CDT which has been further confirmed by our quantum dynamical calculations with the optimized data-sets. Both the field strength and the frequency of the periodic field are kept very low so that CDT can not be obtained by application of a simple monochromatic or bichromatic field. Again, with such a low frequency field ($\sim 10^{-5}$ atomic unit) it is not possible to have transition to the upper excited states. In this communication we have shown that a polychromatic field with six components can lead to CDT only when the field strengths and ratio of the frequencies of the components are suitably optimized. We have used Floquet analysis for a general polychromatic field. We have also presented the $\langle x(t) \rangle$ profiles against time to further illustrate the localization of the particle in one of the wells. This dynamics was carried out by applying TDFGH method. According to Kar et al. CDT results in case of spatial symmetry breaking perturbation only. In this paper we have shown that even a spatially symmetric interaction term, V_{int} driving, can bring in CDT if it is optimized with a suitable optimization scheme. Both for spatially symmetric and anti-symmetric V_{int} , we have designed a suitable polychromatic pulse which localizes the particle in any one of the wells irrespective of overall frequency, strength and the spatial nature of the field. Thus, by only controlling the frequency ratio between the components and their strengths one can achieve localization of the wave function in any one of the wells for external perturbation even for a very low intensity and very low frequency external field.

2. The method

2.1. Floquet theory

We start with a one dimensional bistable potential

$$V(x) = Ax^4 - Bx^2 \quad (1)$$

With this potential, the unperturbed Hamiltonian is represented by $H_0(x) = T(x) + V(x)$, $T(x)$ and $V(x)$ being the kinetic energy and potential energy contribution to the Hamiltonian respectively. This symmetric double well system is now perturbed with a polychromatic field. The time dependent Hamiltonian $H(x, t)$ is expressed as

$$H(x, t) = H_0(x) + V_{int} \quad (2)$$

where

$$V_{int} = |e|x \sum_{i=1}^p \varepsilon_i \cos \omega_i t \quad (3)$$

for dipole interaction and

$$V_{int} = |e|x^2 \sum_{i=1}^p \varepsilon_i \cos \omega_i t \quad (4)$$

for quadruple interaction, where ε_i are the intensities.

The first one does not have any spatial symmetry, so we call it spatial symmetry breaking perturbation throughout the text. Similarly the second one is called as spatial symmetry preserving perturbation.

From the time evolution profile of the Hamiltonian, we obtain the overall fundamental frequency ω for the superharmonics and express all the individual component frequencies as $\omega_i = n_i \omega$, where all the n_i 's are integers. Clearly, the Hamiltonian has the property

$$H(t) = H\left(t + \frac{2\pi}{\omega}\right) \quad (5)$$

Since the Hamiltonian is periodic in time, we can apply Floquet theory [30], the success of which lies in the fact that it replaces the semiclassical time-dependent Hamiltonian with a time-independent infinite matrix. The formalism is developed as a mathematical equivalent to the semiclassical treatment, and interpreted as a classical approximation to the quantum treatment of the field. Applying Floquet theory we obtain a hermitian matrix H_F , the elements of which are defined as

$$\langle \alpha n | H_F | \beta m \rangle = H(x, t)_{\alpha\beta}^{n-m} + n\omega \delta_{\alpha\beta} \delta_{nm} \quad (6)$$

where α and β represents the eigen states of the time periodic Hamiltonian and m , n represents the order of the Fourier components of the Hamiltonian. ω is the frequency of the overall time periodic Hamiltonian. We resolve ω into multiple frequencies i.e. ω_i with the constraint $\omega_i = n_i \omega$, where all n_i 's are integers. Substituting this into Eq. (6) we obtain

$$H(x, t) = H_0 + \sum_{i=1}^p x |e| \varepsilon_i \cos n_i \omega t \quad (7)$$

for spatially asymmetric perturbation and

$$H(x, t) = H_0 + \sum_{i=1}^p x^2 |e| \varepsilon_i \cos n_i \omega t \quad (8)$$

for spatially symmetric perturbation

Our endeavor in this paper is to optimize the time periodic external polychromatic field to achieve CDT. In other sense our optimization technique will search the entire parameter region of frequencies and field strengths such that the effective polychromatic field brings about CDT and the subsequent localisation in quantum phase space dynamics subject to the constraint that the overall strength of the field is of the order of 10^{-4} atomic unit for spatially symmetry breaking perturbation and 10^{-3} atomic unit for spatially symmetry preserving perturbation. Also the frequencies of the individual components are restricted to have values in the order of 10^{-6} atomic unit. The details of the optimization technique is discussed in the next section.

Thus the time dependent problem is transformed into a time independent one. Diagonal elements of this Floquet Hamiltonian H_{FI} can be expressed as

$$\langle \alpha n | H_{FI} | \alpha n \rangle = E_\alpha + n\omega \quad (9)$$

E_α being the eigenvalue of the unperturbed Hamiltonian H_0 at $t = 0$,

$$H_0 \phi_\alpha^0 = E_\alpha \phi_\alpha^0 \quad (10)$$

Off diagonal elements of the Floquet Hamiltonian H_{FI}

$$\langle \alpha n | H_{FI} | \beta m \rangle = \langle \phi_\alpha^0 | x | \phi_\beta^0 \rangle |e| \sum_i \varepsilon_i \Gamma_{nm}^{n_i} \quad (11)$$

or

$$\langle \alpha n | H_{FI} | \beta m \rangle = \langle \phi_\alpha^0 | x^2 | \phi_\beta^0 \rangle |e| \sum_i \alpha_i \Gamma_{nm}^{n_i} \quad (12)$$

depending on the nature of the spatial character of the interaction, where $\Gamma_{nm}^{n_i} = 0$ if $|m - n| \neq n_i$ and $\Gamma_{nm}^{n_i} = 1$ if $|m - n| = n_i$. Diagonalizing this Floquet Hamiltonian, we obtain the quasi energies as q_i . The gap between the two lowest quasi energy states Δq_{21} is given by $\Delta q_{21} = q_2 - q_1$. $\Delta q_{21} = 0$ corresponds to the exact crossing between the two lowest quasi energy states which in turn may cause CDT, as the ground state of the bi-stable potential is supposed to be populated initially.

2.2. TDFGH method

To further illustrate the complete localization of the wave function into one of the wells, we have numerically computed the dynamics of $\langle x(t) \rangle$ with the optimized data sets by using Time dependent Fourier Grid Hamiltonian (TDFGH) method [31,32] on a suitably discretized uniform co-ordinate grid. Using the orthonormalization condition on the grid

$$\langle x_p | x_q \rangle \Delta x = \delta_{pq} \quad (13)$$

the unperturbed i^{th} eigenstate at $t = 0$ is represented on the grid as follows:

$$|\phi_x^0(x, 0)\rangle = \sum_p w_{px}(0) |x_p\rangle \Delta x \quad (14)$$

When the perturbation is switched on, the wavefunction at $t > 0$ is represented on the same grid by making the grid point amplitudes time-dependent:

$$|\phi_x^0(x, t)\rangle = \sum_p w_{px}(t) |x_p\rangle \Delta x \quad (15)$$

The time dependent amplitude $w_p(t)$ is obtained by solving the evolution equation as follows:

$$\dot{w}_p = \frac{1}{\hbar} \sum_i [\langle x_p | H_0 | x_i \rangle + \langle x_p | V'(x, t) | x_i \rangle] w_i(t) \quad (16)$$

These sets of coupled differential equations can be numerically computed once the values of w_p ($t=0$) are provided. The matrix element of H_0 and V' on the right hand side can be evaluated by invoking FGH [33] representation

$$\langle x_i | H_0 | x_j \rangle = \frac{1}{\Delta x} \left(\sum_{l=-n}^n \frac{\exp(2\pi i l(i-j)/n)}{N} \right) T_l + V(x_i) \delta(x_i - x_j) \quad (17)$$

where $T_l = \frac{\hbar^2}{2m} (l\Delta k)^2$, $\Delta k = \frac{2\pi}{n\Delta x}$, $2n = N$. The particle is initially localised in the right well. Localised states (ψ_L or ψ_R) can be obtained by taking linear combination of the two lowest energy eigen states of even (ψ_{0^+}) and odd parity (ψ_{0^-}).

$$\psi_R = \frac{1}{\sqrt{2}} (\psi_{0^+} + \psi_{0^-}) \quad (18)$$

and

$$\psi_L = \frac{1}{\sqrt{2}} (\psi_{0^+} - \psi_{0^-}) \quad (19)$$

ψ_L and ψ_R denote the states localised in the left and right well respectively. To follow the quantum dynamics of the system, we have computed the quantities $\langle x(t) \rangle$ and $\langle p_x(t) \rangle$ as

$$\langle x(t) \rangle = \sum_p (w_{px}(t))^2 x_p \quad (20)$$

$$\langle p(t) \rangle = \sum_{p,q} w_{px} \cdot w_{qx} \cdot K_{p,q} \quad (21)$$

Where

$$K_{p,q} = \langle x_p | K | x_q \rangle \quad (22)$$

i.e.,

$$K_{p,q} = \frac{1}{\Delta x} \sum_{l=1}^N \frac{2i \sin(l2\pi(p-q)/N)}{N} P_l \quad (23)$$

where, the momentum operator $P_l = \hbar l \Delta k$

2.3. The Simulated Annealing method used for optimization

Our target here is to cast the problem as one of optimization, such that we can solve it with the help of stochastic global optimizer, in our case the Simulated Annealing (SA) method [34,35] is used. One could well have used standard deterministic methods Newton Raphson and others, but the attainment of the best possible (global) solution can only be unequivocally guaranteed by using a stochastic one. Simulated Annealing is one of the many stochastic search method in common use. It is simple, easy to understand intuitively but at the same time a very potent technique.

The main objective in our study is to minimize the energy difference between the two lowest quasi energy states. The cost functional for this technique is defined as

$$F = |q_2 - q_1| \quad (24)$$

where q_1 and q_2 are the energies of the first two quasi energy states.

Simulated Annealing mimics the physical process of metallurgical annealing. Like physical annealing a temperature is defined which is set to a high value at the start of the simulation and then gradually decreases the temperature to a very minimal value. This is known as 'annealing temperature' (T_{at}) and the routine of lowering the temperature known as 'annealing schedule'. The annealing temperature has no relation with the system temperature, as it is only the algorithmic parameter by which the extent of search over the solution space is guided. At high T_{at} an increasing amount of the search space is sampled. Gradually, with the lowering of temperature, the sampling space is reduced and finally the process becomes directed towards the optimum solution. If the surface is rugged, there is always a finite probability of being trapped in a local minimum. To escape such local basins, occasionally one needs to accept moves in which the cost function increases, while the eventual goal remains to reduce the cost to zero. This strategy is implemented in SA by controlling the thermal fluctuation, which is induced by the annealing temperature T_{at} . The thermal fluctuation is used to cross the energy barrier separating one minimum from the other. This is technically included by the Metropolis Test. The probability of accepting a move in Metropolis test is

$$P = \exp(-\Delta F/T_{at}) \quad (25)$$

where ΔF is the difference in cost of the two successive moves or the change in the cost functional. P can be between 0 and 1. A random number between 0 and 1 is drawn, and if P is greater than this random number, the move is accepted. At higher T_{at} , P will be close to 1 and more moves will pass the Metropolis test. The physical meaning is that at higher simulation temperature, due to strong thermal fluctuations, a greater length of search space is sampled and nearly all moves become accepted. As the simulation proceeds, T_{at} is gradually decreased. At low T_{at} , less moves pass the Metropolis test and only those moves for which the cost function predominantly decreases are accepted. In the limit $T_{at} \rightarrow 0$, the correct solution or the global minimum is obtained. SA is being used as an efficient optimization tool in several physical problems e.g. searching global geometry of atomic and molecular clusters [36], finding out the Minimum Energy Path (MEP) for cluster transformations on going from one stable geometry to another through a

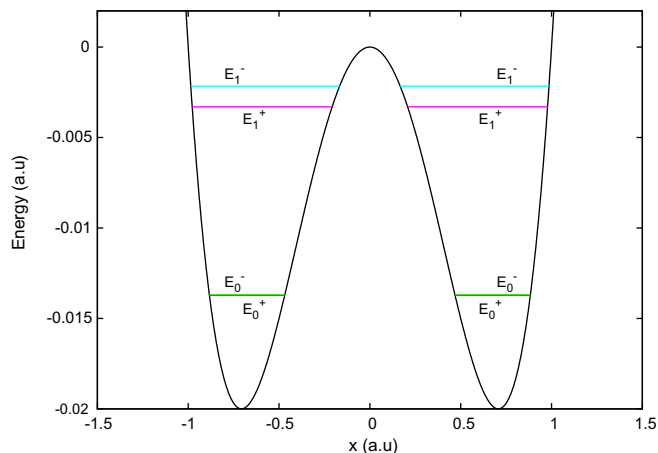


Fig. 1. Symmetric double well with the underbarrier states.

saddle point [37], in basis set optimization [38,39], in biological problems like DNA breathing dynamics etc. [40].

3. Results and discussion

Fig. 1 describes the symmetric double well and its two pairs of underbarrier states. The barrier is at $x = 0$ and the two minima are located at -0.65 atomic unit and 0.65 atomic unit. The Floquet matrix is generated by taking the lowest 25 states of the unperturbed symmetric double well system ($N_{\text{state}} = 25$) and 31 numbers of Fourier components ($N_{\text{fc}} = 31$). N_{state} and N_{fc} are chosen in such a way that further increase in N_{state} and N_{fc} does not change the quasi energies of the system. ΔE_{12} (the energy gap between two lowest states of the H_0) is 2.78×10^{-5} atomic unit. Application of an external field may increase or decrease ΔE_{12} depending on the spatial and temporal nature of the field and consequently tunneling rate increases and decreases respectively. For example, if we choose a monochromatic field with frequency ω of the order of 10^{-5} atomic unit we observe an increase in the Δq_{12} ($\Delta q_{12} = 3.31 \times 10^{-5}$ atomic unit for spatial symmetry preserving and $\Delta q_{12} = 3.07 \times 10^{-5}$ atomic unit for symmetry breaking monochromatic perturbation). By use of a bichromatic field, Δq_{12} is observed to decrease by a factor of 10 but still exact crossing between the two lowest energy Floquet states are not achieved by a general bichromatic field. We have designed a six-frequency polychromatic field which leads to an almost exact crossing of the two lowest energy Floquet states with ($\Delta q_{12} = 7.7 \times 10^{-8}$ atomic unit for spatial symmetry breaking perturbation and $\Delta q_{12} = 2.6 \times 10^{-8}$ atomic unit for symmetry preserving perturbation). In Table 1 we have presented the comparative study of

Table 1

Energy difference between the lowest quasi energy states of symmetric double well potential with different type of perturbations.

Type of field	Δq_{12}
Without field	2.779E-005
Monochromatic (spatial symmetry breaking perturbation)	3.309E-005
Monochromatic (spatial symmetry preserving perturbation)	3.070E-005
unoptimized Bichromatic (spatial symmetry breaking perturbation)	1.187E-006
unoptimized Bichromatic (spatial symmetry preserving perturbation)	3.051E-005
unoptimized polychromatic field (spatial symmetry breaking perturbation)	1.88E-004
unoptimized polychromatic field (spatial symmetry preserving perturbation)	8.64E-006
optimized Bichromatic (spatial symmetry breaking perturbation)	5.497E-007
optimized Bichromatic (spatial symmetry preserving perturbation)	1.040E-007
optimized polychromatic field (spatial symmetry breaking perturbation)	7.709E-008
optimized polychromatic field (spatial symmetry preserving perturbation)	2.611E-008

Δq_{12} for different spatial and temporal nature of perturbation, and we clearly observe the abrupt decrease of Δq_{12} with our optimised polychromatic fields. We have also designed an optimised bichromatic field both for symmetry preserving and symmetry breaking perturbations and obtained $\Delta q_{12} = 1.04 \times 10^{-7}$ and $\Delta q_{12} = 5.49 \times 10^{-7}$ respectively. It is clear that with increasing the number of frequency components in the perturbation we can increase the efficiency of the field in terms of getting lower Δq_{12} . Table 1 gives us a clear conclusion that without optimisation we can not lower Δq_{12} to such an extent that would lead to CDT. It can be stated that with lowering of Δq_{12} the transition rate from $\psi_R \rightarrow \psi_L$ decreases according to Fermi Golden rule which predicts that transition rate will be proportional to $(\frac{\Delta q_{12}}{2})^2$ [41]. The evolution profile of quasi-energies of the two lowest Floquet states with the number of generation for spatial symmetry breaking perturbation, is shown in Fig. 2(a) and (b) represents the corresponding cost profile of SA. The similar profiles are given for spatial symmetry preserving perturbation in Fig. 3. Table 2 presents the optimized data sets of polychromatic fields to achieve the aforementioned minimum energy differences both for symmetry breaking and symmetry preserving perturbations.

We have also computed the dynamics of a particle confined in one of the wells of the bistable potential using TDFGH method driven by the optimally designed polychromatic field. In our attempt at solving the Time dependent Schrodinger Equation the grid length used is 20 a.u and the number of points used to describe the system on the grid being 131. The form of the FGH formulation

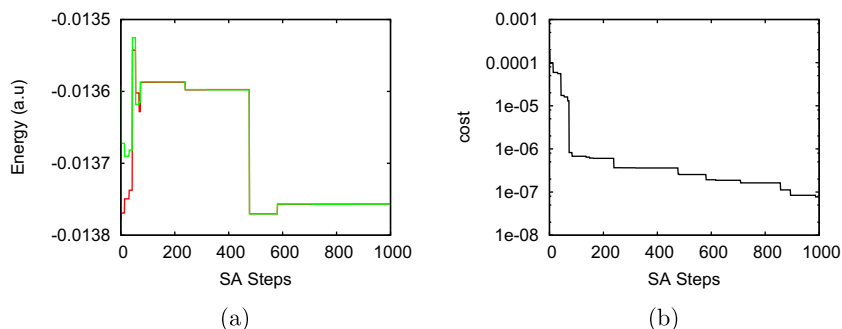


Fig. 2. (a) Evolution profile of quasi-energies of the two lowest Floquet states and (b) Cost function (in log scale) with the number of generation of Simulated Annealing for spatial symmetry breaking perturbation.

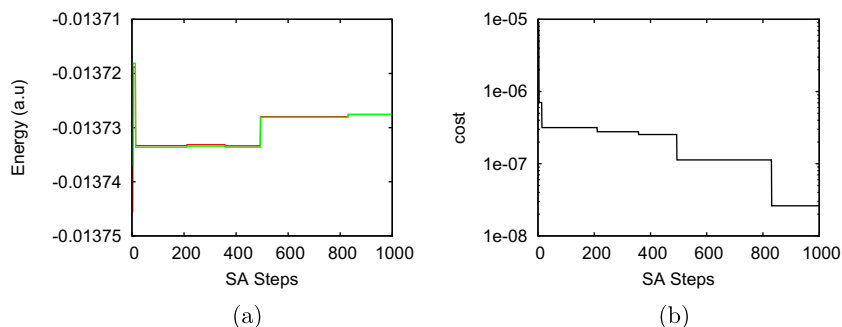


Fig. 3. (a) Evolution profile of quasi-energies of the two lowest Floquet states and (b) Cost function (in log scale) with the number of generation of Simulated Annealing for spatial symmetry preserving perturbation.

Table 2
optimized parameter sets for polychromatic perturbation.

Nature of the field	Frequency ratio	ϵ
Spatial symmetry breaking perturbation	4:8:14:15:26:5	ϵ_1 2.050E-4
		ϵ_2 5.251E-5
		ϵ_3 1.387E-4
		ϵ_4 1.195E-4
		ϵ_5 2.000E-4
		ϵ_6 2.040E-4
Spatial symmetry preserving perturbation	3:4:21:6:20:8	ϵ_1 1.570E-3
		ϵ_2 1.945E-3
		ϵ_3 1.512E-4
		ϵ_4 1.495E-3
		ϵ_5 2.829E-4
		ϵ_6 4.050E-3

which has been used for the present work demands the use of odd number of points. The initial wave function is localized in the right well as $\psi_R = \frac{1}{\sqrt{2}}(\psi_{0^+} + \psi_{0^-})$. In absence of field, the particle tunnels from left well to right well so that $\langle x(t) \rangle$ ranges from $+a$ to $-a$ ($a \approx 0.65$ a.u. for this particular case). Even in presence of a monochromatic field for both symmetry preserving or symmetry breaking perturbation the nature of the overall dynamics does not change much (red lines in Figs. 4 and 5). An unoptimised bichromatic field also fails to destroy the tunneling in the bistable potential, as a result $\langle x(t) \rangle$ oscillates from right to left well in a regular pattern (green lines in Figs. 4 and 5). For the optimized data sets of the polychromatic field, we obtain the $\langle x(t) \rangle$ ranging from $+a$

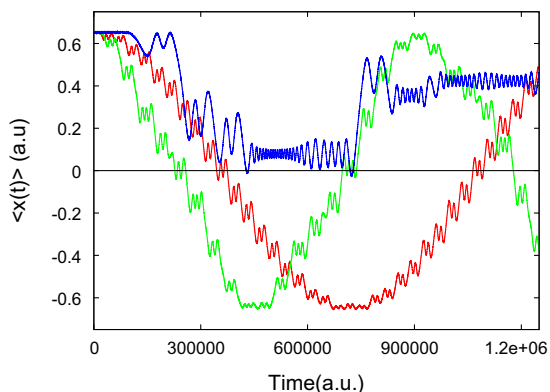


Fig. 4. Computed $\langle x(t) \rangle$ vs time in presence of monochromatic (Red line), Bichromatic (Green line) and Polychromatic (Blue line) spatial symmetry breaking perturbation. (For interpretation of the references to color in this figure legend, the reader is referred to the web version of this article.)

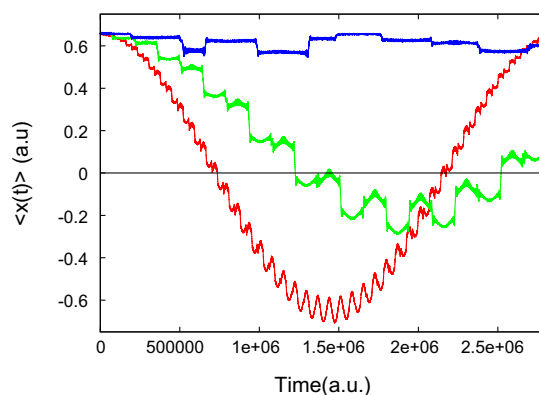


Fig. 5. Computed $\langle x(t) \rangle$ vs time in presence of monochromatic (Red line), Bichromatic (Green line) and Polychromatic (Blue line) spatial symmetry preserving perturbation. (For interpretation of the references to color in this figure legend, the reader is referred to the web version of this article.)

to 0, which means the particle does not tunnel into the left well (Blue line in Figs. 4 and 5). For convenience we have drawn the $x = 0$ line, which clearly shows that the blue lines in Figs. 4 and 5 do not cross the $\langle x(t) \rangle = 0$, where the red and green lines move back and forth with respect to $\langle x(t) \rangle = 0$ line. We have also presented the “quantum phase space” which is characterized by plotting $\langle x(t) \rangle$ against $\langle p_x(t) \rangle$ over regular intervals of time. For the unperturbed bistable potential “quantum phase space” is symmetric both around $\langle x(t) \rangle = 0$ and $\langle p_x(t) \rangle = 0$ lines. With a monochromatic symmetry breaking perturbation and monochromatic symmetry preserving perturbation (Figs. 6(a) and 7(a)) the same symmetry around $\langle x(t) \rangle = 0$ and $\langle p_x(t) \rangle = 0$ lines are still maintained. For our optimally designed polychromatic fields the symmetry of the “quantum phase space” pictures around $\langle x(t) \rangle = 0$ line are lost and localisation in the right side of the $\langle x(t) \rangle$ is observed (Figs. 6(c) and 7(c)). However the symmetry around $\langle p_x(t) \rangle = 0$ is still maintained for our optimally designed fields. Figs. 6(b) and 7(b) presents the “quantum phase space” picture for the unoptimised bichromatic fields for symmetry breaking and symmetry preserving respectively. Fig. 6(b) shows the similar trend as is shown in Fig. 6(a) (the corresponding monochromatic one). The picture of “quantum phase space” in Fig. 7(b) is not symmetric with respect to $\langle x(t) \rangle = 0$, but still the probability of having $\langle x(t) \rangle < 0$ is not negligible. It can be concluded that with increase in number of components, the quantum phase space picture shows a tendency to get localised in coordinate space but without a properly optimised perturbation it is not possible to have CDT, in general.

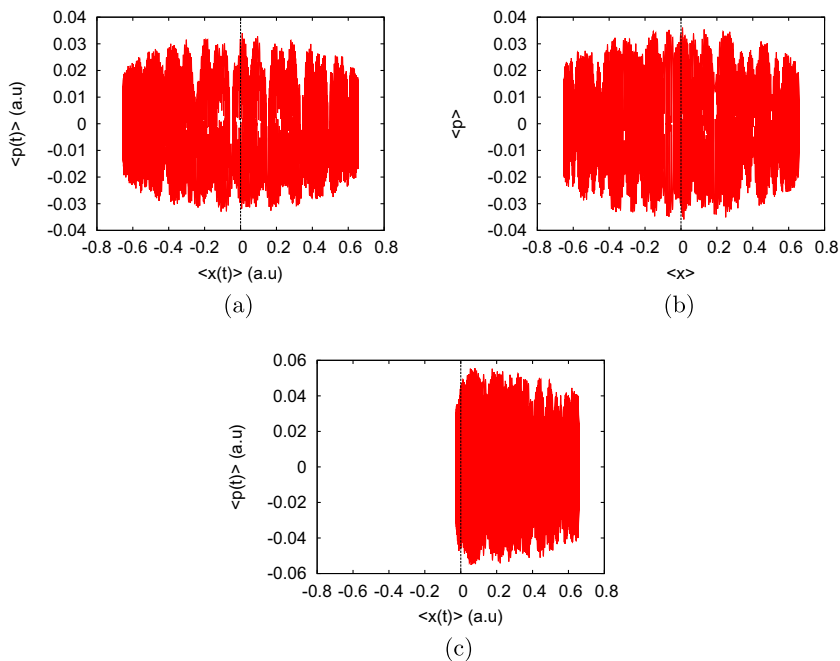


Fig. 6. The quantum phase space picture of Symmetric double well potential in presence of spatial symmetry breaking perturbation. (a) Monochromatic, (b) Bichromatic and (c) Polychromatic field.

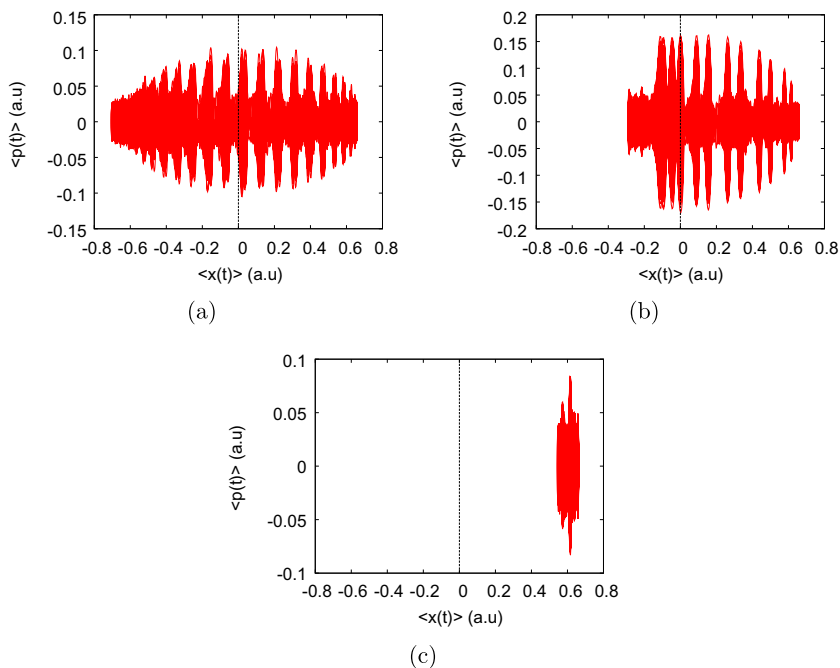


Fig. 7. The quantum phase space picture of Symmetric double well potential in presence of spatial symmetry preserving perturbation. (a) Monochromatic, (b) Bichromatic and (c) Polychromatic field.

4. Conclusion

From the above discussion it is clear that depending on the spatial and temporal nature of a time periodic field, tunneling rate can be enhanced or tunneling rate can also be completely suppressed. Our target has been to design such an external field which can completely localize a particle in one of the wells of a symmetric double well potential. By simulated annealing technique we have designed such a field which minimizes the difference between

the quasi-energies of the two lowest states so that they have an exact crossing among them and with these optimized parameter values we have obtained the dynamics of the system which clearly shows complete localization of the particle in one of the wells.

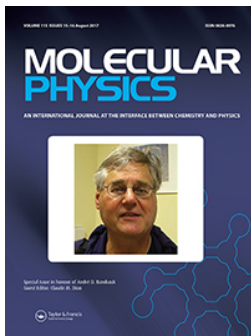
Acknowledgment

One of the authors (ST) would like to thank the UGC, New Delhi, Government of India for the award of senior research fellowship. SS

thanks the UGC, New Delhi for granting a D.S. Kothari post-doctoral fellowship. PC acknowledges the UGC for the major research project.

References

- [1] A.D. Bandrauk (Ed.), Atomic and molecular process with short intense laser pulses, NATO ASF Series B: Physics, vol. 171, Plenum, NewYork, 1988.
- [2] A.D. Bandrauk, S.C. Wallace (Eds.), Coherent phenomenon in atoms and molecules in laser fields, NATO ASF, Series B: Physics, vol. 287, Plenum, NewYork, 1992.
- [3] G.K. Ivanov, M.A. Kozhushner, L.I. Trakhtenberg, J. Chem. Phys. 113 (2000) 1992.
- [4] L.I. Trakhtenberg, V.L. Klochikhin, S. Ya, Chem. Phys. 69 (1982) 121.
- [5] A. Eckardt, T. Jinasundera, C. Weiss, M. Holthaus, Phys. Rev. Lett. 95 (2005) 200401.
- [6] J. Javanainen, Phys. Rev. Lett. 57 (1986) 3164.
- [7] M.W. Jack, M.J. Collett, D.F. Walls, Phys. Rev. A 54 (1996) 4625.
- [8] T. Miyazaki (Ed.), Atom Tunneling Phenomena in Physics, Chemistry and Biology, Springer Publication, Berlin, 2003.
- [9] P. Jung, P. Hanggi, Phys. Rev. A 44 (1991) 8032.
- [10] L. Gammaitoni, P. Hanggi, P. Jung, F. Marchesoni, Rev. Mod. Phys. 70 (1998) 223.
- [11] K.L. Jensen, F.A. Bout, Appl. Phys. Lett. 55 (1989) 669.
- [12] H. Sekiya, Y. Nagashima, Y. Nishimura, J. Chem. Phys. 92 (1990) 5761.
- [13] P. Kral, I. Thanopoulos, M. Shapiro, Rev. Mod. Phys. 79 (2007) 53.
- [14] M. Grifoni, P. Hanggi, Phys. Rep. 304 (1998) 229.
- [15] E. Kierig, U. Schnorrberger, A. Schietinger, J. Tomkovic, M.K. Oberthaler, Phys. Rev. Lett. 100 (2008) 190405.
- [16] G. Lu, W. Hai, H. Zhong, Phys. Rev. A 80 (2009) 013411.
- [17] S. Ghosh, S.P. Bhattacharyya, Int. J. Quantum Chem. 109 (2009) 1177.
- [18] R. Utermann, T. Dittrich, P. Hanggi, Phys. Rev. E 49 (1994) 273.
- [19] D.A. Steck, W.H. Oskay, M.G. Raizen, Science 293 (2001) 274.
- [20] F. Grossmann, T. Dittrich, P. Jung, P. Hanggi, Phys. Rev. Lett. 67 (1991) 516.
- [21] F. Grossmann, P. Jung, T. Dittrich, P. Hanggi, Z. Physik B 84 (1991) 315.
- [22] D. Farrelly, J.A. Milligan, Phys. Rev. E 47 (1993) R2225.
- [23] R. Bavli, H. Metiu, Phys. Rev. Lett. 69 (1992) 1986.
- [24] S. Kar, S. Ghosh, S.P. Bhattacharyya, Chem. Phys. 403 (2012) 12.
- [25] W.A. Lin, L.E. Ballentine, Phys. Rev. Lett. 65 (1990) 2927.
- [26] Y. Kayanuma, K. Saito, Phys. Rev. A 77 (2008) 010101.
- [27] J.S. Shao, P. Hanggi, Phys. Rev. A 56 (1997) R4397.
- [28] G.D. Valle, M. Ornigotti, E. Cianci, V. Fogleitti, P. Laporta, S. Longhi, Phys. Rev. Lett. 98 (2007) 263601.
- [29] G. Lu, W. Hai, H. Zhong, Q. Xie, Phys. Rev. A 81 (2010) 063423.
- [30] J.H. Shirley, Phys. Rev. 138 (1965) B979.
- [31] S. Adhikari, P. Dutta, S.P. Bhattacharyya, Chem. Phys. Lett. 199 (1992) 574.
- [32] S. Adhikari, S.P. Bhattacharyya, Phys. Lett. A 172 (1992) 155.
- [33] C.C. Marston, G.G. Balint-kurti, J. Chem. Phys. 91 (1989) 3571.
- [34] S. Kirkpatrick, C.D. Gelatt, M.P. Vecchi, Science 220 (1983) 671.
- [35] S. Kirkpatrick, J. Stat. Phys. 34 (1984) 975.
- [36] P. Chaudhury, R. Saha, S.P. Bhattacharyya, Phys. Lett. A 291 (2001) 397.
- [37] S.K. Biring, P. Chaudhury, Chem. Phys. 400 (2012) 198.
- [38] S. Nandi, P. Chaudhury, S.P. Bhattacharyya, Adv. Comput. Intell. 61 (2009) 259.
- [39] P. Chaudhury, S.P. Bhattacharyya, Int. J. Quantum Chem. 74 (1999) 153.
- [40] P. Chaudhury, R. Metzler, S.K. Banik, J. Phys. A 42 (2009) 335101.
- [41] K. Maji, S.P. Bhattacharyya, Chem. Phys. Lett. 424 (2006) 218.



Molecular Physics

An International Journal at the Interface Between Chemistry and Physics

ISSN: 0026-8976 (Print) 1362-3028 (Online) Journal homepage: <https://www.tandfonline.com/loi/tmph20>

Selective bond dissociation of HOD molecule by optimally designed polychromatic IR+UV pulse: a genetic-algorithm-based study

Srijeeta Talukder, Pinaki Chaudhury & Satrajit Adhikari

To cite this article: Srijeeta Talukder, Pinaki Chaudhury & Satrajit Adhikari (2017) Selective bond dissociation of HOD molecule by optimally designed polychromatic IR+UV pulse: a genetic-algorithm-based study, *Molecular Physics*, 115:15-16, 1786-1796, DOI: [10.1080/00268976.2016.1277591](https://doi.org/10.1080/00268976.2016.1277591)

To link to this article: <https://doi.org/10.1080/00268976.2016.1277591>

 View supplementary material 

 Published online: 27 Jan 2017.

 Submit your article to this journal 

 Article views: 152

 View related articles 

 View Crossmark data 

 Citing articles: 3 View citing articles 

BANDRAUK

Selective bond dissociation of HOD molecule by optimally designed polychromatic IR+UV pulse: a genetic-algorithm-based study

Srijeeta Talukder^a, Pinaki Chaudhury^b and Satrajit Adhikari^a

^aDepartment of Physical Chemistry, Indian Association for the Cultivation of Science, Jadavpur, Kolkata, India; ^bDepartment of Chemistry, University of Calcutta, Kolkata, India

ABSTRACT

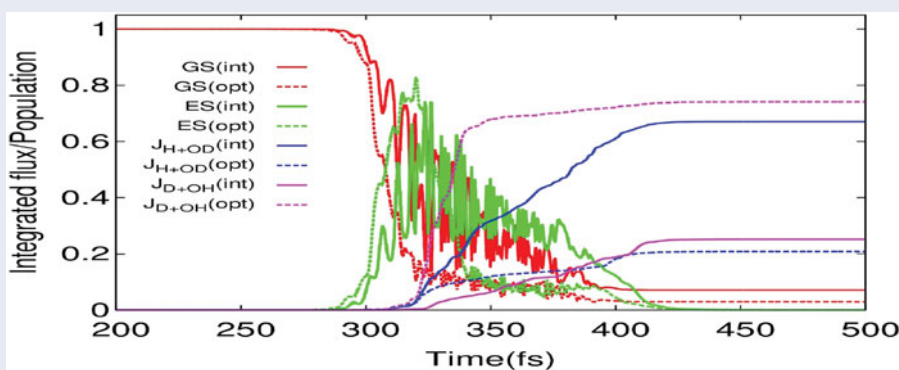
A theoretical investigation of selective bond dissociation of O–H or O–D bond of HOD molecule is carried out by optimally designed electromagnetic field where optimisation is performed by Genetic Algorithm (GA). Two strategies depending upon the objective function and variable space for optimisation have been followed to achieve selective photodissociation. In *Strategy I* flux along a particular channel ($J_{\text{H+O-D}}/J_{\text{D+O-H}}$) in the repulsive excited state of HOD is considered in defining the objective function with a polychromatic IR pulse of eight components and a UV radiation of two components being optimally found out by GA. The polychromatic IR pulse distributes the population among the low quanta vibrational states of O–H or O–D stretching mode in ground electronic state and the subsequent UV pulse transfers the population to the excited state where photodissociation occurs. According to the direction of population along O–H or O–D stretch in ground electronic state, fluxes in the channels may be expected. We have obtained a maximum value of 92.38% and 74.12% along $J_{\text{H+O-D}}$ and $J_{\text{D+O-H}}$ channels, respectively. The *Strategy II* is the conventional strategy of selective vibrational excitation followed by population transfer to excited state by single UV pulse. In this case, the polychromatic IR fields are optimised by GA to achieve selective vibrational excitation on $|1, 0\rangle$, $|2, 0\rangle$, $|0, 1\rangle$ and $|0, 2\rangle$ states and the matching single UV pulse is fired for electronic excitation. The first two states correspond to the O–H stretch and population transfer from these states to excited state result in predominant flux along H+O–D channel and similar scheme from the last two states result in D+O–H dissociation as they are effectively of O–D character. The best values of $J_{\text{H+O-D}}$ and $J_{\text{D+O-H}}$ are 86.91% and 65.94% obtained by using *Strategy II*.

ARTICLE HISTORY

Received 13 September 2016
Accepted 15 December 2016

KEYWORDS

Optimal control; selective dissociation; genetic algorithm; pulse design



1. Introduction

Selective photodissociation of HOD molecule is a problem of interest for both experimentalists and theoreticians for decades. Literature has been enriched with several interesting and noteworthy works on photodissociation of HOD [1–21]. However, both theoretical as well

as experimental works suggest that the O–H bond breaking is more feasible and selective over O–D dissociation [4,11,17–21].

Photodissociation of HOD happens in the first excited electronic state as the state is totally repulsive in nature, only having a potential barrier which effectively segregates the two channels, H+O–D and D+O–H [22,23].

CONTACT Satrajit Adhikari ✉ pcsa@iacs.res.in

Supplemental data for this article can be accessed at <http://dx.doi.org/10.1080/00268976.2016.1277591>.

© 2017 Informa UK Limited, trading as Taylor & Francis Group

Population transfer from ground electronic state to either region of this repulsive excited state leads to molecular dissociation to the corresponding channel. The potential barrier restricts the crossing of population from one channel to another. It is necessary to pre-direct the system along a particular channel (along which the dissociation is desired) in the ground electronic state before transferring the population to the repulsive state.

The low quanta vibrational modes of O–H and O–D are practically decoupled in the ground electronic state [9,11,19–21]. To get selective dissociation one has to make the system initially vibrationally excited along a desired mode. For O–H mode, the electronic excitation from one quanta vibrational excited state of ground electronic state gives effective selective dissociation, but this is not the case for O–D mode. Significant flux is observed in the H+O–D channel if population is transferred from single quanta vibrational mode of O–H bond. Preferential dissociation of O–D bond is reported to be observed by electronic excitation from higher quanta vibrational state along O–D mode, both in experimental and theoretical works [5,7].

Now it is clear that we need a two-tier strategy to selectively cleave a bond in HOD. Optimal IR laser pulse is needed for selective vibrational excitation along O–H or O–D stretching mode and then the application of UV pulse causes population transfer to the excited electronic state followed by splitting of H or D atom as the case might be. Generally, a single resonating frequency UV field is sufficient for the whole population though a combination of UV pulses might also work; however, for selective vibrational excitation optimally designed polychromatic IR pulse is a necessity.

The area of research of doing control of chemical event by radiative perturbation is commonly termed as optimal control theory (OCT) [24–36]. Different methods have been reported to obtain radiative field parameters to achieve desired goal. Most algorithms follow deterministic pathway to optimise the field parameters. However, the use of stochastic optimisers is also not unusual [37–42]. The effectivity of stochastic optimiser over a deterministic algorithm lies in its nature of optimising search direction and inherent quality to overcome potential barrier and thus it generally does not get stuck in local basins and can reach to the global solution unequivocally. Our group has demonstrated the successful use of stochastic optimiser, Simulated Annealing (SA) [43,44] in getting selective bond dissociation [39,42] and controlling tunnelling rate [40,41]. In the present communication, we want to test the potency of another stochastic optimiser, GA [45,46] to achieve selective bond cleaving of HOD molecule.

In our previous attempt for selective photodissociation study for HOD [39], we have optimised (by SA) the polychromatic IR pulse having eight components in order to selectively transfer the population to the desired vibrational state. Electronic excitation from both one and two quanta vibrational states along O–H mode results in complete transfer of population into the flux along H+O–D channel. However, only population transfer from two quanta excitation along O–D mode gives complete transfer of flux in D+O–H channel, whereas crossing of population occurs if one excites from one quanta vibration along O–D mode. Transferring population into higher quanta vibrational states generally requires higher energy and excitation from the single quanta state would be a compromise on selectivity. Thus one should balance these two factors in order to get increased flux along a particular channel along with selectivity. In this work, we want to distribute the population among low quanta vibrational states for a particular stretching and then incident a combination of UV laser pulses to achieve selective dissociation. For this purpose, we have to optimise both IR and UV pulses. The new strategy does not excite specific vibrational mode by optimal IR pulse to get selectivity and thereby, expected to be more robust where bonds are even strongly coupled. We also perform the study in the conventional way, i.e. by doing selective vibrational state excitation followed by electronic excitation and compare the results with our new strategy. We get significantly improved flux along D+O–H channel by applying both optimised polychromatic IR and UV pulses, where as both the approaches perform equally well for the other channel (H+O–D).

The paper is arranged in the following way. In Section 2, we would like to discuss the nature of the system and how the dynamics has been carried out including the process of pulse optimisation using GA. The next section contains the analysis of results obtained followed by concluding remarks.

2. Methodology

2.1. System and dynamics

A two-state model, consisting of ground and totally repulsive excited electronic states, is considered for selective bond cleaving of HOD. The time evolution of the system, i.e. time-dependent Schrödinger equation can be written as

$$i\hbar \frac{\partial}{\partial t} \begin{pmatrix} \Psi_g \\ \Psi_e \end{pmatrix} = \begin{pmatrix} \hat{H}_g + \hat{H}_{ir}(t) & \hat{H}_{uv}(t) \\ \hat{H}_{uv}(t) & \hat{H}_e \end{pmatrix} \begin{pmatrix} \Psi_g \\ \Psi_e \end{pmatrix} \quad (2.1)$$

Ψ_g and Ψ_e are the nuclear wave functions for the ground and excited electronic states, respectively. We neglect the bending motion of HOD and the system then reduces to a two-dimensional problem [11,17,47]. Ψ_j ($j = g, e$) can be expressed as $\Psi_j(r_1, r_2, t)$, where r_1 represents the O–H stretch and r_2 is for O–D stretch. The $\angle\text{HOD}$ (θ) is kept fixed at 104.52° . The concept of working with a Hamiltonian neglecting bending motions has been used earlier also. The rationale behind this is the wide difference in frequencies of the stretching and the bending modes. It can be said with a degree of certainty that while the stretching modes are getting excited with light of a certain frequency, the bending modes will not be affected as the conditions are far from the resonance condition for inducing significant bending motion.

Now the Hamiltonian for ground electronic state (\hat{H}_g) and excited state (\hat{H}_e) can be written as the sum of kinetic energy operator (\hat{T}) and potential energy operator (\hat{V}_g or \hat{V}_e):

$$\begin{aligned}\hat{H}_g &= \hat{T} + \hat{V}_g, \\ \hat{H}_e &= \hat{T} + \hat{V}_e.\end{aligned}\quad (2.2)$$

If p_1 and p_2 are the conjugate momenta along O–H and O–D stretches, the expression of \hat{T} would be

$$\hat{T} = \frac{\hat{p}_1^2}{2\mu_1} + \frac{\hat{p}_2^2}{2\mu_2} + \frac{\hat{p}_1\hat{p}_2}{m_O} \cos\theta, \quad (2.3)$$

where

$$\begin{aligned}\hat{p}_j &= \frac{\hbar}{i} \frac{\partial}{\partial r_j}, \quad j = 1, 2, \\ \mu_1 &= \frac{m_H m_O}{(m_H + m_O)}, \\ \mu_2 &= \frac{m_O m_D}{(m_O + m_D)},\end{aligned}$$

with m_O , m_H and m_D are the masses of O, H and D, respectively.

Well-defined potential functions exist both for the ground and excited states of HOD molecule. The O–H and O–D vibrations are expressed by Morse potentials and a coupling between two Morse is there, whereas the potential surface of repulsive excited state is obtained by fitting *ab initio* data. The detailed discussion of the potential surfaces and the parameters is given elsewhere [19,39,48–50].

The dynamics is started from the ground vibrational state. The vibrational states are obtained by solving time-independent Schrödinger equation for ground electronic state Hamiltonian (\hat{H}_g) using two-dimensional Fourier grid Hamiltonian method. The vibrational state is

denoted as $|n_1, n_2\rangle$, where n_1 and n_2 represent the quantum numbers for O–H and O–D stretches, respectively. At $t = 0$,

$$\begin{aligned}\Psi_g &= |0, 0\rangle \\ \Psi_e &= 0\end{aligned}\quad (2.4)$$

In Equation (2.1), the \hat{H}_{ir} and \hat{H}_{uv} account to the interaction with IR laser pulse and UV pulse, respectively:

$$\hat{H}_{ir}(t) = -\vec{\mu}_g(\mathbf{r}_1, \mathbf{r}_2) \cdot \vec{S}^{ir}(t) \quad (2.5)$$

$\vec{\mu}_g(\mathbf{r}_1, \mathbf{r}_2)$ is the electric dipole moment in ground electronic state where r_1 and r_2 represent the bond length along O–H and O–D directions and $\vec{S}^{ir}(t)$ denotes the electric field vector corresponding to IR pulse. As we have used polychromatic laser pulse for the study, Equation (2.5) takes the following form:

$$\hat{H}_{ir}(t) = -\vec{\mu}_g(\mathbf{r}_1, \mathbf{r}_2) \cdot \sum_i \vec{S}_i^{ir}(t) \quad (2.6)$$

$S_i^{ir}(t)$ depends on the maximum amplitude ($E_{0,i}^{ir}$), frequency ω_i^{ir} and shape of the laser pulse ($a_i(t)^{ir}$). The complete form of $\hat{H}_{ir}(t)$ will be

$$\hat{H}_{ir}(t) = -\mu_g(\mathbf{r}_1, \mathbf{r}_2) \sum_i c_i^{ir} E_{0,i}^{ir} a_i^{ir}(t) \cos \omega_i^{ir} t, \quad (2.7)$$

$$\text{where } \sum_i (c_i^{ir})^2 = 1. \quad (2.8)$$

Here c_i^{ir} is the associated coefficient of each of the components of the polychromatic field with the condition mentioned in Equation (2.8). The shape of the laser is considered as a simple form of Gaussian function for each of the components of the field:

$$a_i^{ir}(t) = \left(\frac{8\gamma_i^{ir} t_l^2}{\pi} \right)^{1/4} \exp[-\gamma_i^{ir}(t - t^{ir})^2]. \quad (2.9)$$

In Equation (2.9), t_l indicates the length of time the pulses being switched on and t^{ir} is the peak time of the pulses. γ_i^{ir} is the parameter by which the full width at half-maximum (FWHM) of the individual Gaussian pulse can be expressed as

$$\text{FWHM} = \sqrt{\frac{4 \ln 2}{\gamma}}. \quad (2.10)$$

The \hat{H}_{uv} can similarly be written as \hat{H}_{IR} :

$$\hat{H}_{uv}(t) = -\mu_{ge}(\mathbf{r}_1, \mathbf{r}_2) \sum_i c_i^{uv} E_{0,i}^{uv} a_i^{uv}(t) \cos \omega_i^{uv} t. \quad (2.11)$$

The ‘ Σ ’ denotes the use of polychromatic UV pulse. The terms imply in a similar way as explained for IR pulse. The form of $a_i^{uv}(t)$ is

$$a_i^{uv}(t) = \exp[-\gamma_i^{uv}(t - t^{uv})^2]. \quad (2.12)$$

The process is started according to Equation (2.4), where the whole population is situated in the lowest vibrational state of ground electronic state. Polychromatic IR pulse is then switched on which is designed to get its maximum potency at the time of 100 fs, i.e. $t^{ir} = 100$ fs. The IR pulse transfers the population to the higher vibrational states. According to the nature of the fields, the modes along O–H stretch or O–D stretch are populated. T_l is set as 250 fs. At 250 fs, the IR pulse is turned down and UV fields are started to play. Transition of population from ground electronic state to excited totally repulsive electronic state occurs. The molecule then dissociates in this state. With respect to the direction of population along O–H or O–D mode, the flux along H+O–D or D+O–H channel is expected. UV light maximises at 350 fs and die down according to the shape function. We have followed the dynamics up to 500 fs. Equation (2.1) is the fundamental working equation and it has to be solved for every time to get the time profile of the system. Fast Fourier transform [51] technique is used to evaluate the kinetic energy operator and Lanczos scheme [52] is employed as a propagator.

2.2. Pulse optimisation

The time-integrated flux can be written as [39,42]

$$J_{\text{H+O-D}} = \int_0^{r_2^d} \int_0^T \Psi^*(r_1, r_2, t) \times \left(\hat{j}_1 + \frac{\mu_2 \cos \theta}{m_o} \hat{j}_2 \right) \Psi(r_1, r_2, t) dr_2 dt, \quad (2.13)$$

$$\text{and } J_{\text{D+O-H}} = \int_0^{r_1^d} \int_0^T \Psi^*(r_1, r_2, t) \times \left(\hat{j}_2 + \frac{\mu_1 \cos \theta}{m_o} \hat{j}_1 \right) \Psi(r_1, r_2, t) dr_1 dt. \quad (2.14)$$

where

$$\hat{j}_i = \frac{1}{2\mu_i} [\hat{p}_i \delta(r_i - r_i^d) + \delta(r_i - r_i^d) \hat{p}_i], \quad (2.15)$$

In Equation (2.15), r_i^d represents the grid point in the asymptotic region for the i th channel.

The objective of the work is to increase the flux along desired channel (H+O–D or D+O–H) as well as reduce the flux in other channel to get selectivity. The goal may be achieved by designing proper electromagnetic field of radiation. The problem is now cast as a problem of optimisation and we need to define the objective function, which directs the search, and the variable space, which is to be optimised to get the objective. First, we define the objective function

$$\text{Obj} = \alpha |1 - J_i| + \beta \frac{J_k}{J_i} \quad (2.16)$$

If $i = \text{H+O-D}$, $k = \text{D+O-H}$ and vice versa, α and β are the scalar parameters and can be manipulated manually. The first term takes care of the gain in flux along the channel we want and the second term accounts for the selectivity, as it will be minimum if the J_k will be zero. As the maximum value of the total time-integrated flux is 1, the value of ‘Obj’ will be the lowest (effectively zero) if J_i reaches to 1 and it also guarantees the flux along other channel to be 0. Following this objective function, the optimisation is named as *strategy I*.

Both IR and UV pulses are optimised in order to achieve the objective. Thus the variable space contains both IR and UV field parameters and it is represented as $\{S_i^{ir}(c_i^{ir}, E_{0,i}^{ir}, \text{FWHM}_i^{ir}, \omega_i^{ir}), i = 1, 8\}$ and $\{S_i^{uv}(c_i^{uv}, E_{0,i}^{uv}, \text{FWHM}_i^{uv}, \omega_i^{uv}), i = 1, 2\}$ for IR and UV fields, respectively. Instead of doing consecutive optimisation of IR and then UV pulses, all the pulse parameters are subjected to optimisation simultaneously with the objective function according to Equation (2.16). The idea behind the strategy is that, the IR pulse distributes the population to the low quanta vibrational states of desired direction and thus more than one UV light are needed for complete transfer of the population to the excited state.

The selective vibrational excitation followed by population transfer via matching UV has also been performed (*Strategy II*) and the results from both the strategies are compared. For selective vibrational excitation, the objective function is set as

$$\text{Obj} = |1 - \text{Pop}_{ij}| \quad (2.17)$$

$$\text{where, } \text{Pop}_{ij} = |\langle n_i, n_j | \Psi_g(t) \rangle|^2 \quad (2.18)$$

GA [45,46] is employed for pulse optimisation. The philosophy behind the algorithm is based on the concept of ‘survival of the fittest’ by Darwin, as nature selects the best possibility to survive, GA searches for the optimal solution for a problem. The algorithm is started with an

arbitrary solution pool. The fitness function for each solution in the solution pool is designed as

$$F = \exp(-\text{Obj}). \quad (2.19)$$

The value of F would be between 0 and 1. When the value of Obj is 0, i.e. F is to be 1, it implies the solution to be the most fit.

3. Results and discussion

Following the objective function demonstrated in Equation (2.16), we first attempt to get selective dissociation along H+O–D mode. The J_i in the equation is thus $J_{\text{H+O–D}}$ and $J_k = J_{\text{D+O–H}}$. In doing optimal control, the generous use of polychromatic field is observed in recent research over the use of monochromatic ones [37–42,53–55]. A possible reason may be the breakdown of periodicity in polychromatic field which gives the flexibility to the system to move in a direction where reinforcing or suppressing a quantum event occurs. We have taken a linear combination of eight IR pulses (polychromatic) instead of single-frequency pulse (monochromatic), with similar associated coefficients c_i^{ir} ; however, the constraint mentioned in Equation (2.8) is maintained. The initial guess of $E_{0,i}^{ir}$, FWHM_i^{ir} , ω_i^{ir} are chosen according to the previous works on HOD photodissociation [11,39]. The ω_i^{ir} s are chosen arbitrarily around the value of resonating frequency of vibrational transition from $|0, 0\rangle$ to $|1, 0\rangle$ states. The normal femtosecond pulses ranging from 50fs to 90 fs are taken as initial FWHM_i^{ir} . As *Strategy I* is based on the idea to distribute the population over the vibrational state of predominating O–H/O–D mode, single UV pulse would not be expected to be sufficient for population transfer from ground to excited electronic states. This is the reason why we have chosen a combination pulse of two UV frequencies. The initial guess for selective dissociation along H+O–D mode optimisation, these two UV frequencies are taken as the resonating frequencies for electronic transition from $|1, 0\rangle$ and $|2, 0\rangle$ vibrational states of ground electronic state. The other parameters of UV pulses, i.e. c_i^{uv} , $E_{0,i}^{uv}$, FWHM_i^{uv} , are of the same value for both the components at the stage of initialisation of the optimisation. The initial guess solutions are then subjected to the GA optimisation and GA, and then sample the parameter space to select the optimal IR and UV pulses which results in a high and selective population along H+O–D channel on application. The evolution of the fitness function with GA step is presented in Figure 1(a) and the pictorial representation of the IR pulses is given in Figure 1(b). The initial and optimised pulse parameters for both the IR

Table 1. The initial and optimised population at different vibrational levels (after completion of IR pulse) and final fluxes at excited state (after completion of IR+UV pulses) for optimisation performed followed by *Strategy I* using IR polychromatic pulse of eight components.

Optimising the channel	Pulse type	Population at vibrational state	$J_{\text{H+O–D}}$	$J_{\text{D+O–H}}$	
H+O–D	in	$ 1, 0\rangle$	16.90%	40.24%	13.67%
		$ 2, 0\rangle$	6.33%		
	opt	$ 1, 0\rangle$	69.79%	92.38%	5.92%
		$ 2, 0\rangle$	29.62%		
D+O–H	in	$ 0, 1\rangle$	12.51%	67.10%	25.21%
		$ 0, 2\rangle$	2.38%		
		$ 0, 3\rangle$	0.23%		
	opt	$ 0, 1\rangle$	11.65%	20.81%	74.12%
		$ 0, 2\rangle$	41.82%		
		$ 0, 3\rangle$	35.56%		

and UV fields are tabulated in supplementary information. We now plot the dynamical profile of the system on the application of the optimised field as well as the initial field in Figure 1(c,d). Figure 1(c) depicts the picture of population distribution over different vibration levels of ground electronic state after applying IR frequencies. As the optimisation is performed with the goal of getting maximum flux along H+O–D channel, the population gets distributed among the low quanta vibrational state of predominant O–H character, $|1, 0\rangle$ and $|2, 0\rangle$, on application of the optimised pulse. Optimised pulse results in population of 69.79% at $|1, 0\rangle$ and 29.62% at $|2, 0\rangle$ state at time 250 fs, while the application of initial pulse gives 16.90% and 6.33% population on $|1, 0\rangle$ and $|2, 0\rangle$, respectively. The flux along both of the channel on repulsive excited state as well as ground state are plotted in Figure 1(d) for initial and optimised IR+UV pulses. We get $J_{\text{H+O–D}}$ for optimised pulse is about 92.4% while the flux for initial guess pulse is only 40.24% (Table 1). The flux along another channel, i.e. $J_{\text{D+O–H}}$, is of 13.67% and 5.92%, respectively, for initial and optimised pulses. We have presented the contours of population obtained by applying both initial and optimised pulses in Figure 2. Figure 2(a,b) represents the snapshots of contours in ground electronic level at 175 fs for the initial and optimised fields, respectively. 175 fs is a time when the IR frequencies practically die off and UV field is not switched on. Contours of population at excited electronic state, after completion of both IR and UV pulses (at 325 fs), are plotted in Figure 2(c,d) for initial and optimised pulse parameters.

To get selective photodissociation along D+O–H channel, we start optimisation in a similar manner as done for the case of flux optimisation along H+O–D channel. A linear combination of eight IR components are chosen arbitrarily within a range of fundamental frequency along O–D mode. The initial UV frequencies

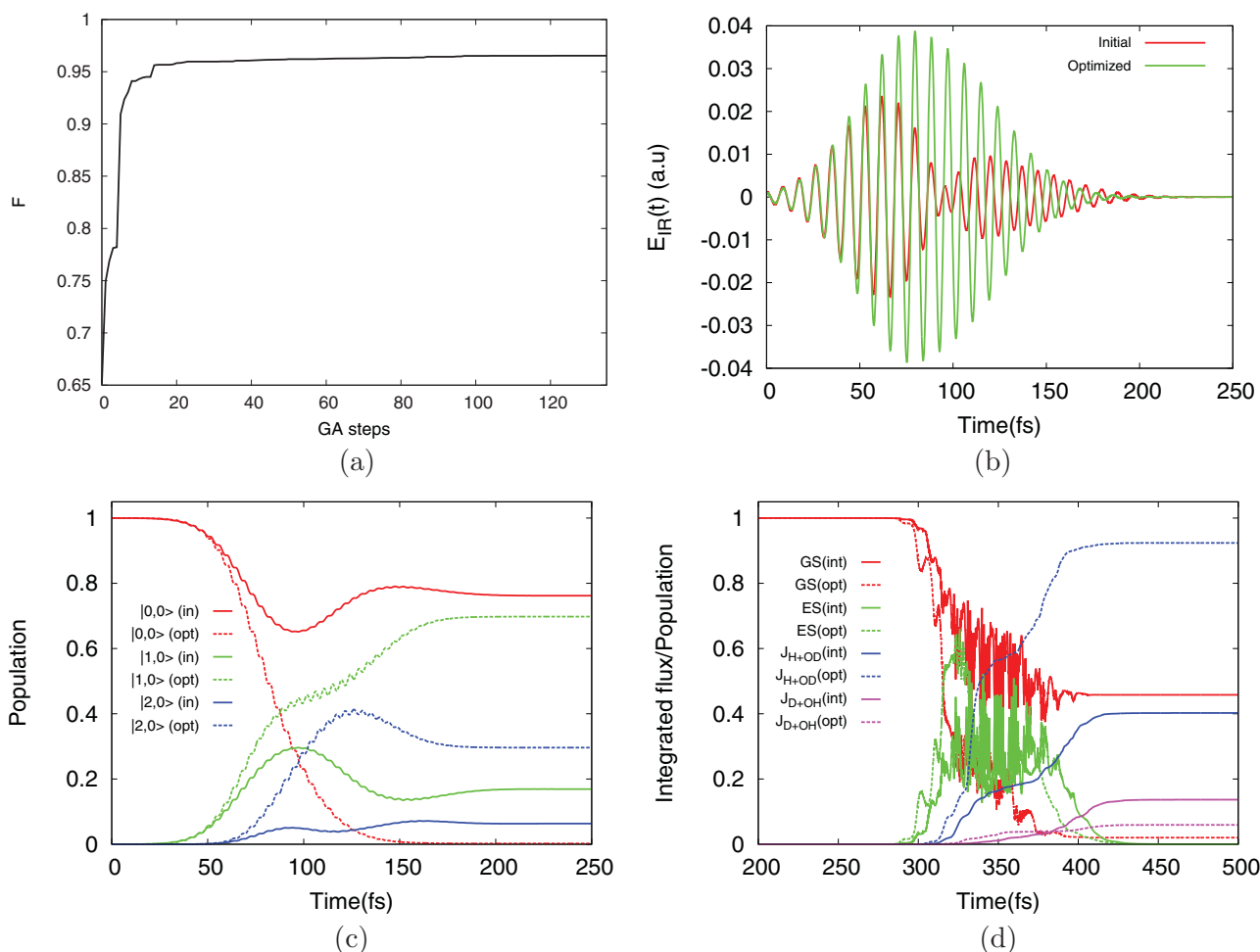


Figure 1. (Colour online) The plots are obtained while optimising the J_{H+O-D} (following *Strategy I*). GS and ES denote populations in ground and excited electronic states, respectively. (a) The fitness function vs. GA step. (b) Pictorial representation of IR pulses both for initial (red) and optimised (green) one. (c) Population at different vibrational levels of ground electronic state while applying IR pulse. The solid line denotes the initial state and dashed line is for optimised state. (d) Overall population in ground (red line) and excited (green line) electronic states and fluxes along J_{H+O-D} (blue line) and J_{D+O-H} (magenta line) for both ground and excited states on the application of initial (solid line) and optimised (dashed line) IR+UV pulses.

are taken equal to the matching frequencies to excited electronic state from the $|0, 1\rangle$ and $|0, 2\rangle$ vibrational states of ground electronic state. The objective function in Equation (2.16) is used with $J_i = J_{D+O-H}$ and $J_k = J_{H+O-D}$. The fitness profile and the pulse shapes (both initial and optimised) are portrayed in Figure 3(a,b). We have plotted the population vs. time profile for vibrational states in ground electronic state in Figure 3(c), likewise Figure 1(c). Here we found the majority of the population more or less equally distributed among $|0, 2\rangle$ and $|0, 3\rangle$ states and a significant population is also there in $|0, 1\rangle$ state. The population obtained at 250 fs for optimised field is 11.6%, 41.8% and 35.6% for $|0, 1\rangle$, $|0, 2\rangle$ and $|0, 3\rangle$ states, respectively. If we follow the time profile (Figure 3(d)) of the flux in excited state after applying both IR and UV frequencies, we will see that $J_{D+O-H} = 74.1\%$ and $J_{H+O-D} = 20.8\%$ for optimised pulses, where

initial pulses result 25.2% and 67.0% along D+O-H channel and H+O-D channel, respectively. The details of results of the fluxes along both the channels as well as the populations on different vibrational states of ground electronic state, for initial and optimised pulses are tabulated in Table 1 and the pulse parameters are given in supplementary information. The contoural evolution also justifies the results in Table 1. From Figure 4, it is clear that the population in ground electronic is directed predominantly along r_2 bond for the optimised pulse (see figures for 175 fs) making the O-D bond dissociation more feasible while transfer to the excited state, where as the initial pulse cannot produce any significant likelihood towards any mode. The characteristic of these contour sustained in the contoural evolution after addressing both optimised pulses, i.e. IR and UV pulses. The snapshots at 325 fs (Figure 4(d)) for optimised pulse show principal

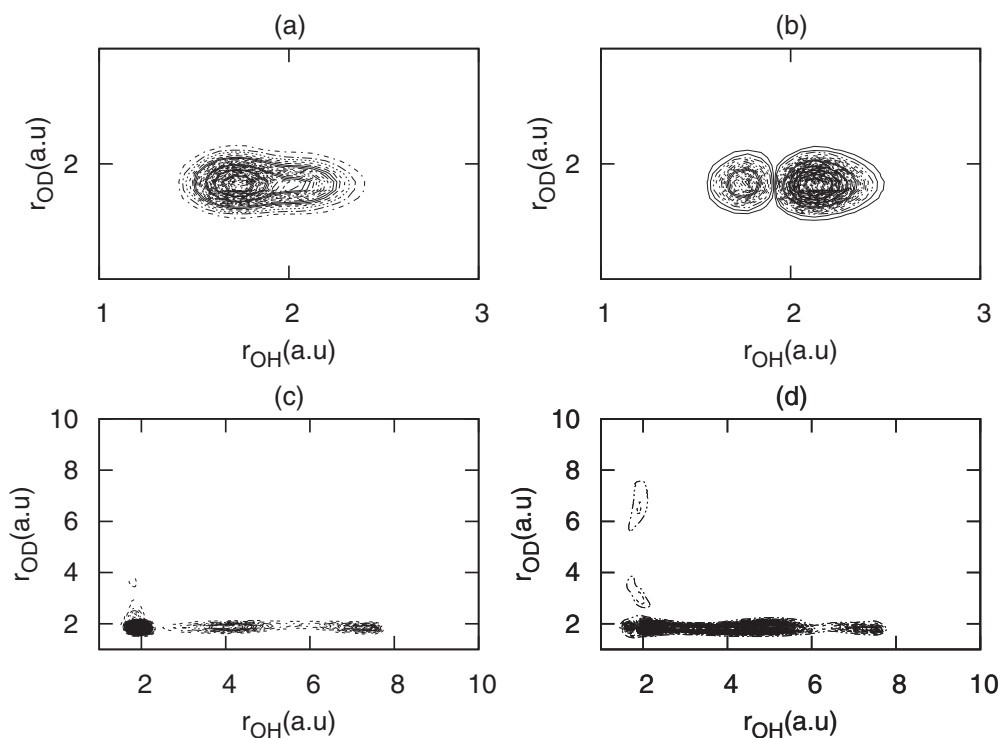


Figure 2. Snapshot of contours of population while optimising the $J_{\text{H+O-D}}$ (a) at 175 fs in ground electronic state for initial pulse; (b) at 175 fs in ground electronic state for optimised pulse; (c) at 325 fs in repulsive excited electronic state for initial pulse; (d) at 325 fs in repulsive excited electronic state for optimised pulse.

amount of flux along D+O-H channel; however, the plots for initial pulse in Figure 4(c) present reverse picture, i.e. $J_{\text{H+O-D}} > J_{\text{D+O-H}}$.

We have also performed the optimisation to get the selective vibrational excitation as was done in our previous work for selective photodissociation of HOD by using SA as optimiser [39]. According to the nature of vibrational state, i.e. whether it corresponds to O-H stretch or O-D stretch, the selective dissociation may be achieved by population transfer from the selectively populated vibrational state to the repulsive excited state by single-matching UV frequency. The low quanta vibrational excited states are chosen as target state and optimisations are conducted with the objective function in Equation (2.17), i.e. population at ground electronic state is controlled rather than the flux in excited state. Target population is achieved for $|1, 0\rangle$ and $|2, 0\rangle$ to get selective dissociation along H+O-D and for the other channel, i.e. to maximise $J_{\text{D+O-H}}$, $|0, 1\rangle$ and $|0, 2\rangle$ vibrational states are selected. The parameters of initial and optimised pulses for $|1, 0\rangle$, $|2, 0\rangle$, $|0, 1\rangle$, $|0, 2\rangle$ states are given in supplementary information. The detail results from these optimisations, the population at target states and flux obtained after completion of the IR+UV pulses along both the channels are furnished in Table 2 for initial as well as optimised pulses.

Table 2. The initial and optimised population at target vibrational levels (after completion of IR pulse), final fluxes (after completion of IR+UV pulses) for optimisation using Strategy II using IR polychromatic pulse of eight components.

Target level	Pulse type	Population	$J_{\text{H+O-D}}$	$J_{\text{D+O-H}}$
$ 1, 0\rangle$	in	10.02%	10.22%	0.94%
	opt	87.96%	84.31%	5.56%
$ 2, 0\rangle$	in	0.72%	1.47%	0.03%
	opt	86.76%	86.91%	2.23%
$ 0, 1\rangle$	in	12.51%	53.97%	26.63%
	opt	79.68%	38.49%	56.72%
$ 0, 2\rangle$	in	2.38%	0.05%	2.3%
	opt	66.75%	11.89%	65.94%

We obtain 87.9% and 86.8% population at states $|1, 0\rangle$ and $|2, 0\rangle$, respectively, by applying the optimised IR perturbations. The initial pulse cannot transfer the population to the higher vibrational states and the whole population practically remains in the ground vibrational state. With the optimised pulses we get selective population transfer to target states, where only a 7%–8% population remains in the $|0, 0\rangle$ state. The $J_{\text{H+O-D}}$ obtained by transferring population to excited electronic state from respective vibrational states, $|1, 0\rangle$ and $|2, 0\rangle$, are 84.3% and 86.9% (see Table 2). From direct flux optimisation we

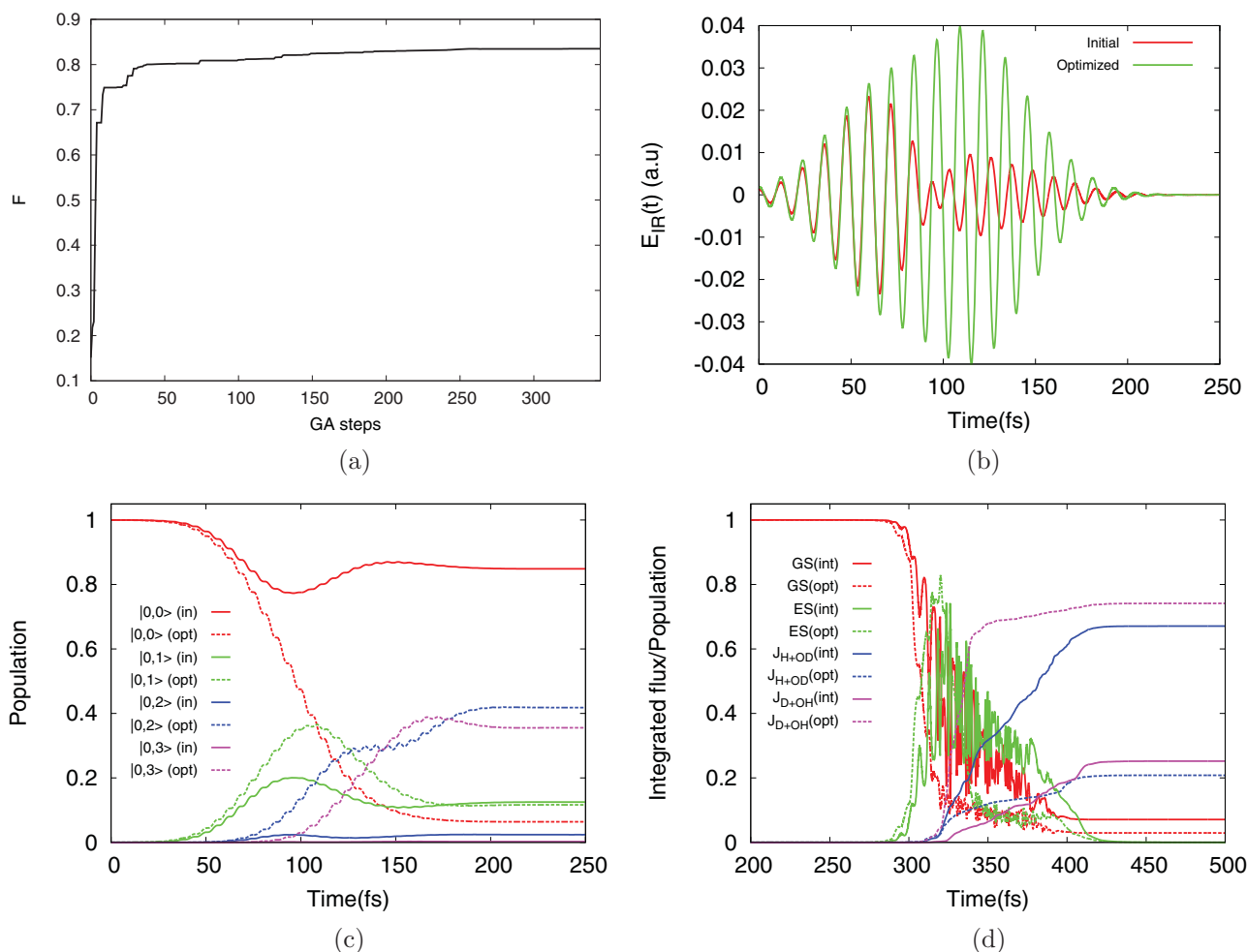


Figure 3. The plots are obtained while optimising the J_{D+O-H} (following *Strategy I*). GS and ES denote populations in ground and excited electronic states, respectively. (a)–(d) depict similarly as in [Figure 1](#).

get $J_{H+O-D} = 92.4\%$, which is $\approx 5\%$ higher than the fluxes obtained by *Strategy II*.

Now we come to the picture of D+O–H channel. Using *Strategy II* we get population 79.7% and 66.7% for target state $|0, 1\rangle$ and $|0, 2\rangle$ after optimisation. Here also the initial field cannot transfer population to the target vibrational excited state for both the cases of optimisation (see [Table 2](#)). In the case of $|0, 2\rangle$ optimisation, a significant amount of populations are there in other vibrational states of O–D mode such as $|0, 1\rangle$ (16.67%), $|0, 3\rangle$ (14.30%) after completion of the IR field, whereas during the other optimisation (i.e. for optimising $|0, 1\rangle$ state) 8.65% population is there in $|0, 2\rangle$. But when comes the time of population transfer to excited state, only 56.7% flux in D+O–H channel is observed though the population is 79.7% at state $|0, 1\rangle$ and the value of J_{H+O-D} obtained for that of the pulse is 38.49%. Thus it is not effective to use *Strategy II* on $|0, 1\rangle$ state to achieve selective photodissociation along D+O–H channel. However,

applying matching UV frequency from $|0, 2\rangle$ with population 66.7% results $J_{D+O-H} = 65.9\%$ in the excited state. The overall results using GA study shows that maximum J_{D+O-H} is achieved by applying *Strategy I* (74.1%) which is more than 8% greater than that we have obtained by applying *Strategy II*. One of the plausible reasons for the success of *Strategy I* over *Strategy II* is that in *Strategy I*, GA is able to induce a frequency chirp which resulted in greater distribution of population over the bunch of excited vibrational states.

To make a critical examination of the rationale behind the choice of taking eight components to design polychromatic field, we have repeated the whole study of *Strategy I* and *Strategy II* with polychromatic field with four components. The results are summarised in [Table 3](#). Considering *Strategy I*, the optimised fluxes obtained for both the channels, i.e. optimised $J_{H+O-D} = 84.13\%$ and $J_{D+O-H} = 64.0\%$ values, are substantially less (around 8% and 10% respectively) than that obtained by using

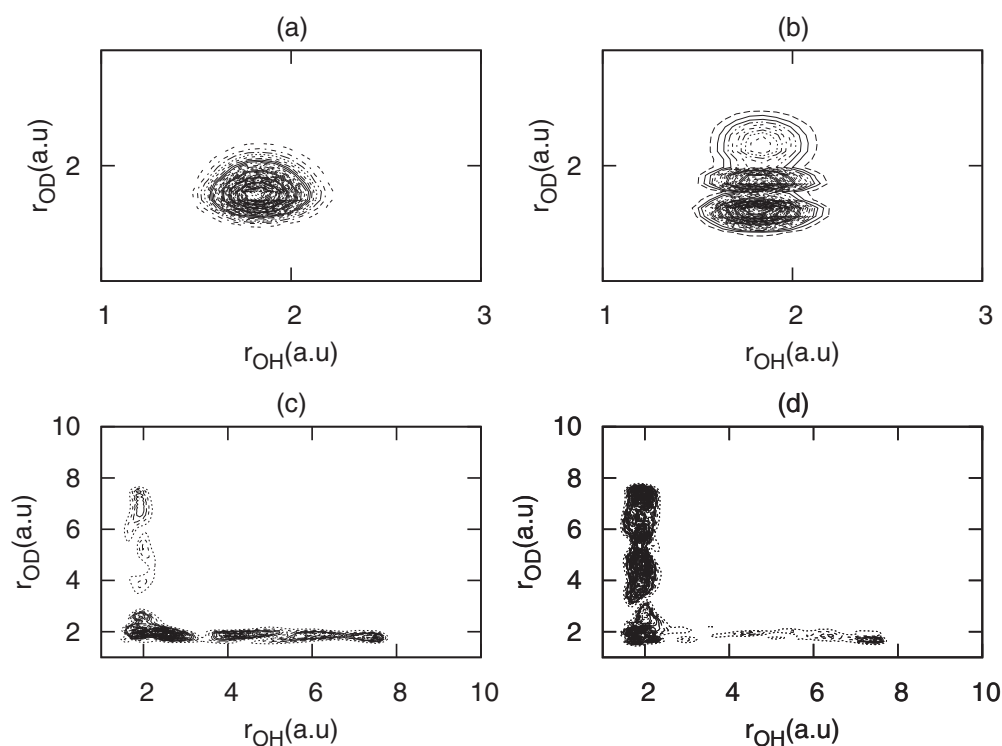


Figure 4. The plots are obtained while optimising the J_{D+O-H} . (a)–(d) depict similarly as in Figure 2.

Table 3. The optimised population at vibrational levels (after completion of IR pulse) and final fluxes (after completion of IR+UV pulses) for IR polychromatic field of four components using both *Strategy I* and *Strategy II*.

<i>Strategy I</i>				
Optimising the channel	Population at vibrational state		J_{H+O-D}	J_{D+O-H}
H+O–D	$ 1, 0\rangle$	76.50%	84.13%	14.08%
	$ 2, 0\rangle$	19.50%		
D+O–H	$ 0, 1\rangle$	25.89%	32.08%	64.00%
	$ 0, 2\rangle$	40.91%		
	$ 0, 3\rangle$	19.53%		
<i>Strategy II</i>				
Optimising level	Population type		J_{H+O-D}	J_{D+O-H}
$ 1, 0\rangle$	84.57%		85.10%	6.14%
$ 2, 0\rangle$	77.72%		80.41%	2.57%
$ 0, 1\rangle$	61.52%		41.03%	51.37%
$ 0, 2\rangle$	58.20%		9.16%	54.37%

optimised polychromatic field of eight components. The maximum fluxes obtained in H+O–D channel by applying optimised polychromatic pulse of four components with *Strategy II* (85.10%) are comparable with the fluxes achieved by optimised pulse of eight components, however optimisation to maximise J_{D+O-H} (54.37%) with lesser number of frequency components fails to give sufficient flux. In this scenario, we may comment that pulse with eight components performs in a better way than that of four-component pulse.

4. Conclusion

We have discussed strategies for obtaining selective dissociation in HOD molecule by designing optimum laser pulses. The pulse design is carried out by the use of GA, a well established and potent stochastic optimisation procedure. The optimisation was affected on both the IR as well as the UV pulse. The dissociation took place from the excited electronic state, which is repulsive, by the use of optimally selected UV pulse. Our study focused on two different ways to achieve selective control. The first one (*Strategy I*) focused on distributing the population in the ground electronic states among the low quanta vibrational states along the desired mode (O–H or O–D), as opposed to the other strategy (*Strategy II*) where the effort was to maximise the initial population along a particular excited vibrational state. Our results clearly show that the first alternative is better and robust with the flux along H+O–D dissociating channel being 92.38% as opposed to 86.91% in the second strategy. For D+O–H channel which is relatively difficult to dissociate, we again find that the first strategy is overwhelmingly better giving us a flux of 74.12% as opposed to 65.94% in the second route.

Finally, the point to be emphasised is whether the proposed strategy of distributing populations in a bunch of vibrational excited states (*Strategy I*) as opposed to a single one (*Strategy II*) can be a general scheme which one can follow in a host of molecular systems. We believe that

though our study is on HOD, it is sufficiently general to shed light on what should be an ideal general mechanism for optimal control of bond dissociation dynamics. We, in one of our earlier communication [42], have worked on $O^{16}O^{16}O^{18}$ system which has very strong Intramolecular Vibrational Redistribution (IVR) and selective cleavage of bonds is difficult to achieve using light. However, a strategy of non-specific vibrational excitation in ground electronic state followed by a UV excitation to the excited electronic state is able to generate reasonably good flux along dissociation channels. The success of this strategy (*Strategy I*) on these systems gives us confidence to say that it has mechanistic implications.

Acknowledgments

S. Talukder would like to thank Indian Association for the Cultivation of Science for granting research fellowship. P. Chaudhury and S. Adhikari acknowledge UGC for the funding through Major Research Project.

Disclosure statement

No potential conflict of interest was reported by the authors.

Funding

UGC.

References

- [1] N. Shafer, S. Satyapal, and R. Bersohn, *J. Chem. Phys.* **90**, 6807 (1989).
- [2] R.L. Vander Wal, J.L. Scott, and F.F. Crim, *J. Chem. Phys.* **92**, 803 (1990).
- [3] I. Bar, Y. Cohen, D. David, S. Rosenwaks, and J.J. Valentini, *J. Chem. Phys.* **93**, 2146 (1990).
- [4] R.L. Vander Wal, J.L. Scott, F.F. Crim, K. Weide, and R. Schinke, *J. Chem. Phys.* **94**, 3548 (1991).
- [5] I. Bar, Y. Cohen, D. David, T. Arusi-Parper, S. Rosenwaks, and J.J. Valentini, *J. Chem. Phys.* **95**, 3341 (1991).
- [6] Y. Cohen, I. Bar, and N. Rosenwaks, *J. Chem. Phys.* **102**, 3612 (1995).
- [7] H. Akagi, H. Fukazawa, K. Yokoyama, and A. Yokoyama, *J. Chem. Phys.* **123**, 184305 (2005).
- [8] E. Segev and M. Shapiro, *J. Chem. Phys.* **77**, 5604 (1982).
- [9] J. Manz and G.K. Paramonov, *J. Phys. Chem.* **97**, 12625 (1993).
- [10] W. Jakubetz, E. Kades, and J. Manz, *J. Phys. Chem.* **97**, 12609 (1993).
- [11] B. Amstrup and N.E. Henriksen, *J. Chem. Phys.* **97**, 8285 (1992).
- [12] M. Amstrup and P. Brumer, *J. Chem. Phys.* **98**, 201 (1993).
- [13] N.E. Henriksen and B. Amstrup, *Chem. Phys. Lett.* **123**, 65 (1993).
- [14] N.E. Henriksen, K.B. Møller, and V. Engel, *J. Chem. Phys.* **122**, 204320 (2005).
- [15] M. Sarma, S. Adhikari, and M.K. Mishra, *J. Chem. Phys.* **127**, 024305 (2007).
- [16] M. Sarma, S. Adhikari, and M.K. Mishra, *Mol. Phys.* **107**, 939 (2009).
- [17] V. Engel and R. Schinke, *J. Chem. Phys.* **88**, 6831 (1988).
- [18] J. Zhang and D.G. Imre, *Chem. Phys. Lett.* **123**, 233 (1988).
- [19] J. Zhang, D.G. Imre, and J.H. Frederick, *J. Phys. Chem.* **93**, 1840 (1989).
- [20] D. G. Imre and J. Zhang, *Chem. Phys.* **123**, 89 (1989).
- [21] B. Hartke, J. Manz, and J. Mathis, *Chem. Phys.* **139**, 123 (1989).
- [22] V. Engel, R. Schinke, and V. Staemmler, *J. Chem. Phys.* **88**, 129 (1988).
- [23] V. Staemmler and A. Palma, *Chem. Phys.* **93**, 63 (1985).
- [24] H. Rabitz, *Science*. **314**, 264 (2006).
- [25] P. Gross, D. Neuhauser, and H. Rabitz, *J. Chem. Phys.* **96**, 2834 (1992).
- [26] P. Gross, D.M. Bairagi, M.K. Mishra, and H. Rabitz, *Chem. Phys. Lett.* **223**, 263 (1994).
- [27] P. Gross, A.K. Gupta, D.M. Bairagi, and M.K. Mishra, *J. Chem. Phys.* **104**, 7045 (1996).
- [28] K. Vandana and M.K. Mishra, *J. Chem. Phys.* **110**, 5140 (1999).
- [29] K. Vandana and M.K. Mishra, *J. Chem. Phys.* **113**, 2336 (2000).
- [30] S.A. Rice, *Nat. (Lond.)* **409**, 422 (2001).
- [31] D.J. Tannor and S.A. Rice, *Adv. Chem. Phys.* **70**, 441 (1988).
- [32] C. Kalyanraman and N. Sathyamurti, *Chem. Phys. Lett.* **209**, 52 (1993).
- [33] C. Shu, T. Rozgonyi, L. González, and N.E. Henriksen, *J. Chem. Phys.* **136**, 174303 (2012).
- [34] S.K. Lee, A.G. Suits, H.B. Schlegel, and W. Li, *J. Phys. Chem. Lett.* **3**, 2541 (2012).
- [35] S.K. Lee, H.B. Schlegel, and W. Li, *J. Phys. Chem. A* **117**, 11202 (2013).
- [36] M.E. Corrales, J. González-Vázquez, G. Balerdi, I.R. Solá, R. de Nalda, and L. Bañares, *Nat. Chem.* **6**, 785 (2014).
- [37] S. Sharma, H. Singh, and G.G. Balint-Kurti, *J. Chem. Phys.* **132**, 064108 (2010).
- [38] S. Sharma, H. Singh, J. Harvey, and G.G. Balint-Kurti, *J. Chem. Phys.* **133**, 174103 (2010).
- [39] B.K. Shandilya, S. Sen, T. Sahoo, S. Talukder, P. Chaudhury, and S. Adhikari, *J. Chem. Phys.* **139**, 034310 (2013).
- [40] S. Ghosh, S. Talukder, S. Sen, and P. Chaudhury, *Chem. Phys.* **425**, 73 (2013).
- [41] S. Ghosh, S. Talukder, S. Sen, and P. Chaudhury, *Mol. Phys.* **113**, 3826 (2015).
- [42] S. Talukder, S. Sen, B.K. Shandilya, R. Sharma, P. Chaudhury, and S. Adhikari, *J. Chem. Phys.* **143**, 144109 (2015).
- [43] S. Kirkpatrick, C.D. Gelatt, and M.P. Vecchi, *Science*. **220**, 671 (1983).
- [44] S. Kirkpatrick, *J. Stat. Phys.* **34**, 975 (1984).
- [45] D.E. Goldberg, *Genetic Algorithm in Search, Optimization and Machine Learning* (Addison Wesley, Reading, MA, 1989).
- [46] J. Holland, *Adaptation in Natural and Artificial Systems* (MIT Press, Ann Arbor, MI, 1992).
- [47] A.K. Tiwari, K.B. Møller, and N.E. Henriksen, *Phys. Rev. A* **78**, 065402 (2008).

- [48] J.R. Reimers and R.O. Watts, *Mol. Phys.* **52**, 357 (1984).
- [49] K.S. Sorbie and J.N. Murrell, *Mol. Phys.* **29**, 1387 (1975).
- [50] K.S. Sorbie and J.N. Murrell, *Mol. Phys.* **31**, 905 (1976).
- [51] D. Kosloff and R. Kosloff, *J. Comput. Phys.* **52**, 35 (1983).
- [52] C. Leforestier, R. Bisseling, C. Cerjan, M.D. Feit, R. Friesner, A. Guldborg, A. Hammerich, G. Jolicard, W. Karrlein, H.-D. Meyer, N. Lipkin, O. Roncero, and R. Kosloff, *J. Comput. Phys.* **94**, 59 (1991).
- [53] K. Hoki and Y. Fujimura, *Chem. Phys.* **267**, 187 (2001).
- [54] O. Atabek, C.M. Dion, and A.B. Haj-Yedder, *J. Phys. B* **36**, 4667 (2003).
- [55] C.M. Dion, A.B. Haj-Yedder, E. Cancés, C. Le Bris, A. Keller, and O. Atabek, **123**, 063408 (2002).